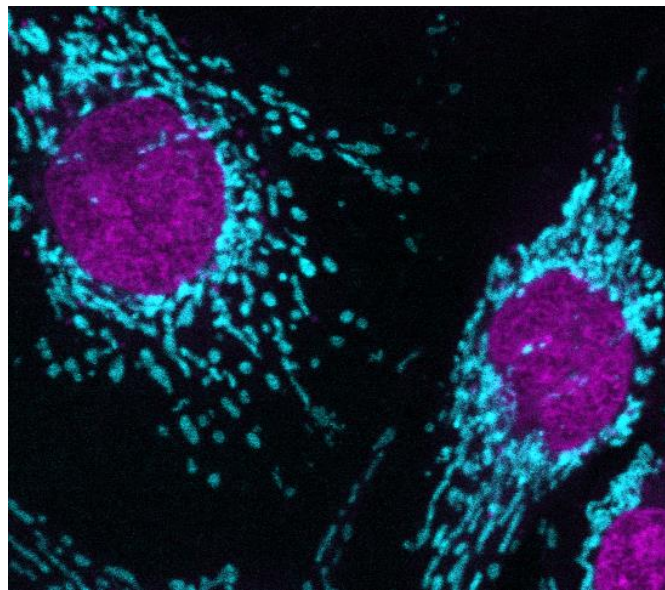


MAX-PLANCK-INSTITUT
FÜR POLYMERFORSCHUNG



JOHANNES GUTENBERG
UNIVERSITÄT MAINZ

Synthesis of Furin-Responsive Depsipeptides for Intracellular Self-Assembly



Master Thesis

Max Planck Institute for Polymer Research, Mainz

Johannes Gutenberg University of Mainz

Jana Fetzer

born May 30th, 1998 in Worms

September 2022

The present work was prepared from March 2022 to September 2022 in the work group of Prof. Dr. Tanja Weil (subgroup of Dr. David Ng) at the Max Planck Institute for Polymer Research in Mainz.

Submission date: 30th September 2022

1. Reviewer: Prof. Dr. Tanja Weil

2. Reviewer: Prof. Dr. Andreas Walther

Eigenständigkeitserklärung

Masterarbeit im Studiengang Chemie, Biomedizinische Chemie oder Polymerchemie
an der Johannes Gutenberg-Universität Mainz

Ich, Jana Fetzer, Matrikelnummer 2740862, versichere, dass ich meine Masterarbeit selbstständig verfasst und keine anderen als die angegebenen schriftlichen und elektronischen Quellen sowie andere Hilfsmittel benutzt habe. Alle Ausführungen, die anderen Schriften wörtlich oder sinngemäß entnommen wurden, habe ich kenntlich gemacht.

Mainz, 30.09.22

(Ort, Datum)

J. Fetzer

(Unterschrift)

Table of Contents

List of Abbreviations	III
Abstract.....	V
Kurzfassung	VII
1 Introduction	1
1.1 Self-Assembly	1
1.2 Peptides and Proteins.....	6
1.3 Furin	11
1.4 Fluorescence and Fluorophores	12
2 Motivation and Aim	15
3 Results and Discussion.....	19
3.1 Synthesis and Characterization of Peptides.....	19
3.2 Analysis of Enzymatic Conversion	25
3.3 Analysis of Self-Assembly Behavior	28
3.4 Cell Uptake Studies and Intracellular Structure Formation.....	35
3.5 Cell Viability	39
4 Conclusion and Outlook.....	41
5 Experimental Section	44
5.1 Instruments and Methods	44
5.2 Synthesis.....	48
6 References	61
7 List of Figures and Schemes	65
8 Attachment	71

List of Abbreviations

Ac	acetyl	HOBt	1-hydroxybenzotriazole
ACN	acetonitrile	HPLC	high performance liquid chromatography
Ala/A	alanine	IC₅₀	half maximal inhibitory concentration
Arg/R	arginine	Ile/I	isoleucine
BOP	benzotriazolylxytris(dimethylamino)phosphonium hexafluorophosphate	LC-MS	liquid chromatography - mass spectrometry
BSA	bovine serum albumin	Lys/K	lysine
C343	coumarin-343	MALDI-TOF	matrix-assisted laser desorption ionization-time offlight
CD	circular dichroism	MeOH	methanol
CH	cyclohexane	MF	molecular formula
CHCA	α -cyano-4-hydroxycinnamic acid	MW	molecular weight
DBCO	dibenzocyclooctine	NHS	<i>N</i> -hydroxysuccinimide
DCM	dichloromethane	NMR	nuclear magnetic resonance
DIC	diisopropylcarbodiimide	PB	phosphate buffer
DIPEA	diisopropylethylamine	Pbf	2,2,4,6,7-pentamethyl-1,2,3,4-tetrahydro-1H-benzotriazol-5-yl
DMAP	4-(dimethylamino)pyridine	PBS	phosphate-buffered saline
DMEM	Dulbecco's Modified Eagle's Medium	Py	pyrene
DMF	dimethyl formamide	PyBOP	benzotriazol-1-ylxytripyrrolidinophosphonium hexafluorophosphate
DMSO	dimethyl sulfoxide	Py-COOH	1-pyrenylacetic acid
DNA	deoxyribonucleic acid	R_F	relate-to-front
EA	ethylacetate	RNA	ribonucleic acid
Fmoc	fluorenylmethoxycarbonyl	ROS	reactive oxygen species
HEPES	2-(4-(2-hydroxyethyl)-1-piperazinyl)-ethanesulfone acid	R_T	retention time
HMPT	hexamethylphosphoric triamide	Ser/S	serine
HOAt	1-hydroxy-7-azabenzotriazole	SPPS	solid phase peptide synthesis

List of Abbreviations

TAT	trans-activator of transcrip- tion
TCEP	tris(2-carboxyethyl)phos- phine
TEM	transmission electron microscopy
TFA	trifluoroacetic acid
THF	tetrahydrofurane
TIPS	triisopropylsilane
UV	ultraviolet
Val/V	valine

Abstract

The research area of synthetic supramolecular chemistry within biological systems is inspired by natural phenomena that drive the creation of living matter. The formation of self-assembled structures can be observed in almost every biological process and is therefore fundamental for cellular life. A major focus of mimicking such processes to build artificial supramolecular structures within the cell is being able to control the complex dynamics of self-assembly. This can be realized by incorporating stimulus-responsive structural elements into the molecular design of an assembly precursor. Specific biological or chemical cues within the cellular environment can trigger the transformation of the precursor-molecule into an active monomer capable of self-assembly. In this thesis, a new system for enzyme-induced intracellular self-assembly was developed to achieve the stimulus-responsive formation of nanostructures inside cancer cells. For this purpose, a peptide sequence that is cleavable by the enzyme furin was incorporated into the molecular design of a precursor molecule. Furin is a protease that is associated with the Golgi apparatus of eukaryotic cells and is overexpressed in some cancer cells. Prior to the formation of fibrillar architectures inside the cell, the enzyme-responsive precursor molecule has to go through several steps, starting with cellular uptake, subcellular diffusion to the Golgi and subsequent cleavage by furin. This proteolytic cleavage initiates the in situ generation of linear self-assembling peptides. Within this thesis, the enzyme-induced self-assembly of furin-responsive peptides was analyzed to study their bio-responsiveness and the kinetics of the enzyme-triggered reaction cascade, as well as the supramolecular properties of the resulting self-assembling monomers. Additionally, cell studies with furin-overexpressing breast cancer cells were carried out showcasing the efficient in vitro conversion of the precursor and the formation of intricate intracellular nanostructures. These artificial structures were shown to exhibit low cytotoxicity making them highly interesting for various applications in synthetic biology and nanomedicine.

Kurzfassung

Das Forschungsgebiet der synthetischen supramolekularen Chemie in biologischen Systemen ist inspiriert von Naturphänomenen, welche die Entstehung lebender Materie vorantreiben. Die Bildung selbstassemblierender Strukturen ist in nahezu jedem biologischen Prozess vorzufinden und damit einhergehend fundamental für zelluläres Leben. Ein großer Fokus bei der Nachahmung solcher Prozesse, zum Aufbau synthetischer supramolekularer Strukturen innerhalb der Zelle, liegt darauf, die komplexe Dynamik der Selbstorganisation kontrollieren zu können. Dies kann realisiert werden, indem stimulusabhängige Strukturelemente in das molekulare Design eines assemblierenden Präkursors integriert werden. Spezifische biologische oder chemische Bestandteile innerhalb der zellulären Umgebung können die Umwandlung des Vorläufermoleküls in ein aktives Monomer auslösen, welches zur Selbstassemblierung fähig ist. In dieser Arbeit wurde ein neues System zur enzyminduzierten intrazellulären Selbstorganisation entwickelt, um die stimulusabhängige Bildung von Nanostrukturen innerhalb von Krebszellen zu erreichen. Dazu wurde eine durch das Enzym Furin spaltbare Peptidsequenz in das molekulare Design eines Präkursormoleküls eingebaut. Furin ist eine Protease, die mit dem Golgi-Apparat eukaryotischer Zellen assoziiert und in einigen Krebszellen überexprimiert wird. Vor der Bildung fibrillärer Architekturen innerhalb der Zelle muss das enzymresponsive Vorläufermolekül mehrere Schritte durchlaufen, beginnend mit der zellulären Aufnahme, der subzellulären Diffusion zum Golgi und der anschließenden Spaltung durch Furin. Diese proteolytische Spaltung initiiert die In-situ-Erzeugung von linearen selbstassemblierenden Peptiden. Im Rahmen dieser Arbeit wurde die enzyminduzierte Selbstorganisation Furin-responsiver Peptide analysiert, um ihre Bioresponsivität und die Kinetik der enzymgetriggerten Reaktionskaskade sowie die supramolekularen Eigenschaften der resultierenden selbstorganisierenden Monomere zu untersuchen. Zusätzlich wurden Zellstudien mit Furin-überexprimierenden Brustkrebszellen durchgeführt, welche die effiziente In-vitro-Umwandlung des Präkursors und die Bildung komplizierter intrazellulärer Nanostrukturen demonstrierten. Es wurde gezeigt, dass diese synthetischen Strukturen eine geringe Zytotoxizität aufweisen, was sie für verschiedene Anwendungen in der synthetischen Biologie und Nanomedizin interessant macht.

1 Introduction

In nature, the formation of sophisticated structures via secondary interactions of self-assembling monomers can be observed in a multitude of cases. Within the eukaryotic cell, supramolecular structures are strongly represented, with self-assembly of biomolecules being essential for the foundation of life.^[1] One example of supramolecular interactions inside the cell is the hydrogen bonding driven interactions of nucleotides which are the basic building blocks of deoxyribonucleic acid (DNA), the biomacromolecule that stores genetic information within the nucleus. In order to find space in the relatively small cell nucleus, the DNA must be compressed, which is achieved by wrapping it around positively charged histones, reducing its size by a factor of 40,000. The cytoskeleton, a dynamic network of self- and co-assembling proteins, located in the cytoplasm of the eukaryotic cell, represents another example of naturally occurring supramolecular structures.^[2] Through the creation of different fibrillar architectures, the cytoskeleton ensures cell stability, motility and division, among other things. This ability to generate function through structure formation is a common property of all the afore-mentioned natural assemblies. The development of life-like bionanomaterials that can form artificial nanostructures in the complex intracellular environment represents a major milestone in supramolecular chemistry, nanomedicine and synthetic biology. The mimicking of natural supramolecular networks inside cells might help to analyze molecular mechanisms of naturally occurring cellular processes, thereby aiding the investigation into the origin of life.^[3] Furthermore, materials that transform into synthetic supramolecular nanostructures in situ have many potential uses for therapeutic and diagnostic applications, since they circumvent many of the limitations of small molecule drug and imaging agents, such as drug resistance in cancer cells caused by efflux pumps.^[4,5] The ability of supramolecular monomers to form large aggregates within the cell forces their accumulation at the target site and enhances their pharmacokinetics.^[6]

1.1 Self-Assembly

1.1.1 General Theoretical Background

The discovery of self-assembling molecules are attributed to *Jean-Marie Lehn* who demonstrated in 1990 the first supramolecular polymer based on hydrogen bonds between small molecules.^[7] A new field in chemistry was created which deals with larger structures formed via non-covalent reversible interactions including hydrogen bonds, hydrophobic and electrostatic interactions, *Van-der-Waals* forces and π - π stacking. These intermolecular interactions are the equivalent to intramolecular covalent bonds between atoms in molecules.^[8]

Introduction

Because of the low binding energy of non-covalent interactions (< 30 kJ/mol) compared to covalent bonds (> 100 kJ/mol) multivalent forces are necessary to build stable supramolecular networks.^[9] The process of forming such sophisticated structures is called self-assembly, which is described as a spontaneous (or in response to a specific stimulus) organization of compounds into large, rigid, organized architectures. A distinction is made between static and dynamic self-assembly. The former may require energy for the formation of the ordered structures, but once formed, a stable equilibrium is established that does not dissipate energy. The latter process is less investigated and is merely able to occur if the system dissipates energy. A simple example for dynamic self-assembly would be a competitive process between reaction and diffusion in oscillating chemical reactions.^[10]

The research interest in self-assembling systems arises from the fact that several biological systems are based on such complex interactions like the cell membrane, consisting of assembling amphiphilic lipids or the two complementary single strands that form the DNA double helix which are connected through hydrogen bonds.^[2,11] The most popular bioinspired building blocks to form synthetic self-assembling structures are peptides because of their attractive properties like structural programmability, biocompatibility and -degradability, versatile functionality, good availability and cost-effectiveness.^[12] Peptides provide an abundance of hydrogen-bond-formation sites because of their amide bonds in the backbone such as several other functional groups depending on their side chains. The selectivity and high directionality of these interactions lead to a stabilization of the peptide secondary structure which can induce the formation of 1D, 2D and 3D nanostructures.^[12] Also, π - π stacking of aromatic side chain groups or added aromatic moieties can drive peptide self-assembly and can lead to directional growth. These interactions are very robust in water because of the containing nonpolar aromatic groups.^[13] Aromatic residues of peptide building blocks can be also involved in hydrophobic interactions which leads to disordered structures while π - π stacking induces well-organized structures.

Self-assembly can be controlled through different factors such as the increasing of temperature which can lead to weaker or broken hydrogen bonds while hydrophobic interactions get stabilized through this environmental change. Also, the solvent can influence non-covalent interactions by changing the pH which affects the competing solvation between donor and acceptor sites of hydrogen bonds.^[12] *Kim* and *Ihee* published a system for a significantly example of kinetic control of thermodynamic interactions by using diphenylalanine in water and showed an alternating structural transition between nanowires and nanotubes.^[14] In

general, ultrasonication is an effective method to overcome energy barriers of intermolecular non-covalent interactions for the reconfiguration of nanostructures.^[15]

1.1.2 Assembly Formation Triggered by Intracellular Stimuli

Within the cell, different naturally occurring stimuli can be exploited to trigger self-assembly of active monomers which are formed in situ from pro-assembling precursors. Such targeted intracellular stimuli include changes of pH during endocytosis and the presence of certain enzymes, as well as redox-active molecules such as reactive oxygen species (ROS) or glutathione (Figure 1.1).^[16] These compartments within the cell can be compared to reaction vessels which offer different reaction conditions for chemical transformations.

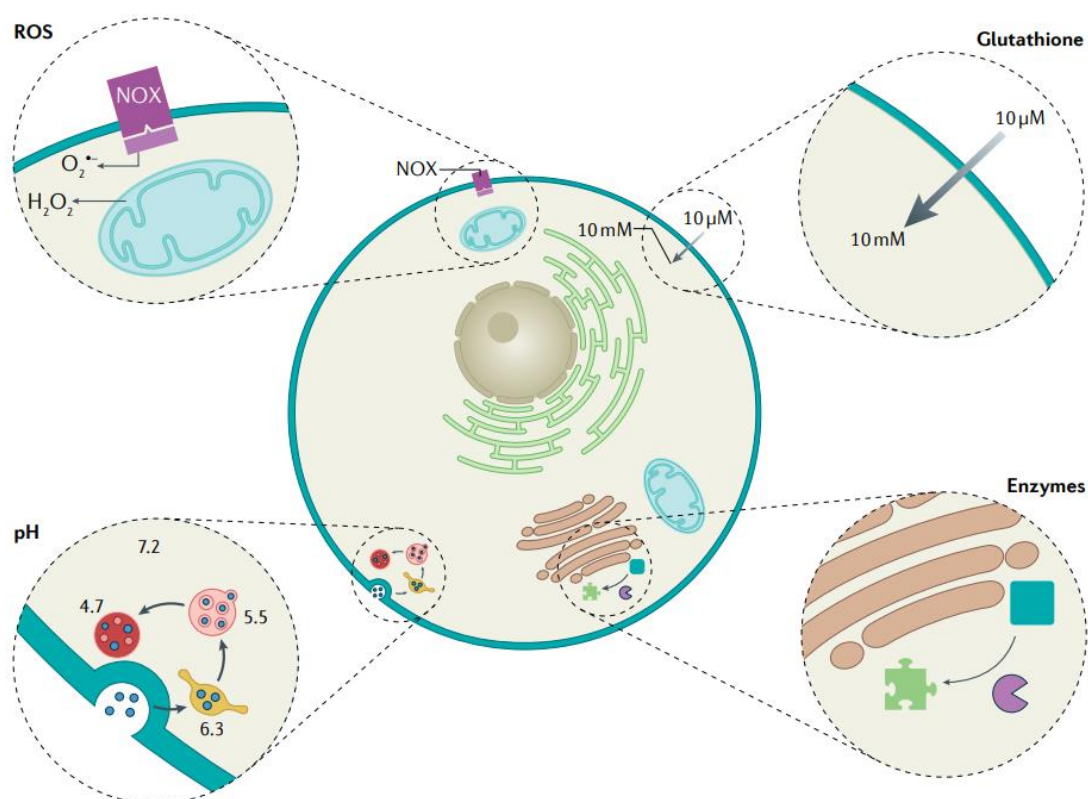


Figure 1.1: Schematic representation of the eukaryotic cell and its compartments harboring different conditions in terms of self-assembly triggers such as ROS, glutathione, pH or enzymes.^[17]

For example, the physiological pH in tissues and inside cellular organelles can vary significantly. The tumor microenvironment, for instance displays a slightly acidic pH (6.7-7.1) compared with healthy tissue (pH 7.2).^[18] Besides, within the cell a change in pH value can be observed during the endocytic pathway which entails the formation of distinct membrane compartments. These vesicular compartments are called endosomes and serve to internalize molecules from the outside of the plasma membrane, whereby their internal pH level ranges

Introduction

from 6.3 in the early endosomes to 5.5 in the late endosomes and 4.7 in the finally formed lysosome (Figure 1.1).^[19] These localization-dependent pH changes within the cell can trigger self-assembly or morphological transformation of a pH-responsive nanomaterial like peptides, since certain side chains of amino acids can be protonated or deprotonated changing the hydrophilic-hydrophobic balance within the molecule (Figure 1.2 a).^[20] Another possible trigger for self-assembly inside cells is glutathione which is a tripeptide that acts as reducing agent. Its concentration varies greatly within human tissues and is especially high in cytosolic nuclear compartment (up to 10 mM^[21]) transforming this subcellular space into a reducing environment. Due to its thiol group owing to cysteine, glutathione can also act as nucleophile in addition to its reducing properties as cell-protective antioxidant. Its capability to efficiently reducing disulfide bonds and the difference in concentration inside and outside of the cell make glutathione an attractive endogenous trigger for intracellular self-assembly.^[22] Through the cleavage of disulfide bonds, hydrophilic units of the precursor molecule can be removed inside the cell which leads to the formation of peptides capable of self-assembly. The attachment of hydrophilic motifs is essential to enable cell entry and to prevent the formation of supramolecular structures outside the cell (Figure 1.2 b).^[23]

In contrast to the reducing agent glutathione, ROS perform the task of oxidizing agents within cells. They are generated during oxidative mitochondrial metabolism and as cellular response to xenobiotics, cytokines and bacterial invasion.^{[24][25]} As mitochondria produce ROS due to the electron transport chain, the surrounding environment represents an attractive subcellular target for ROS-sensitive materials to create supramolecular architectures inside cells.^[26,27] For example, thioketal groups can be degraded in the presence of sufficient amounts of ROS.^[28] In combination with a mitochondria-targeting group as part of the chemical design of an assembly precursor, ROS-responsive materials can be efficiently transported to the oxidative environment of the mitochondria. The principle of the triggered self-assembly after degradation of the thioketal is analogous to the assembly formation caused by the cleavage of a disulfide bond whereby hydrophilic units can be removed (Figure 1.2 b). Another type of an endogenous stimulus that has been frequently exploited for intracellular self-assembly is the biocatalytic transformation of precursor molecules by specific enzymes. A multitude of different enzymes can be found within the cellular environment fulfilling various functions within the cell at their respective subcellular locations.^[2] By using enzyme-specific recognition motifs within the precursor design, a targeted bio-responsiveness towards a certain enzyme can be implemented. The concept of triggering the formation of

intracellular superstructures via enzymatic conversion has largely been based on the removal of hydrophilic groups to generate self-assembling monomers (Figure 1.2 b).

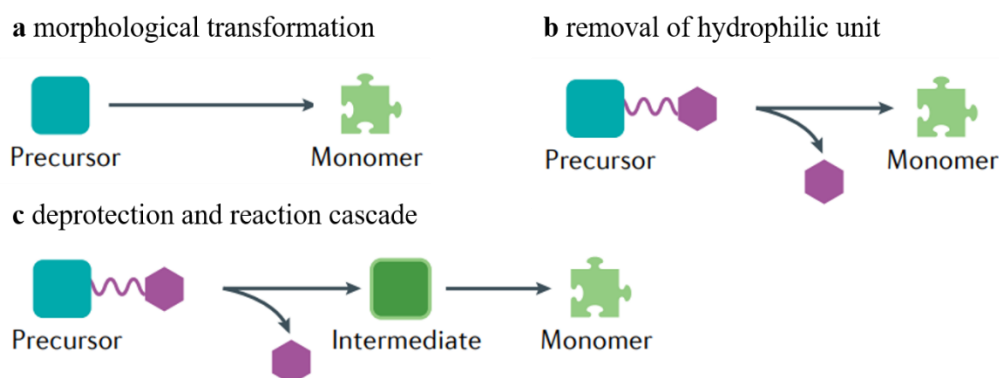


Figure 1.2: Possible chemical transformations of precursors induced by different intracellular stimuli which lead to the generation of self-assembling monomers.^[17]

However, for enhancing the spatiotemporal control over the transformation of a precursor into a self-assembling monomer, having more than one conversion step, can be advantageous. Starting with the stimulus-induced generation of a reactive intermediate, this approach combines several transformation steps (Figure 1.2 c). Since the intermediate can only be converted into the final self-assembling monomer given the appropriate chemical reaction conditions, this allows a more sophisticated design of the reaction sequence within the cell, potentially including more than one intracellular stimulus for self-assembly.^[29]

1.1.3 Nanomaterials for Intracellular Self-Assembly

For intracellular self-assembly of synthetic materials, several criteria regarding biocompatibility and environmental responsiveness must be fulfilled. For instance, the precursor molecule should be able to enter the cell without immediately causing cell death or disrupting cellular functions. To pass the phospholipid bilayer of the cell membrane, cell-penetrating peptides,^[27] containing positively charged moieties can be used which has been shown to be an efficient strategy. Furthermore, self-assembly must take place within crowded and complex environments and the self-assembling monomer needs a critical aggregation concentration which is sufficiently low for physiological conditions.^[30] A general overview of four material classes which are commonly used for intracellular self-assembly, including their type of supramolecular structures, is given in Figure 1.3. These materials include peptides, polyaromatic compounds, polymers and metal nanoparticles.

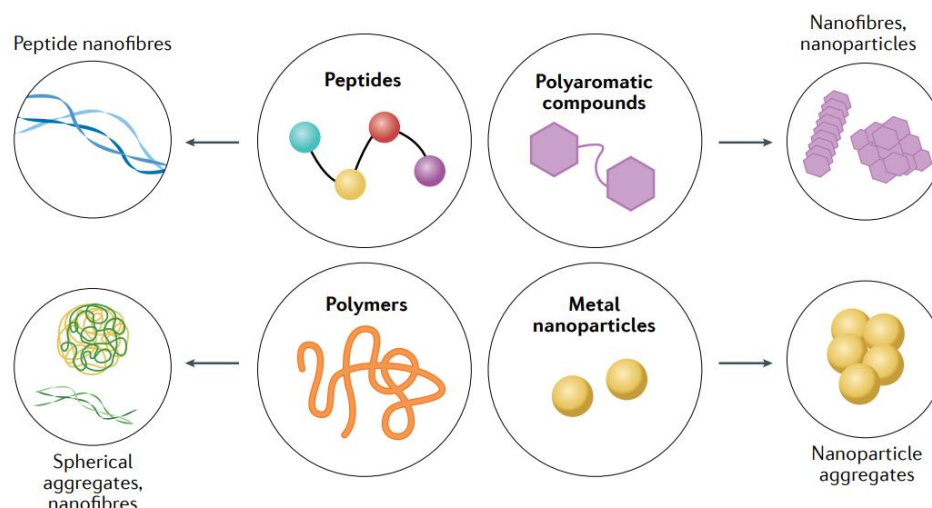


Figure 1.3: Material classes for intracellular self-assembly and their supramolecular structures.^[17]

Because of the relevance of peptides within this work, the following chapter 1.2 describes their properties, structures and possibilities for synthesis.

1.2 Peptides and Proteins

Proteins represent biological macromolecules which have the largest proportion in the cell in terms of quantity and have crucial functions in almost all biological processes. The building blocks of proteins are amino acids which form directed chains connected by peptide or rather amide bonds. The number of amino acids determines the nomenclature: structures with more than 100 amino acids are referred to as proteins, whereas those with fewer amino acids are called peptides. Amino acids are chiral and can either display a L- or D-configuration. In general, there are 20 proteinogenic amino acids which can be found in proteins. They have different side chains that differ in size, shape, charge, hydrogen bonding ability, hydrophobic character and chemical reactivity. This particular set of amino acids exhibits diverse structural and chemical properties which cover a wide range of functions that are crucial to protein function.^[31,32]

1.2.1 Hierarchy of Protein Structures

The biological function of peptides and proteins results from their 3D structure, whereby a distinction is made between four structural levels of increasing complexity. The amino acid sequence in a peptide is called the primary structure and determines its properties due to the different side chain residues. When forming a peptide bond, the α -carboxyl group of one amino acid will be linked with the α -amino group of another, releasing a water molecule. At first glance, the backbone of a peptide sequence contains only single bonds whereby a free

rotation of all three bonds is expected, but the peptide bond has the character of a partial double bond at which all four bonds are in one plane. This structural motif characterizes the properties of the peptides, such as hydrolytic stability, and can be described by two mesomere boundary structures where the electrons oscillate between the nitrogen and oxygen atom (Figure 1.4).^[31,32]

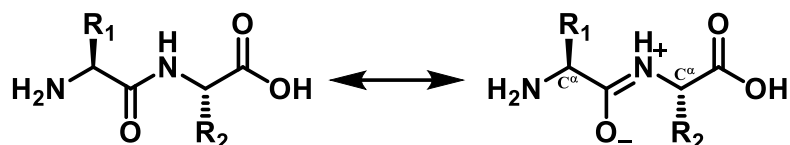


Figure 1.4: Mesomeric structures of the peptide bond to show its partial double bond character.

The double bond character of the peptide bond allows two configurations of the atoms around the bond, in detail the *trans* and *cis* configuration. With the former the C^α atoms are on the same side of the bonding plane while the latter has the two C^α atoms on opposite sites (Figure 1.4). Because of steric reasons the *trans* configuration is favored with the exception of the secondary amide bond of proline. In solution, an equilibrium between *trans* and *cis* is observed. Despite the restriction in rotation of the peptide bond, the most peptides can form several conformations in solution because of the two free rotational single bonds (C^α-C and C^α-N). This allows protein folding, stabilized by interactions between amino acid side chain residues.^[31,32]

The ability of the peptide backbone to form hydrogen bonds between NH- and CO-groups leads to the occurrence of a large number of defined superstructures called as secondary structure. Arrangements that do not follow a specific pattern are referred to as *random coils*. Some conformations can be found frequently which include the α -helix and the β -pleated sheet. They were already described in 1951 by *L. Pauling* and *R. Corey*,^[33] even before the first protein structures were elucidated by X-ray crystallography.^[34] Later on, further structural elements like β -turns or Ω -loops were verified which do not have regular periodic structures but they are mostly well-defined and rigid. The α -helix, a rod-shaped, chiral element (Figure 1.5 **a**, **b**) is one of the possible structures. The backbone forms the inner part of the rod, while the side chains point outwards in a helical arrangement. The helix is stabilized by hydrogen bonds of the carbonyl oxygen and the amide proton between every fourth amino acid. *Van-der-Waals* forces also ensure stabilization due to the dense packing inside the helix. Furthermore, the stability can be enhanced by hydrogen bonds between the side chains of the amino acids. However, there are also amino acids which disturbs the stability of α -helices, in fact such with branches at the C^β atom like valine, threonine or isoleucine but also

Introduction

proline with a missing hydrogen atom at the nitrogen. In addition, the side chains of serine, aspartate or asparagine can form competing hydrogen bonds with the peptide backbone which also disturbs the α -helix. Both, right-handed and left-handed α -helices exist, behaving like image and mirror image.^[35] The right-handed α -helix is energetically more favorable because there are fewer steric hindrances between the side chains. Therefore, almost all α -helices in proteins are right-handed.^[31,32]

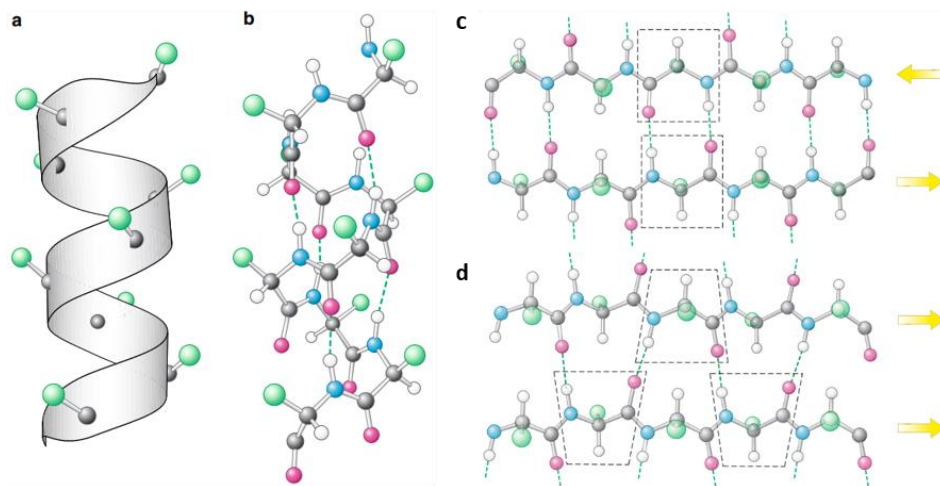


Figure 1.5: Schematic representations of the α -Helix (left) and two types of β -pleated sheets (right). **a** C α atoms (black) and side chains (green) in a helical band. **b** Illustration of the hydrogen bonds (dashed lines) between carbonyl oxygens (black, next to pink oxygen atoms) and amide protons (white). **c** Antiparallel β -pleated sheet with the β -strands running in opposite directions. **d** Parallel β -pleated sheet with the β -strands running in the same direction.^[31]

A second periodic structure discovered by *Pauling* and *Corey* is called β -pleated sheet.^[36] In contrast to the α -helix, the peptide backbone of the β -pleated sheet has an almost completely stretched conformation and the side chains of neighboring amino acids point in opposite directions. A distinction is made between the antiparallel and the parallel β -pleated sheet. In the former, the β -strands exhibit opposite directionality regarding their *N*- and *C*-terminus (Figure 1.5 c). In this arrangement, the carbonyl oxygen and the amide proton of one amino acid are hydrogen bonded to the opposite atoms of an amino acid in the adjacent β -strand. In the parallel arrangement, adjacent β -strands have the same directionality regarding their *N*- and *C*-terminus (Figure 1.5 d). Here, the carbonyl oxygen and amide proton of one amino acid are linked to the opposite atoms of two different amino acids that are two residues apart in the adjacent strand. The antiparallel β -pleated sheet is more stable compared to the parallel sheet because more hydrogen bonds for the same number of amino acids are present. In most cases, there is a mixture of parallel and antiparallel strands, so that it is called a mixed β -pleated sheet. Often amino acids like isoleucine, valine or tyrosine can be found in the

β -pleated sheet secondary structure.^[31,32]

The tertiary structure do not follow any symmetry and represents the spatial arrangement of the secondary structure elements. The spatial folding of proteins is based on physical interactions within the protein and between protein and solvent, so that a specific three-dimensional folding pattern is induced. This includes electrostatic and hydrophobic interactions such as *Van-der-Waals* forces and intramolecular hydrogen bonds. Covalent bonds between amino acids within the sequence like disulfide bonds can additionally promote the stabilization of the structure. A crucial aspect of protein folding is that the inner part of such investigated structures only contains nonpolar sidechains while the surface consists of polar such as nonpolar side chains. This phenomenon is due to the aqueous environment and the associated increase in hydrophobic interactions between non-polar side chains. The last and most complex structure level of proteins is the quaternary structure which occurs in proteins that are made up of several polypeptide chains that are able to be linked together. It is responsible for specific protein properties which means that little changes in the structure can cause significant changes in the overall protein behavior. Examples for this are the regulation of oxygen transport through hemoglobin and the control of catalytic enzyme activities.^[31,32]

1.2.2 Synthesis of Peptides

In the human body, proteins are synthesized in cells via protein biosynthesis within a few seconds.^[32] To synthetically acquire peptides, the solid-phase peptide synthesis, developed by *R. B. Merrifield*^[37] is the state-of-the-art technique, whereby a specific peptide sequence is sequentially grown upon a stationary carrier material. The advantage of the solid-phase synthesis is that the entire peptide sequence is attached to the support material and is therefore immobilized, so that the reactants used in excess can be easily separated from the product by simple washing steps.^[38] These reactants entail the individual amino acids as building blocks of the peptide, as well as peptide coupling agents, such as carbodiimides or benzotriazole compounds, that drive the formation of new amide bonds. The direction of synthesis starts from the *C*-terminus of the peptide and grows further via *N*-terminal attachment of the next amino acid. To prevent unwanted side reactions, an appropriate use of protecting groups is crucial for solid-phase peptide synthesis. For this reason, amino acids with a *N*-terminal protecting group, typically a base-sensitive fluorenylmethoxycarbonyl (Fmoc) group, and nucleophilic side chain groups, such as the thiol group of cysteine or the amino group of lysine, are blocked as well. In the first step of the solid-phase peptide synthesis, the *C*-terminal amino acid of the desired peptide must be attached to an insoluble resin or the resin

Introduction

can be purchased commercially. This and the following steps of the solid-phase peptide synthesis can be performed on-machine by a peptide synthesizer. At the beginning, the (pre-loaded) resin must swell in a solvent to increase the diffusion of the reactants and to ensure access to the loaded areas inside the carrier material to achieve the highest possible conversion.^[37] Before the next amino acid can be attached, the protecting group at the *N*-terminus must be removed. The next building block of the peptide sequence is now attached to the free *N*-terminus of the immobilized amino acid. After the desired peptide sequence has been completely constructed, the final step is to cleave it off from the solid carrier material as well as to remove the side chain protecting groups, typically under acidic conditions.

1.2.3 Depsipeptides

Depsipeptides are a specific type of peptides which are defined as oligomers that contain other bifunctional acids (mostly hydroxy acids) next to amino acids.^[39] While amino acids form amide bonds, ester bonds result from hydroxy acids. Naturally occurring depsipeptides have been the subject of extensive research due to their promising biological activities, including anticancer, antifungal, anti-inflammatory, anticlotting or anti-atherogenic properties.^[40] In most literature, depsipeptides are described as a linear sequence with a mixture of ester and amide bonds. Herein, the ester bond results from the side chain of serine which is linked with the *C*-terminus of another amino acid. This results in a branching of the previously linear peptide chain.^[27] This type of depsipeptides were developed to facilitate the chemical synthesis and purification of long peptides circumventing aggregation phenomena. In order to subsequently achieve the desired target peptide, an *O,N*-acyl shift is necessary after deprotecting the amino group of the serine bearing the ester bond (Figure 1.6).^[41]

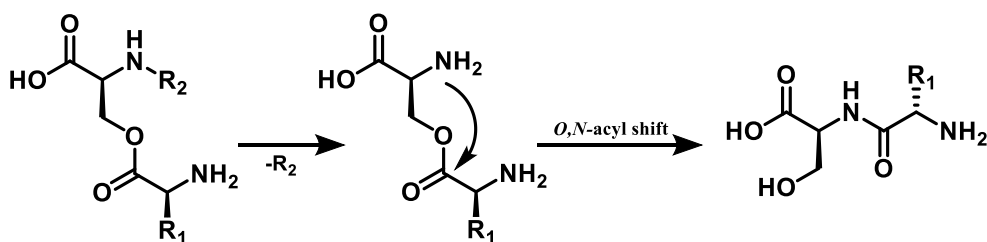


Figure 1.6: Conversion of a depsipeptide to a linear peptide through the removal of a *N*-terminal protecting group (R₂) and a subsequent *O,N*-acyl shift.

In this work, depsipeptides are used as non-assembling precursor molecules to build sophisticated artificial structures in cells. For this purpose, the *N*-terminus of the ester-bearing serine is modified with a bio-responsive protecting group that can be removed via a specific

stimulus inside the cell. This hydrophilic moiety also serves the function of enabling cell penetration and preventing premature assembly.^[27]

1.3 Furin

Enzymes are proteins that act as the catalysts of biological systems and since they can speed up reactions by decreasing the required activation energy. Besides their outstanding catalytic properties, they typically show a high specificity towards the substrate and the reaction they catalyze, such as the forming, the degradation and the remodeling of molecules which take place in the active center of the enzyme.^[31,32]

Furin is a serine endoprotease which means that it is able to hydrolyze specific amide bonds within a protein or peptide. The recognition sequence cleaved by furin contains the amino acid arginine in P₁ as well as in P₄ position (Figure 1.7, left).^[42] The optimal cleavage sequence is **Arg-X-Arg/Lys-Arg** (with **X** as any amino acid) because of the negatively-charged residues of the binding pockets in the active center of furin which results in a prioritization of amino acids with positive charged side chains like arginine or lysine.^[43]

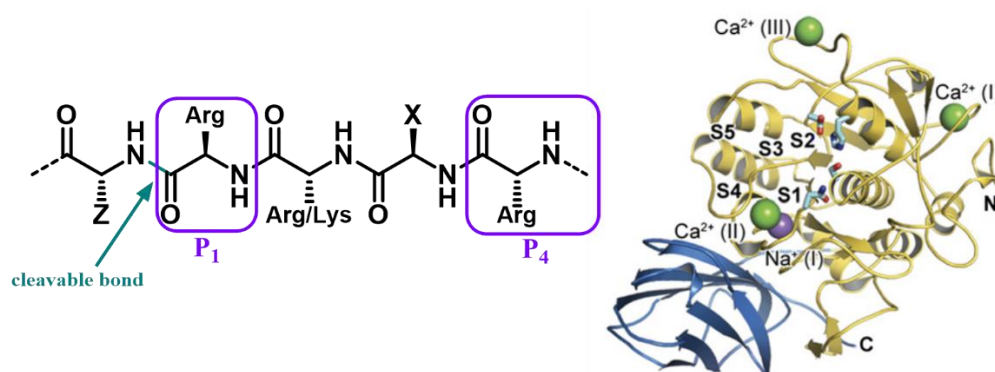


Figure 1.7: **Left:** Optimal recognition sequence of the enzyme furin. (Arg = arginine, Lys = lysine, X, Z = any amino acids). **Right:** Overall structure of human unliganded furin (catalytic domains = gold, P-domains = blue). The catalytic residues (cyan stick model), the substrate binding pockets (labeled S1–S5), and bound ions (Na⁺ (purple), Ca²⁺ (green)) are indicated.^[44]

Some conditions are necessary to reach the optimal enzyme activity for furin. This includes a pH range from 7 to 7.5 but more than 50% of the enzymatic activity remains between pH 5 and 8, depending on the cleavable substrate.^[42] In addition, furin is strictly calcium dependent and needs a concentration of at least 1 mM calcium for full activity. This results from the two calcium binding pockets contained in the enzyme and additionally it was shown that a weak bond to potassium can be formed which results in an increasing activity with the presence of 20 mM potassium.^[42,45] Within cells, furin is localized at the *trans*-Golgi network, a late Golgi structure that is responsible for sorting secretory pathway proteins to their

final destinations.^[46] Different cancer cell lines are also known to express high levels of furin making them interesting candidates for furin-related in vitro experiments. Several cell lines that were shown to exhibit furin overexpression via immunoblotting are HCT 116 cells, MDA-MB-468 cells and MDA-MB-231 cells.^[47] For the cell studies in this thesis furin overexpressing MDA-MB-231 breast cancer cells were used.

1.4 Fluorescence and Fluorophores

Fluorescence is a spontaneous emission of photons after a previous excitation with light. Because light is an electromagnetic wave, it is able to interact with electrons within molecules, promoting them into an excited state. Depending on the multiplicity of the excited state, another luminescence process besides fluorescence is possible, namely phosphorescence. The former is a spin-allowed process which results in a rapidly photon emission with a typical fluorescence lifetime of 10 ns. Phosphorescence is a transition between a triplet excited state and a singlet ground state (or vice versa) and therefore spin-forbidden which results in phosphorescence lifetimes in the range of milliseconds to seconds.^[48] To reach a triplet excited state, intersystem crossing is necessary which is an isoenergetic change between two states with different multiplicity, thereby populating a different vibrationally excited state. With a few rare exceptions, luminescence processes take place from the lowest vibrational level of S_1 (*Kasha* rule) because of the more rapidly vibrational relaxation (10^{-12} s), called internal conversion which leads to a higher priority of this process. This also occurs when the photon returned to an excited vibrational level of the ground state and causes the emission spectrum to be a mirror image of the absorption spectrum of the $S_0 \rightarrow S_1$ transition.^[49]

To illustrate such molecular processes, occur in excited states, so-called *Jablonski* diagrams can be employed (Figure 1.8).^[49]

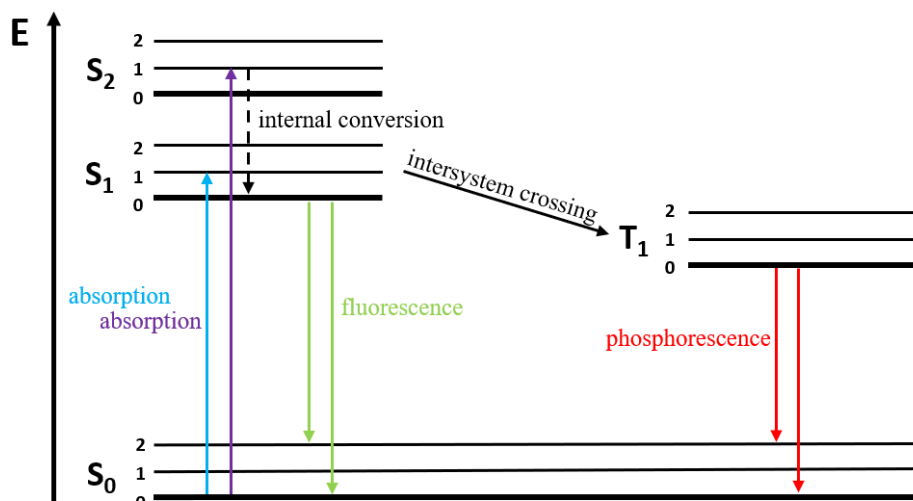


Figure 1.8: Possible depiction of a *Jablonski* diagram. S_0 , S_1 , S_2 : singlet ground/excited states; T_1 : triplet excited state; 0, 1, 2: vibrational states within an electronic energy level.

Fluorescent molecules can be made visible with confocal microscopes, especially structures within biological cells because the investigation with a traditional wide field microscope is disturbed by a high background attributed to the thickness of cells. The principle is that light from a point light source is focused on one point of the sample. Reflected light such as fluorescence photons from the radiated point are selected by a lens and focused onto a pinhole. Only light from the excitation focus can pass through the pinhole and reaches the detector which ensures a better signal-to-noise ratio. A full image can be received when fluorescence of many sample points is detected making confocal microscopy a scanning method.^[50]

1.4.1 Coumarin and Pyrene

The two fluorophores employed in this work are coumarin and pyrene, more specifically the derivatives coumarin-343 (C343) and 1-pyrenylacetic acid (Py-COOH) (Figure 1.9). Typical for fluorophores are several aromatic groups or other forms of conjugated π -systems which are responsible for the property to re-emit light after excitation. The absorbed wavelength, the energy transfer efficiency as well as the fluorescence lifetime of each fluorophore is influenced by the chemical structure and the environment such as the solvent or other molecules that can interact with the fluorophore in its excited state.^[51]

Often fluorophores are used as labels for bioactive agents like peptides, antibodies or nucleic acids and are linked to them via covalent bonds. This allows the application of analytical methods like fluorescence imaging or spectroscopy as part of biological experiments.

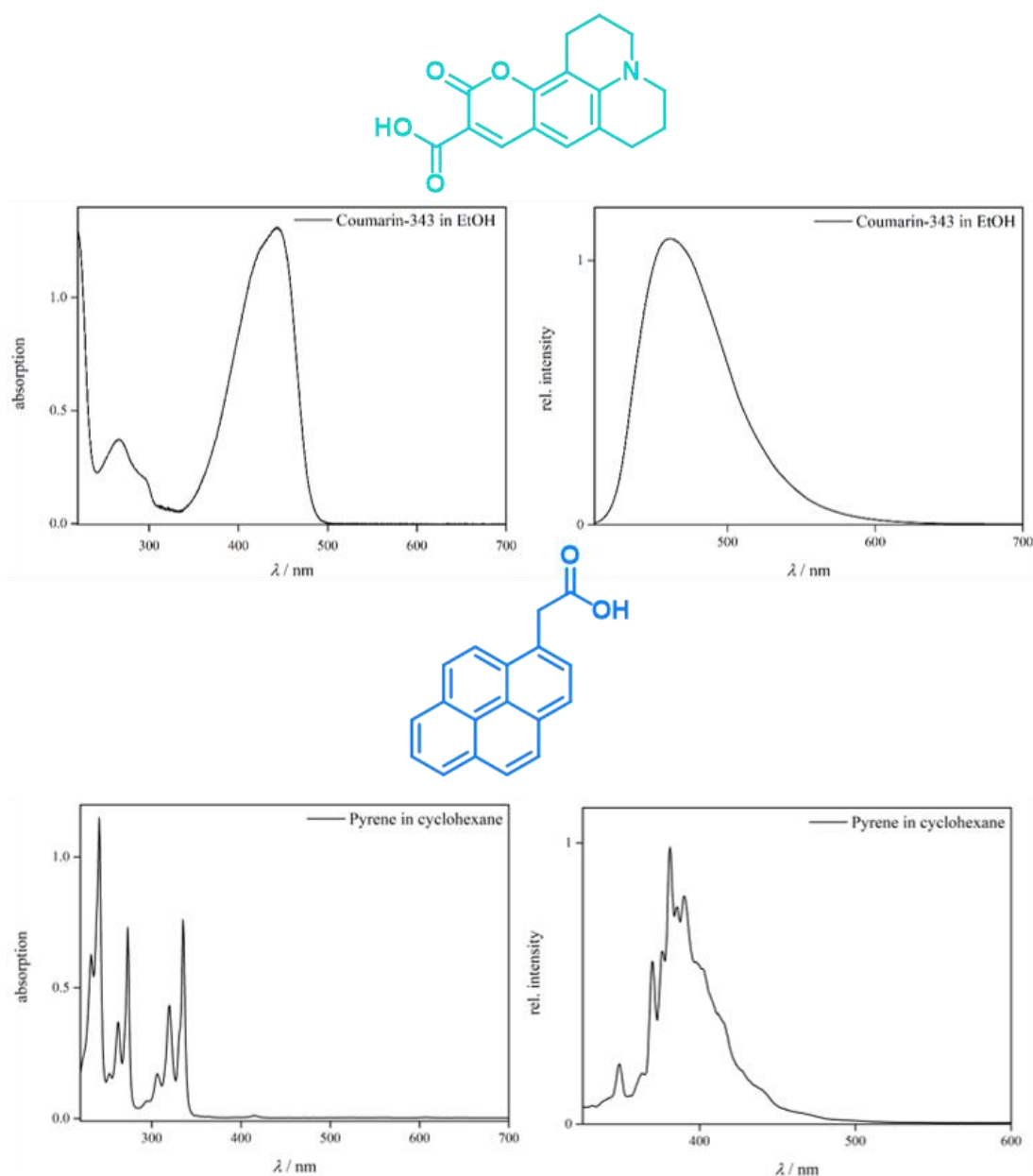


Figure 1.9: Chemical structures as well as absorption and emission spectra of the fluorophores coumarin-343 (top)^[52] and 1-pyrene acetic acid (bottom).^[53]

The absorption maximum of C343 in ethanol is situated at 443 nm^[52] while pyrene in cyclohexane shows more than one absorption maximum (335 nm, 272 nm and 241 nm) (Figure 1.9). All absorption maxima of pyrene appear in combination with another peak of lower wavelength (320 nm, 262 nm and 232 nm).^[53] The emission spectrum of C343 in ethanol shows also one maximum at 460 nm and is a mirror image of its absorption spectrum.^[52] The emission spectrum of pyrene in cyclohexane shows a broad emission band at around 380 nm with several maxima.^[53]

2 Motivation and Aim

The formation of supramolecular structures is fundamental for cellular life. Mimicking natural self-assembling structures via synthetic molecules has been a focus in research for the last few decades. One reason for this is that the in situ creation of synthetic structures inside cells circumvents the limitations of small molecule drugs regarding efflux-induced drug resistance in cancer cells.^[5] By using bio-responsive assembly precursors, intracellular triggers can be exploited to specifically control the self-assembly behavior within the dynamic cellular environment. Targeted stimuli include changes in pH^[20,54], or redox environment^[23,27] as well as various enzymes^[55] which are often characteristic for a certain subcellular location. Recently, the *Weil* group developed a system for the controlled formation of peptide nanostructures inside living cells via a multistage reaction cascade exploiting the pH changes during endocytosis and the presence of ROS inside the cell.^[27] In order to extend the toolbox of available bio-responsive systems for intracellular self-assembly it is crucial to explore various chemical and biological triggers inside the cell to advance molecular design concepts. Due to their diverse functions and cellular localizations, enzymes are generally a promising option as intracellular stimuli for in situ structure formation, as they potentially allow for subcellular specificity of the assembly generation. Especially those enzymes that have a pathological relevance (e.g. enzymes which are overexpressed in certain cancers) represent interesting targets for biomedical application.

The aim of this thesis is the development of an enzyme-responsive peptide nanomaterial for controlled intracellular self-assembly. More specifically, the objectives in this work include the synthesis, characterization and biological investigation of furin-responsive depsipeptides containing the furin-responsive cleavage motif (RVRR) (Figure 2.1). Due to the positively charged side chain groups of the arginine-rich enzyme-responsive sequence it also serves as a cell-penetrating moiety. The kinked ISA motif that is attached to the furin cleavage site is incapable of fiber formation prior to cell uptake and linearization and therefore serves as the pro-assembling unit in the precursor molecules. The aromatic group connected to the isoleucine can fulfill multiple functions: firstly, aromatic units increase the propensity for self-assembly in the aqueous cellular environment due to their π - π stacking ability. Secondly, they can contribute fluorescent properties to the molecule, thereby, enabling the investigation of intracellularly formed structures via confocal laser scanning microscopy. In this thesis different molecular design strategies are pursued regarding the aromatic head group of the peptides. A previously examined combination of both Fmoc- and coumarin-343-functionalized peptides will be used which has been shown to successfully co-assemble inside and outside

Motivation and Aim

the cell.^[27] In this co-assembly system, the Fmoc-group provides a strong tendency for self-assembly, while the fluorophore coumarin-343 contributes the fluorescence to the peptide nanostructures. Additionally, another system with pyrene as aromatic group will be synthesized and investigated, as pyrene combines the properties of strong self-assembling behavior and an emission maximum at visible wavelengths in one compound (Figure 2.1).

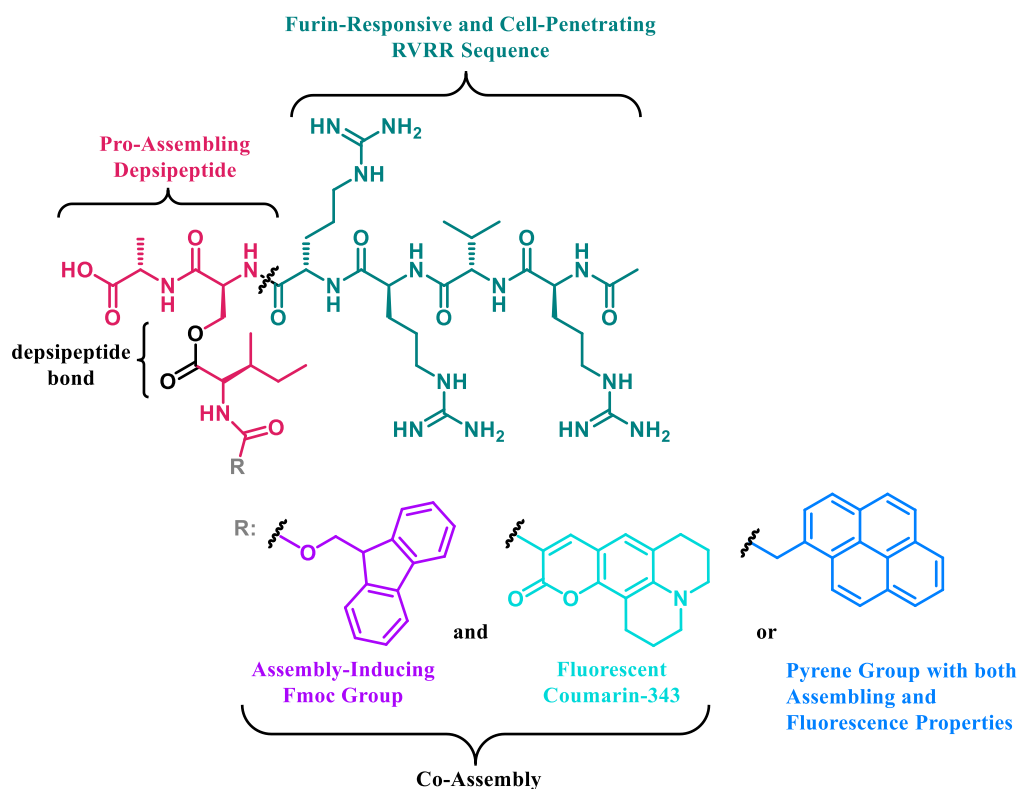


Figure 2.1: Chemical structures of furin-responsive depsipeptides with Fmoc (violet), coumarin-343 (turquoise) and pyrene (blue) as aromatic residues.

Generally, the chemical design of the herein presented furin-sensitive depsipeptides accounts for all necessary properties of nanomaterials capable of triggered structure formation inside cells: the ability to enter cells, the targeted bio-responsiveness and the self-assembling nature of the in situ formed monomers.^[17] An overview of the intracellular behavior of the furin-responsive depsipeptides is given in Figure 2.2: firstly, the depsipeptides **3** enter the cell due to the cell-penetrating properties of the oligoarginine *N*-terminal sequence; secondly, the Golgi-associated enzyme furin cleaves the R_VR_RR motif, thereby, deprotecting the amino group of the serine. Consequently, the free amino group of the depsipeptide **3.2** can perform a nucleophilic attack on the adjacent ester bond causing an *O,N*-acyl shift. This rearrangement reaction results in the linearization of the peptides yielding the self-assembling tripeptide monomers **5**.

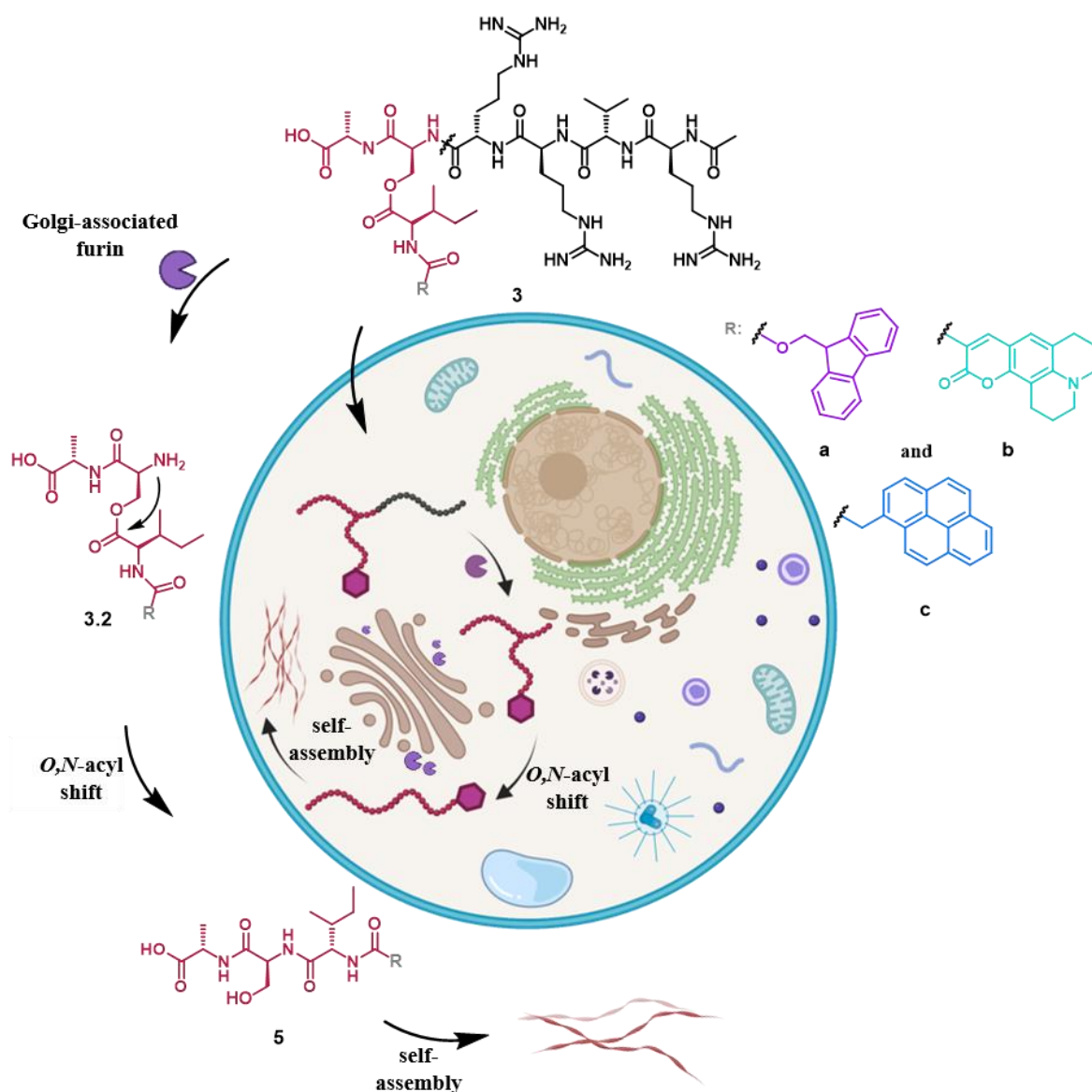


Figure 2.2: Reaction cascade to induce self-assembly inside and outside cells. Depsipeptide **3** is uptaken by the cell due to the polar arginine's (black) and subsequently cleaved by the enzyme furin resulting in peptide **3.2**. The subsequent *O,N*-acyl shift linearizes the peptide, enabling it to self-assemble and generate supramolecular networks.

To study the individual reaction steps outside the cell, commercial furin will be used to perform a kinetic analysis of the enzyme-induced transformation. For this reason, the cleavage and subsequent linearization of the depsipeptides in the presence of furin will be analyzed via analytical high performance liquid chromatography studies (HPLC). In addition, the linear peptides **5** will be synthesized in order to investigate their self-assembly behavior using various analytical methods. For instance, temperature-dependent nuclear magnetic resonance (NMR) measurements will provide information about the π - π -stacking behavior of the aromatic fluorophores, while circular dichroisms (CD) studies will be performed at different temperatures, to obtain more information about the stability of the self-assembled structures.

Motivation and Aim

In order to get an insight into the morphology of the peptide nanostructures, they will be visualized using transmission electron microscopy (TEM). This method will also be used to determine the critical fibrillation concentration, which is an important parameter for intracellular self-assembly. Furthermore, the optical properties of coumarin-343 and pyrene-modified peptides will be investigated using UV/VIS spectroscopy, looking into the effects of self-assembly on the spectra.

Finally, cell uptake studies will be carried out in collaboration with *Sarah Chagri* to examine the intracellular accumulation, transformation and assembly of the furin-responsive depsipeptides via confocal laser scanning microscopy. In addition, the cytotoxicity of the enzyme-responsive depsipeptides will be studied using a cell viability assay allowing the determination of the half maximal inhibitory concentration (IC_{50}).

The experiments presented in this thesis were carried out under the supervision of *Sarah Chagri* and the synthetic procedures were partly based on her work. Therefore, the following results will be included in her dissertation.

3 Results and Discussion

The following chapter describes the synthesis and characterization of the peptides used in this thesis. The depsipeptides **3/6** were synthesized by solid-phase peptide synthesis (SPPS) followed by the attachment of a *N*-terminally modified isoleucine **1** (Ile/I) at the unprotected serine side chain. For the linear peptide **5c**, pyrene acetic acid was coupled to the free *N*-terminus after the linear tripeptide ISA was synthesized via SPPS (Figure 3.1). The other linear peptides Fmoc-ISA **5a** and C343-ISA **5b** were previously synthesized by other people or purchased commercially.

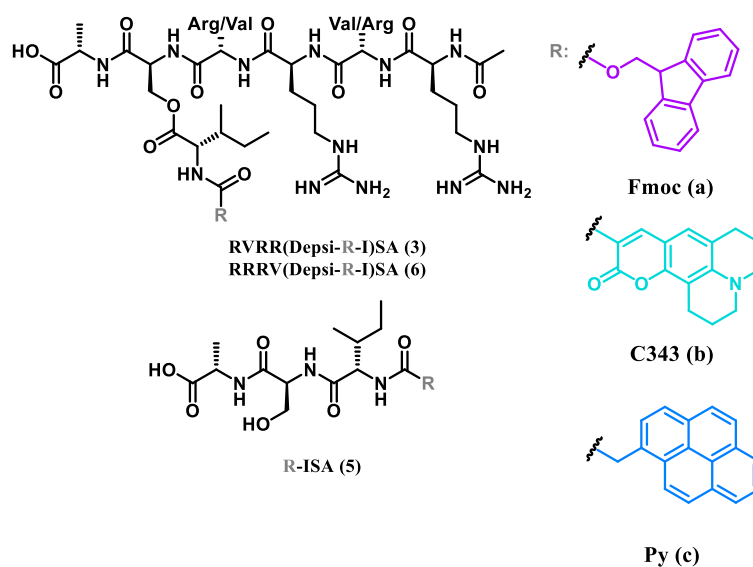


Figure 3.1: Chemical structures of the depsipeptides **3/6** and the linear peptide sequences **5**.

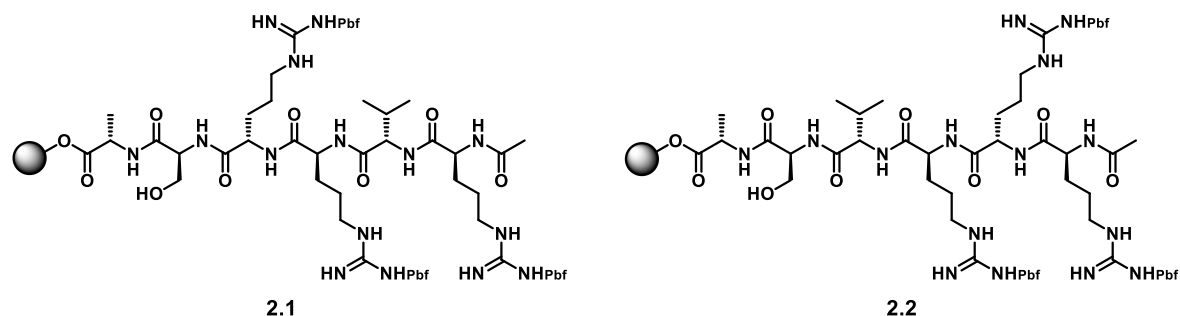
Furthermore, the enzymatic conversion and subsequent linearization of the depsipeptides **3/6** in the presence of furin was investigated using high performance liquid chromatography (HPLC) studies. In addition, a detailed analysis of the peptide nanofibers, formed by the self-assembling linear peptides **5** was performed via transmission electron microscopy (TEM), circular dichroism (CD) and nuclear magnetic resonance (NMR) spectroscopy. Lastly, the depsipeptides **3/6** were used for cell uptake and cell viability studies to investigate the intracellular structure formation and the cytotoxicity of the peptide nanomaterials.

3.1 Synthesis and Characterization of Peptides

For this thesis, six different depsipeptides **3/6** were synthesized, as for each furin-sensitive depsipeptide a non-cleavable peptide with a scrambled version of the cleavage motif was required as a control compound. Therefore, two peptide sequences **2.1** and **2.2** were synthesized via SPPS: the furin cleavable sequence (**RVRRSA**) and the non-cleavable control

Results and Discussion

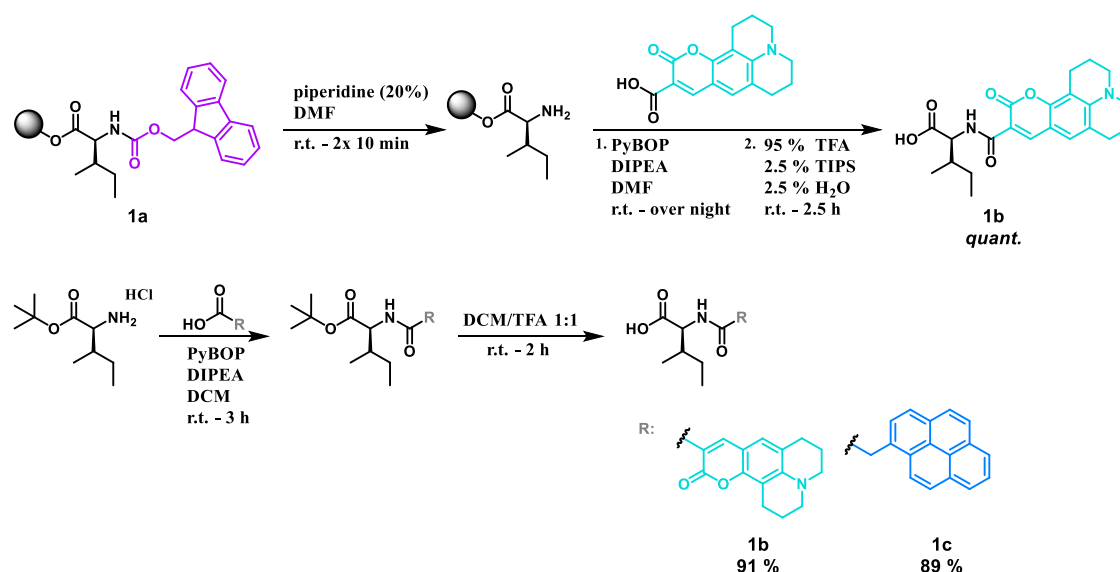
sequence (**RRRVSA**) (Scheme 3.1). In the following, the sequence cleavable by furin is called “active sequence” **2.1** whilst the other one is named “scrambled sequence” **2.2**.



Scheme 3.1: Both synthesized peptide sequences. **Left:** active sequence **2.1** (**RVRRSA**), cleavable by furin. **Right:** scrambled sequence **2.2** (**RRRVSA**), not cleavable by furin.

The acetyl protecting group at the *N*-terminal arginine can be introduced into the peptide sequences in two ways. On the one hand, Fmoc-Arg(Pbf) can be used so that the *N*-terminus of the peptide sequence (**RVRRSA**/**RRRVSA**), synthesized via SPPS, is free after a final Fmoc deprotection step. Subsequently, the acetyl protecting group can then be introduced by an amide coupling with acetic acid. In the second and less complex method, Ac-Arg(Pbf) is used in the SPPS, so that a subsequent synthesis step is not necessary.

Using serine with an unprotected side chain, allows the synthesis of a depsipeptide while the peptide is still connected to the solid-phase. The aromatic compounds (**C343**, Py-COOH) were each coupled with isoleucine (Scheme 3.2) to generate the fluorescently labeled isoleucine derivatives **1b** and **1c** that could then be introduced to the peptide via *Steglich* esterification on the serine side chain.



Scheme 3.2: Synthesis scheme of **C343-Ile 1b** and **Py-Ile 1c** at the solid-phase and in solution.

C343-Ile **1b** was synthesized via two different methods, at the solid-phase and in solution. For the first variant, the base labile Fmoc group of isoleucine loaded *Wang* resin was removed by using piperidine (20 %) in DMF. Then the free amine was coupled with the carboxylic acid group of C343 using the peptide coupling reagent benzotriazol-1-yloxytripyrrolidinophosphonium hexafluorophosphate (PyBOP) and the base diisopropylethylamine (DIPEA). In a last step, the compound had to be removed from the solid support material by adding an acidic cleavage solution consisting of trifluoroacetic acid (TFA), triisopropylsilane (TIPS) and H₂O. After removal of the cleavage solution, the crude product was purified via flash column chromatography yielding C343-Ile (*quant.* yield).

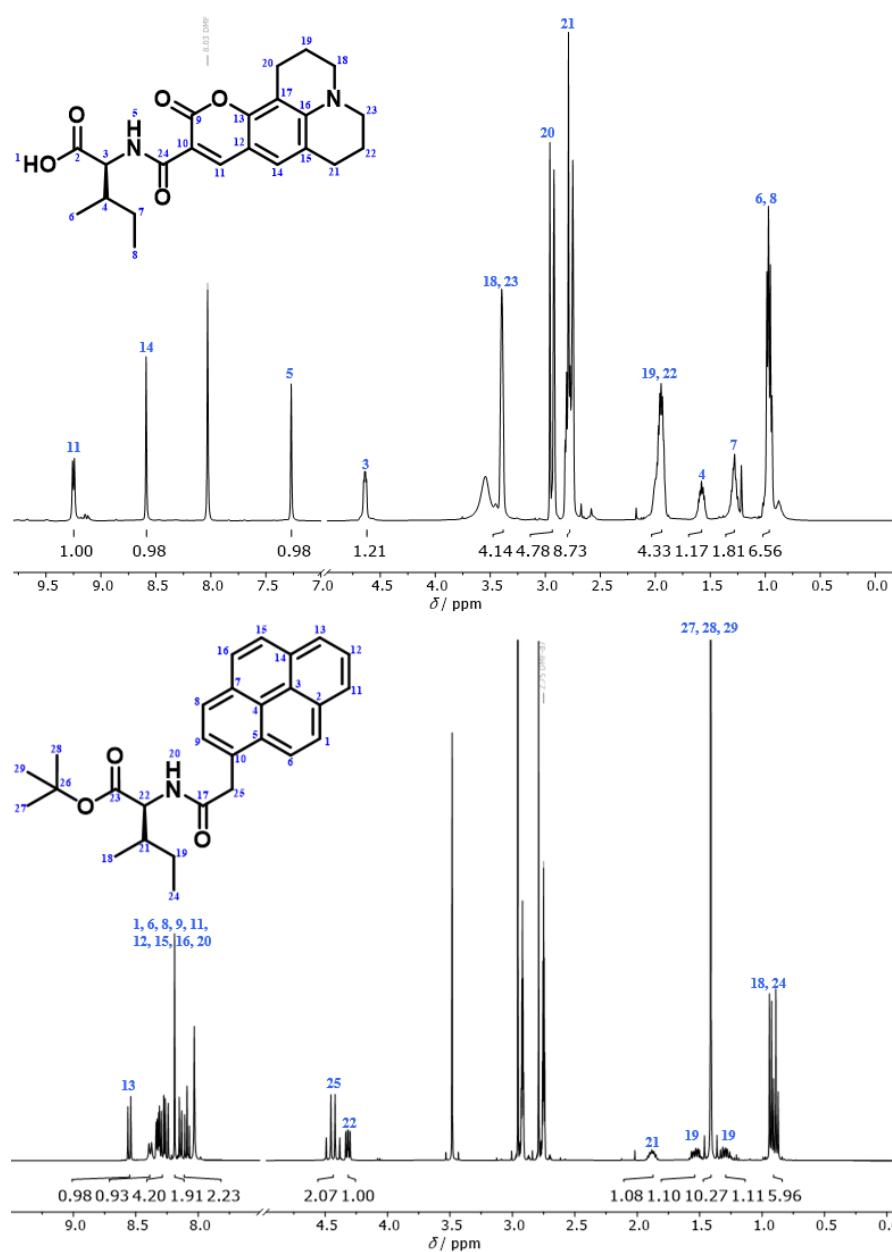
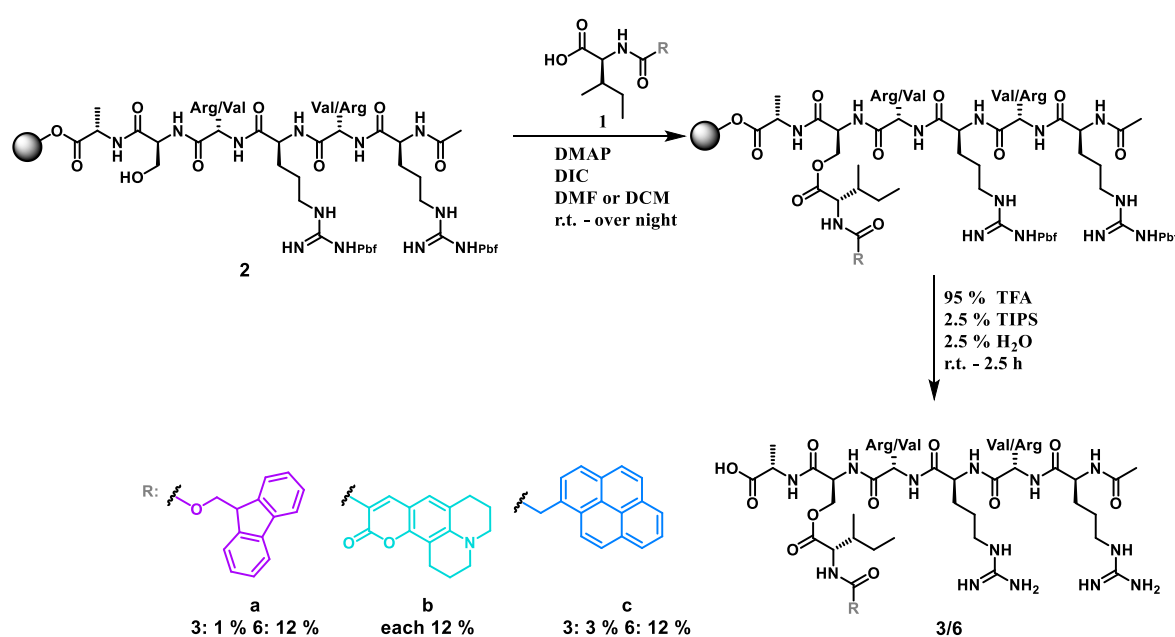


Figure 3.2: ¹H-NMR spectra of C343-Ile **1b** (top, DMF-*d*₇, 500 MHz, 298 K) and Py-Ile-¹BuO (bottom, DMF-*d*₇, 400 MHz, 298 K).

Results and Discussion

As the free carboxylic acid of C343-Ile made the purification via flash column chromatography quite difficult, the next synthesis attempts of C343-Ile **1b** and also of Py-Ile **1c** were performed in solution with an at the C-terminus ^tBu-protected isoleucine as starting material which offered the possibility to remove this protecting group after the purification step (Scheme 3.2, second row). The coupling step was performed analogous to the solid-phase synthesis with the peptide coupling reagent PyBOP and the base DIPEA. Both ^tBu-protected C343-Ile and Py-Ile were obtained in good yields (yields: C343-Ile-^tBuO: 91 %, Py-Ile-^tBuO: 89 %). The cleavage of the C-terminal ^tBu-group with TFA in dichloromethane (DCM) was a quantitative reaction and the final products **1b** and **1c** were filtered over silica gel with pure ethyl acetate to remove TFA.

To obtain the final depsipeptides **3/6**, the isoleucine derivatives Fmoc-Ile **1a**, C343-Ile **1b** and Py-Ile **1c** were reacted with the unprotected serine side chain of the linear peptide sequences **2** via *Steglich* esterification using 4-(dimethylamino)pyridine (DMAP) and DIC as reagents (Scheme 3.3).



Scheme 3.3: Synthesis scheme of the final synthesis step of the depsipeptides **3/6** and subsequent cleavage from the resin.

For the synthesis of the pyrene modified depsipeptides **3c/6c** a better conversion was observed when using DCM instead of DMF as a solvent which could be attributed to the enhanced solubility of Py-Ile **1c** in DCM. In a last step the depsipeptides **3/6** were cleaved from the solid-phase using TFA, TIPS and H₂O as described above. The peptides were precipitated in ice cold diethyl ether and purified via preparative HPLC (yields: see Scheme 3.3).

The MALDI-TOF spectra and the analytical HPLC traces show that the purification was successful and the pure products **3/6** were obtained (Figure 3.3).

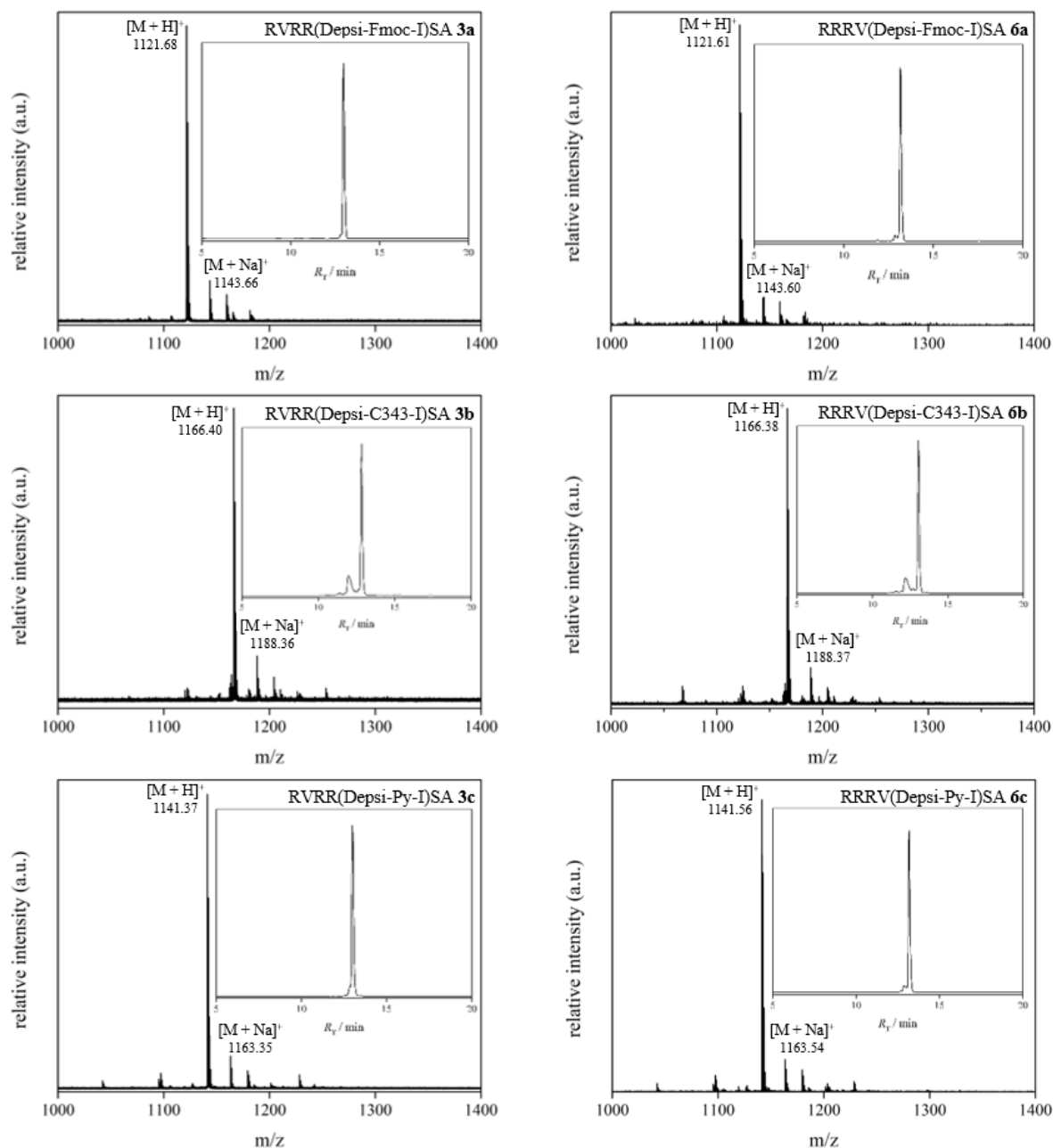
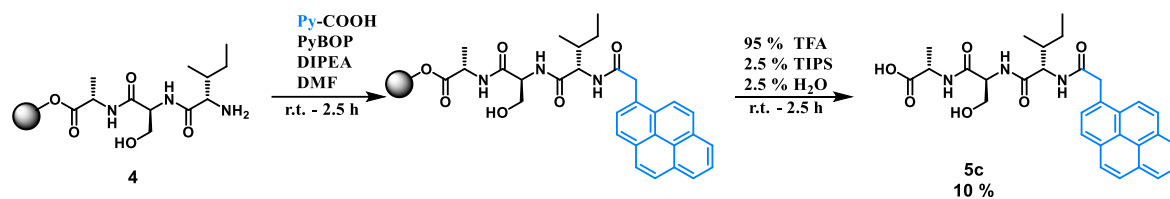


Figure 3.3: MALDI-TOF spectra and HPLC traces of the synthesized with Fmoc-, C343- and pyrene-modified depsipeptides **3** and **6**.

To investigate the self-assembly behavior outside the cell, it was necessary to synthesize the linearized peptides **5** which result from the enzyme cleavage and the subsequent *O,N*-acyl shift starting from the depsipeptides **3**. As described above Fmoc-ISA **5a** and C343-ISA **5b** were received otherwise and only Py-ISA **5c** was self-synthesized (Scheme 3.4).

Results and Discussion



Scheme 3.4: Synthesis scheme of the linear pyrene-modified peptide **5c** and subsequent cleavage from the resin.

The peptide sequence ISA **4** was synthesized via SPPS. For the attachment of Py-COOH to the *N*-terminus of ISA **4**, the coupling reagent PyBOP and the base DIPEA were used. The final linear peptide **5c** was removed from the resin by using a cleavage solution of TFA, TIPS and H₂O, then precipitated in ice cold diethyl ether and purified via preparative HPLC (yield: 10 %).

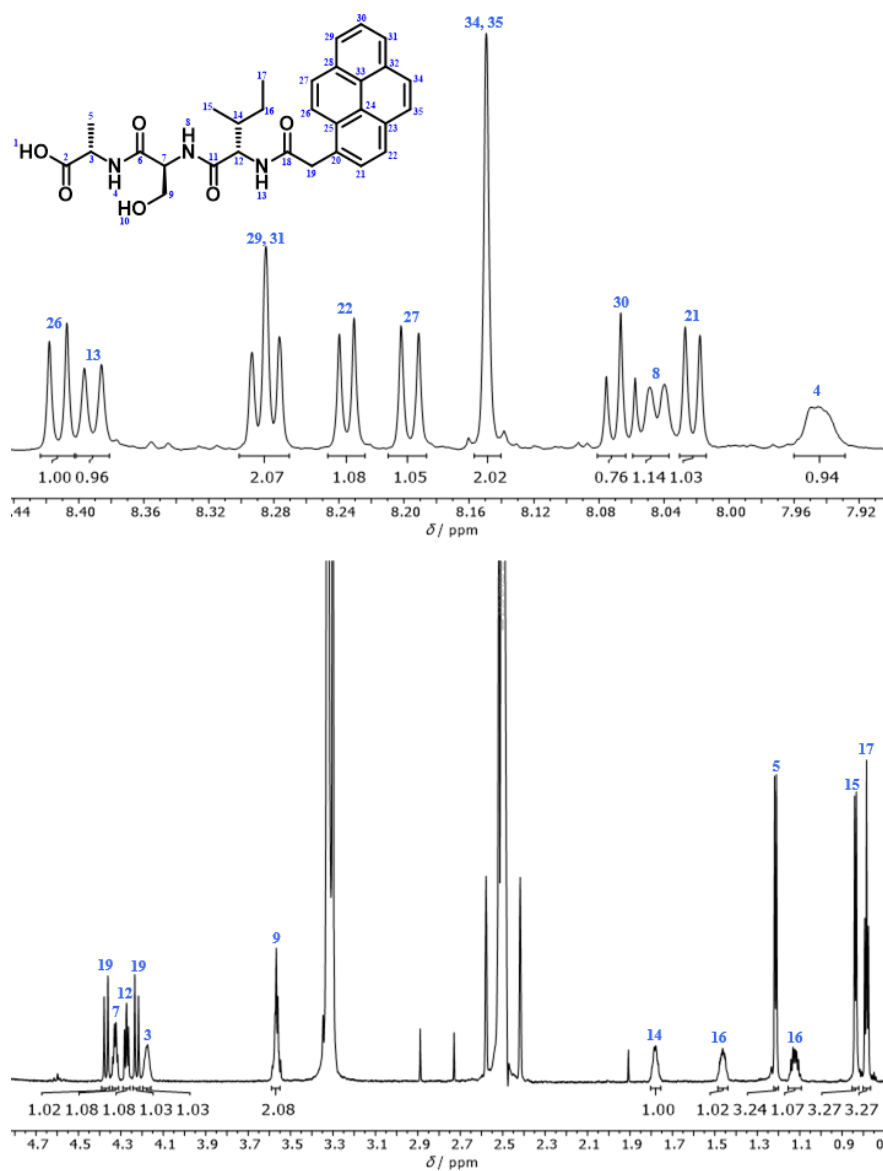
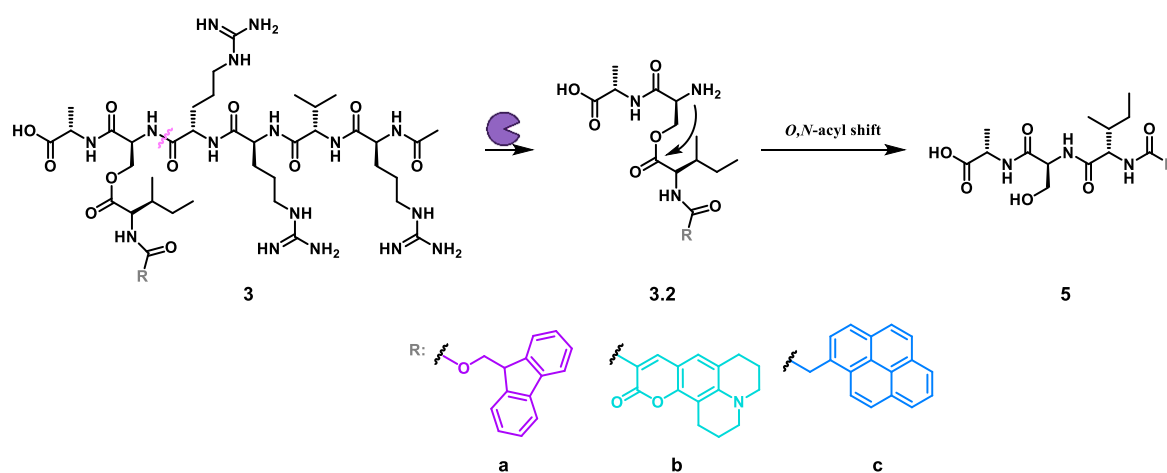


Figure 3.4: ¹H-NMR spectrum of Py-ISA **5c** (DMSO-*d*₆, 850 MHz, 298 K).

3.2 Analysis of Enzymatic Conversion

Next, the enzyme-responsiveness of the three furin-sensitive depsipeptides **3** was analyzed. The non-cleavable scrambled depsipeptides **6** served as controls. Using commercially available furin and a HPLC setup, the conversion of the depsipeptides by the protease was investigated.



Scheme 3.5: Cleavage of depsipeptides **3** by the enzyme furin at the RVRR cleavage site and a subsequent *O,N*-acyl shift to get the linearized peptides **5**.

For the analysis, the compounds were each dissolved at a concentration of 100 μM in a buffered solution (pH 7.4) prepared from 2-(4-(2-hydroxyethyl)-1-piperazinyl)-ethanesulfonic acid (HEPES) (100 mM), CaCl_2 (1 mM) and tris(2-carboxyethyl)phosphine (TCEP) (1 mM). The commercial furin (2 μg) was added to the mixture and the samples were incubated at 37 $^\circ\text{C}$. At different timepoints, samples of the mixtures were taken out and methanol was added to precipitate the enzyme and to stop the enzymatic reaction. After centrifugation of the samples, they were injected into an analytical HPLC to analyze the progression of the enzymatic cleavage and the subsequent formation of the linearized peptides **5** over time (Scheme 3.5). In Figure 3.5 the HPLC traces of the analysis of the pyrene-modified active depsipeptide **3c** and its scrambled control depsipeptide **6c** are shown.

Results and Discussion

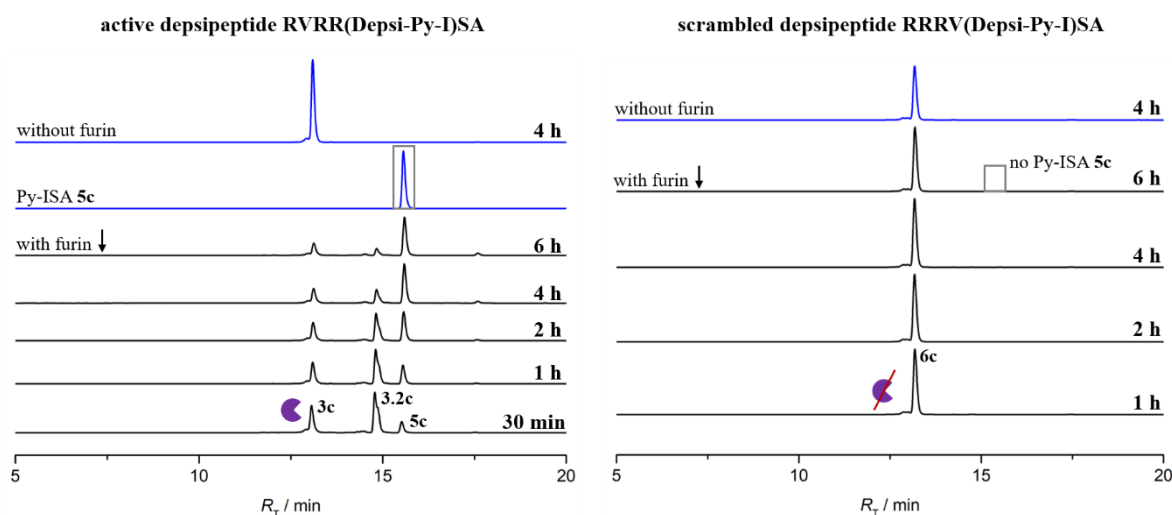


Figure 3.5: **Left:** HPLC traces of furin ($c = 25.6$ nM) induced removal of the RVRR cleavage site to get **3.2c** and linearization to **5c** and its reference spectrum (blue, second row). HPLC trace without furin (blue, first row) to show the stability of **3c** in HEPES buffer solution. **Right:** HPLC traces to show the stability of **6c** in the presence ($c = 21.4$ nM) and absence (blue) of furin in HEPES buffer solution.

The HPLC traces shown in Figure 3.5 (left) indicate a cleavage of the depsipeptide **3c** by furin as the peak of the starting material **3c** ($R_T = 13.1$ min) decreased significantly over time. After an incubation time of 30 min, two new signals **3.2c** ($R_T = 14.8$ min) and the product of the *O,N*-acyl shift, the linearized peptide **5c** ($R_T = 15.6$ min) were observed. While the peak of the cleaved depsipeptide **3.2c** also decreases over time due to the rearrangement of the free depsipeptide, the peak of the final linearized peptide **5c** increases. After 6 h of incubation with furin the conversion of the depsipeptide **3c** into the linear Py-ISA **5c** was at 64 %. For the sample without furin only one peak in the HPLC trace is visible showing the overall stability of the depsipeptide **3c** in the buffer solution.

The control experiment performed with the scrambled depsipeptide **6c** showed no conversion, as only the peak of the starting material ($R_T = 13.2$ min) was observed in the HPLC traces throughout the 6 h incubation time (Figure 3.5, right). This result showcased the stability of the depsipeptide **6c** with the non-cleavable scrambled RRRV sequence in the presence of furin making it a suitable control substance for further biological studies.

Similar experiments were performed for the Fmoc-modified depsipeptides **3a/6a** ($R_T = 12.7$ min, 13.1 min) (Figure 3.6) and the C343-modified depsipeptides **3b/6b** ($R_T = 12.8$ min, 13.0 min) (Figure 3.7). The depsipeptides **3a** and **3b** containing the RVRR motif showed a comparable susceptibility to enzymatic conversion by furin as the pyrene-modified depsipeptide **3c**: 81 % of the Fmoc-substituted depsipeptide **3a** was enzymatically converted to the linearized Fmoc-ISA **5a** ($R_T = 15.5$ min) after 6 h (89 % after 8 h)

(Figure 3.6) and 61 % of the C343-substituted depsipeptide **3b** was converted to the linearized C343-ISA **5b** ($R_T = 15.2$ min) after 6 h (Figure 3.7).

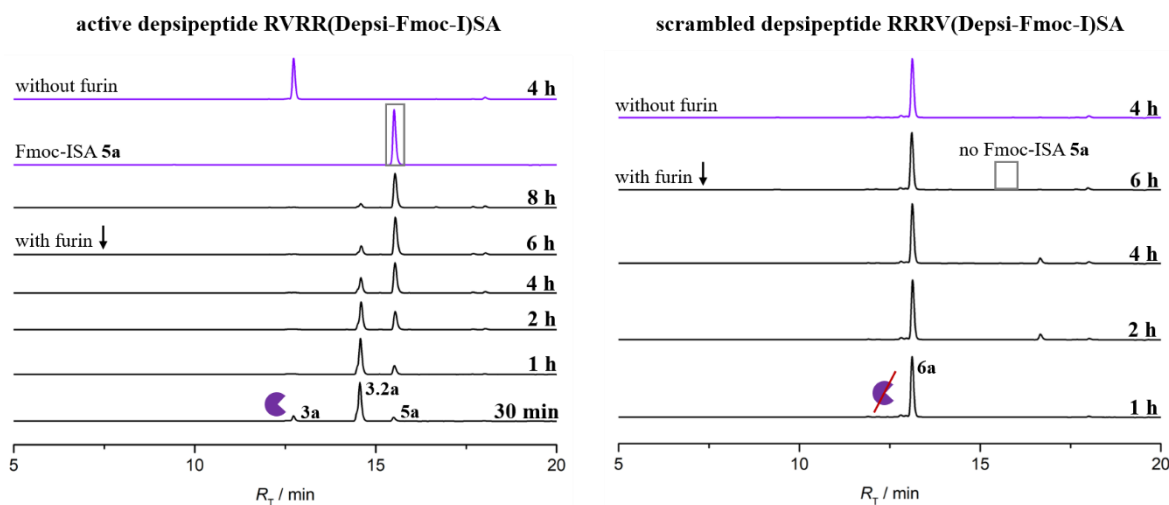


Figure 3.6: **Left:** HPLC traces of furin ($c = 14.7$ nM) induced removal of the RVRR cleavage site to get **3.2a** and linearization to **5a** and its reference spectrum (violet, second row). HPLC trace without furin to show the stability of **3a** in HEPES buffer solution (violet, first row). **Right:** HPLC traces to show the stability of **6a** in the presence ($c = 19.8$ nM) and absence (violet) of furin in HEPES buffer solution.

Based on these observations it could be concluded that the Fmoc- and C343-modified depsipeptides **3a/b** containing the RVRR motif can be cleaved in the presence of furin and can subsequently rearrange via *O,N*-acyl shift yielding the final linear peptide monomers **5a/b**. As for the control depsipeptides **6a/b** with the scrambled RRRV motif, no conversion by the enzyme was detected (Figure 3.6, Figure 3.7).

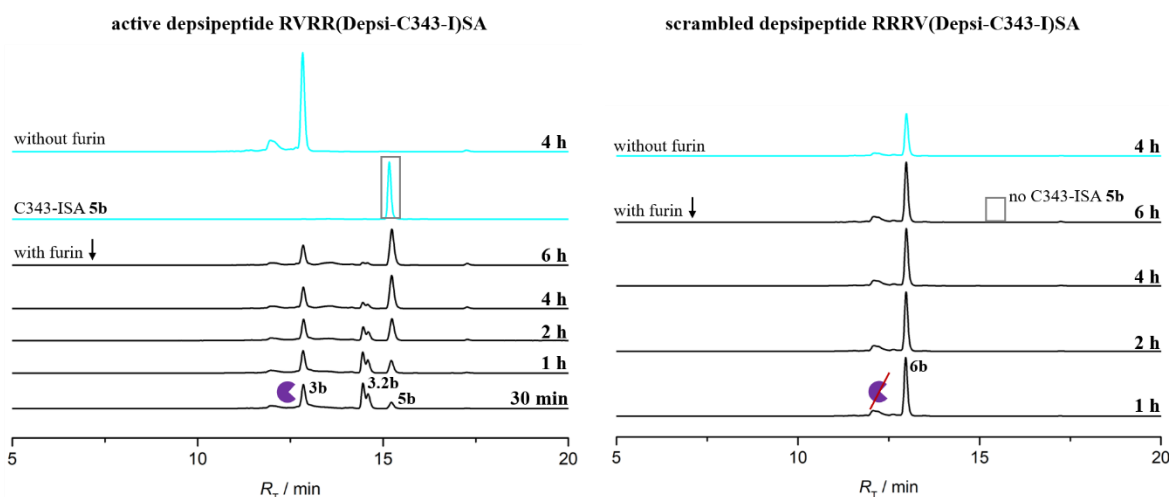


Figure 3.7: **Left:** HPLC traces of furin ($c = 15.0$ nM) induced removal of the RVRR cleavage site to get **3.2b** and linearization to **5b** and its reference spectrum (turquoise, second row). HPLC spectrum without furin to show the stability of **3b** in HEPES buffer solution (turquoise, first row). **Right:** HPLC traces to show the stability of **6b** in the presence ($c = 23.8$ nM) and absence (turquoise) of furin in HEPES buffer solution.

Results and Discussion

As a proof-of-concept experiment the HPLC study of the enzymatic conversion of depsipeptides demonstrated that furin can cleave the unnatural substrates containing the R_VR_R cleavage motif despite their branched structure and the large aromatic group bound to isoleucine. This is an important finding since enzyme-responsiveness of the depsipeptides **3** is crucial for their intracellular transformation.

3.3 Analysis of Self-Assembly Behavior

The self-assembly behavior was investigated via different methods, namely TEM, UV/VIS and CD spectroscopy as well as temperature-dependent NMR experiments. Because of the previous published work^[27] in which the linear peptide sequences Fmoc-ISA **5a** and C343-ISA **5b** were analyzed in detail, the focus in the following sections was placed on the linear Py-ISA **5c**.

3.3.1 TEM Analysis

Samples of the linear peptide **5c** with varying concentrations were prepared to determine the critical fibrillation concentration (Figure 3.8), as this parameter is important to determine the materials suitability for intracellular self-assembly.

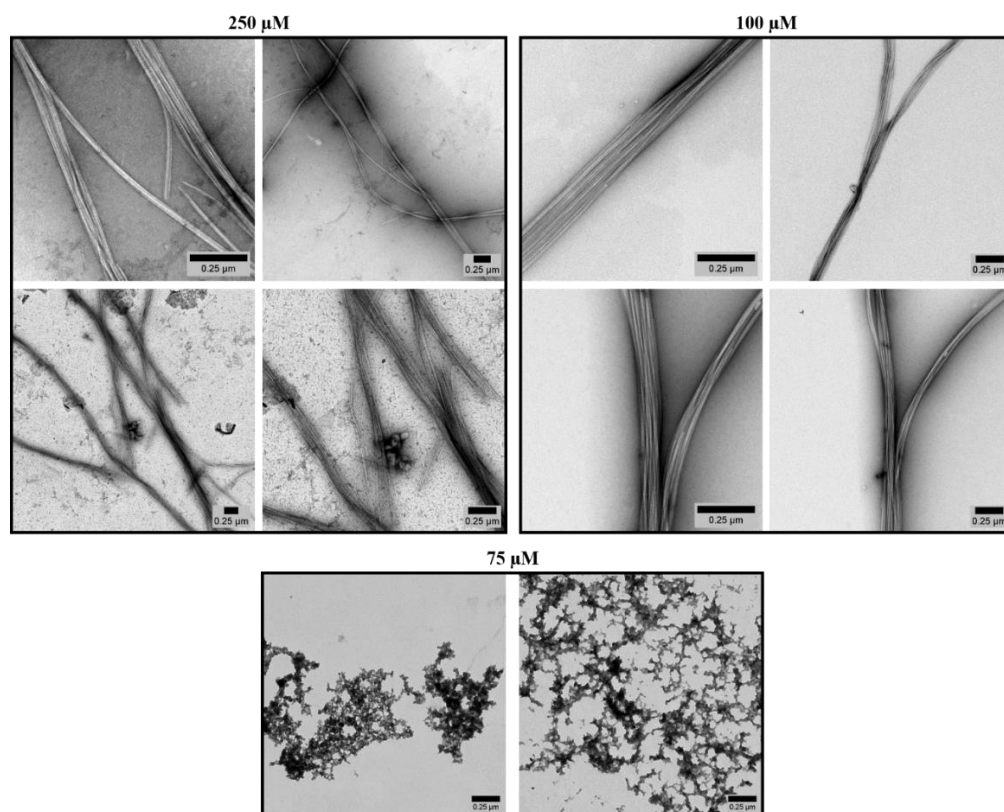


Figure 3.8: TEM images of Py-ISA **5c** at different concentrations in 9:1 PBS/DMSO (pH 7.4). Scale bars = 250 nm.

All samples were made by preparing a DMSO stock solution of the linear peptide and diluting it with phosphate-buffered saline (PBS) in a 1:9 ratio. After 24 h incubation time at room temperature, the sample solutions were applied to freshly etched Formvar/carbon coated copper grids.

The TEM images show the self-assembling capability of the linear peptide Py-ISA **5c**. At concentrations of 100 μM and higher long peptide fibers can be observed that create bundles (Figure 3.8, top), while at a concentration of 75 μM only amorphous aggregates are visible (Figure 3.8, bottom). As the single fibers are twisted into each other, this results in strands up to a thickness of approximately 150 nm. The length of the fibers cannot be determined because they extend beyond the edge of the images. In future experiments, concentrations between 75 μM and 100 μM could be investigated to determine the critical fibrillation concentration more accurately. Nevertheless, these preliminary results already suggest that the material is suited for intracellular assembly formation, as it does not require extensive amounts of peptide to form ordered structures.

To check that the depsipeptides do not self-assemble and form fibers before furin cleavage and linearization takes place, TEM studies of the pyrene-modified active depsipeptide **3c** were performed (Figure 3.9).

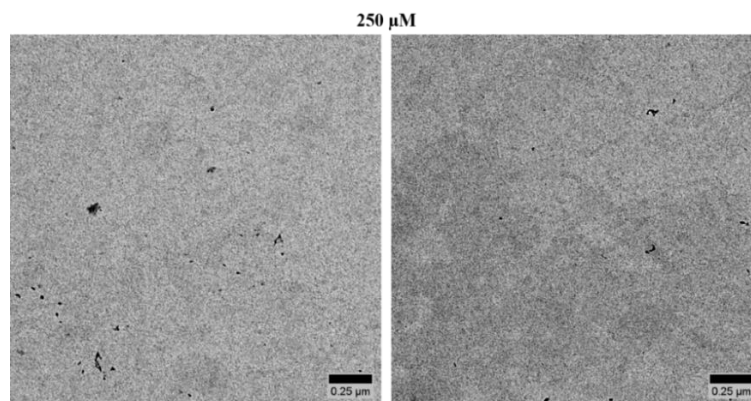


Figure 3.9: TEM images of RVR(R(Depsi-Py-I)SA **3c** at a concentration of $c = 250 \mu\text{M}$ in 9:1 PBS/DMSO (pH 7.4). Scale bars = 250 nm.

The TEM images of RVR(R(Depsi-Py-I)SA **3c** show no fibers which proves that there is no self-assembling behavior of the enzyme-responsive precursor that is comparable to the linear fibrillating Py-ISA **5c**.

3.3.2 UV/VIS Spectroscopy

Using absorbance and fluorescence measurements the optical properties of Py-ISA **5c** above and below the critical fibrillation concentration were investigated. Additionally, solvent

Results and Discussion

effects were studied by varying the ratio of DMSO and PBS in the samples. For the concentration-dependent measurements samples with concentrations of 1 mM, 100 μ M and 10 μ M of the linear peptide **5c** in PBS/DMSO 9:1 were prepared and subsequently analyzed (Figure 3.10). In addition, Py-COOH was also examined regarding its optical properties because this compound is well-known in literature^[56] and can be used as a reference compound to identify characteristic signals of the pyrene unit.

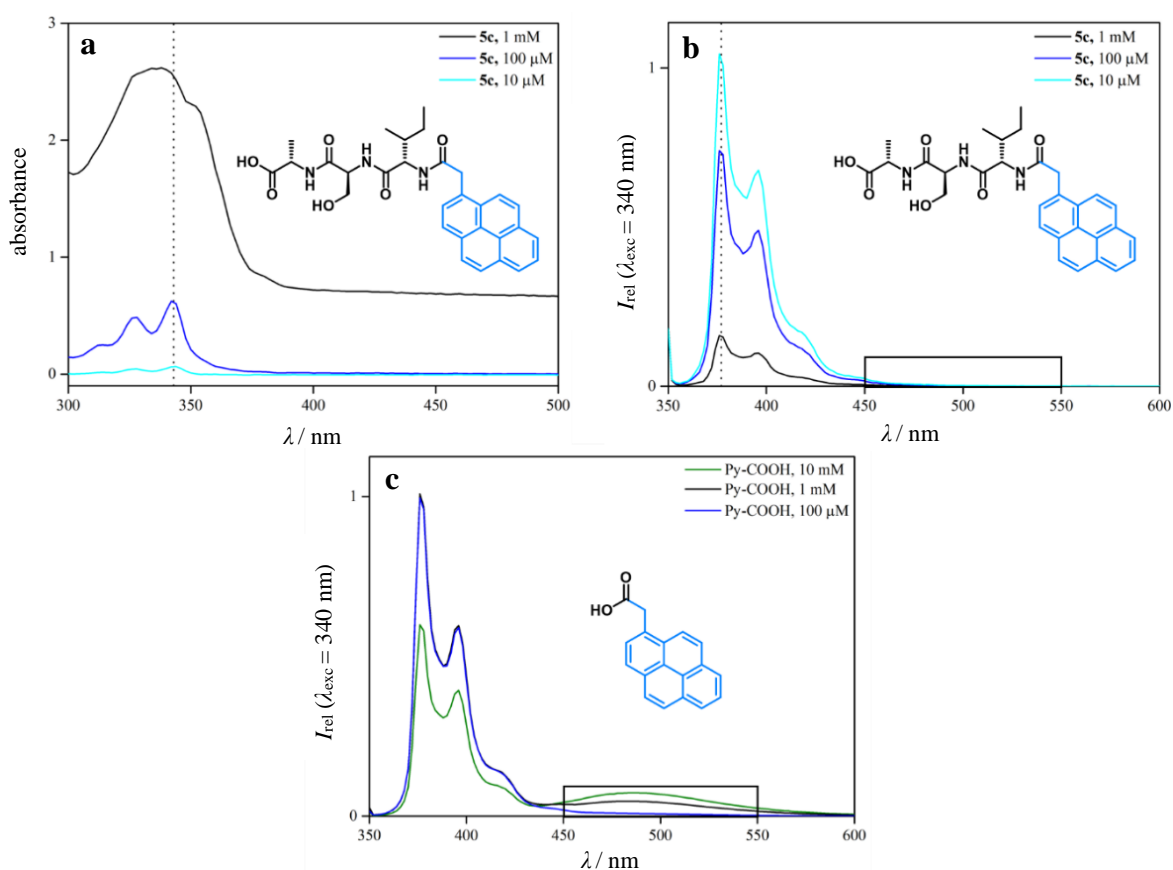


Figure 3.10: Absorption (a) and emission spectra of Py-ISA **5c** (b) and Py-COOH (c) with different concentrations in PBS/DMSO 9:1.

The optical spectra of the samples with varying concentrations of Py-ISA **5c** only differ in the intensity of the signals but they all show similar absorbance and fluorescent fingerprints. The strong increase of the absorption intensity signals when increasing the concentration of **5c** from 10 μ M to 100 μ M could result from enhanced exciton migration in the closely packed pyrene cores^[57] and indicates self-assembly of **5c** at higher concentration. This is in line with the results of the TEM studies (Figure 3.8) which showed the formation of peptide nanofibers at a concentration of 100 μ M.

The linear peptide **5c** has two high energy absorption bands with vibronic features at 343 nm and 327 nm which can be assigned to the π - π^* -transitions of the pyrene group. The spectrum of

the 1 mM sample does not have a high resolution and just one broad absorption band around 335 nm is visible which could also result from stacked pyrene groups. The emission spectra are vertically mirrored to the absorption spectra and also show two maxima at 396 nm and 377 nm after an excitation at 340 nm. Here, the sample with the highest concentration (1 mM) show the lowest fluorescence intensity signals. Normally, pyrene forms complexes with itself which can be seen in the emission spectrum of Py-COOH with a broad emission band at around 470 nm.^[49] The relative intensity of the excited-state dimer (excimer) peak is proportional to the concentration of pyrene and is slightly visible at 1 mM (Figure 3.10, bottom, black curve) and more intense at 10 mM (green curve). Py-ISA **5c** do not display this excimer peak at 470 nm. This could be due to the analyzed concentrations being too low to observe this phenomenon. Besides, it is possible that the chemical environment of the pyrene moiety, namely the peptide sequence ISA, disturbs the complex formation between the aromatic units via steric hindrance, for instance, caused by the branched isoleucine side chain.

In another experiment the effect of the solvent, more specifically the ratio of DMSO to PBS, on the optical properties of **5c** was investigated. (Figure 3.11). For this purpose, samples with a constant peptide concentration ($c = 100 \mu\text{M}$) and varying ratios of PBS/DMSO were prepared and analyzed via UV/VIS spectroscopy.

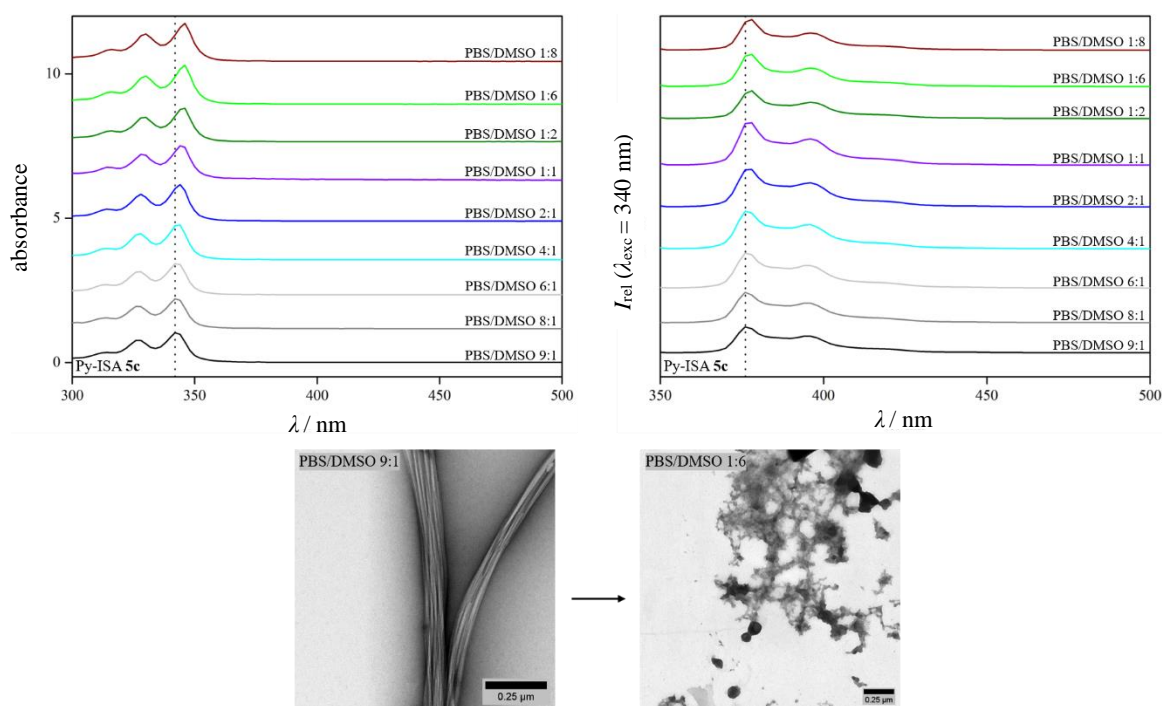


Figure 3.11: **Top:** Absorption (left) and emission (right) spectra of Py-ISA **5c** ($c = 100 \mu\text{M}$) with different ratios of PBS/DMSO. **Bottom:** TEM images of Py-ISA **5c** ($c = 100 \mu\text{M}$) with two different ratios of PBS/DMSO.

Results and Discussion

In both, the absorbance and the emission spectrum, a bathochromic shift could be observed when the PBS/DMSO ratio decreased and more DMSO was present in the sample (Figure 3.11, top). The red shift was more pronounced in the absorption spectra. This data was compared with TEM images that were taken to investigate the impact of changing the ratio of PBS/DMSO on the structure formation (Figure 3.11, bottom). At a 9:1-ratio of PBS/DMSO the TEM image shows fiber formation of Py-ISA **5c**, while at an 1:6-ratio of PBS/DMSO (86 % DMSO) only aggregates are formed. This indicates that the bathochromic shift in the optical spectroscopic measurements potentially marks the ratio of PBS/DMSO that is no longer suited for the fibrillar structure formation of Py-ISA **5c**. Nonetheless, also the effect of the solvent can play a role in the shifted spectra because in the concentration dependent measurements no shift was observed (Figure 3.10).

3.3.3 CD Spectroscopy

To further investigate the structure formation and the secondary structure of Py-ISA **5c** and to compare it to RVRR(Depsi-Py-I)SA **3c**, CD spectroscopy experiments were performed (Figure 3.12). The spectra were measured in Milli-Q water and phosphate buffer without sodium or potassium salts (PB, 10 mM).

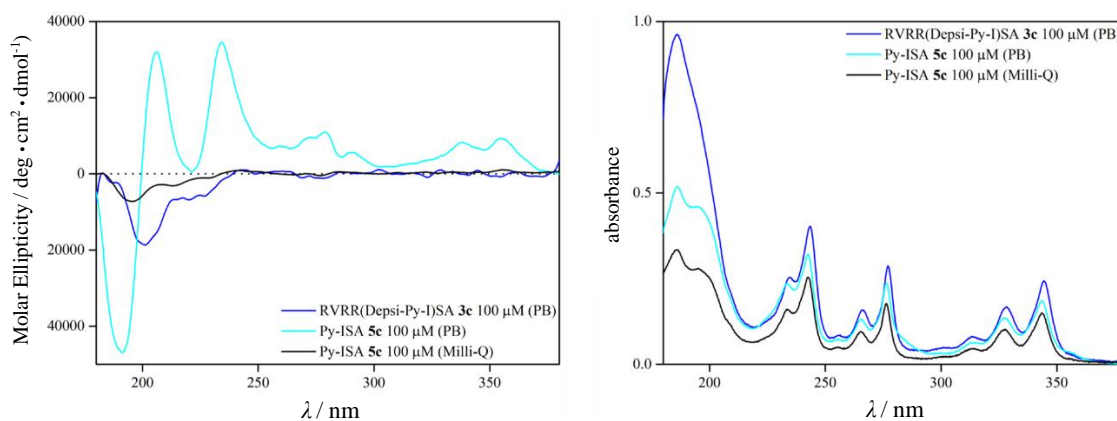


Figure 3.12: CD spectra (left) and absorption spectra (right) of Py-ISA **5c** ($c = 100 \mu\text{M}$) in phosphate buffer (PB, 10 mM) (turquoise curves) and Milli-Q (black curves) and RVRR(Depsi-Py-I)SA **3c** ($c = 100 \mu\text{M}$) in phosphate buffer (PB, 10 mM) (blue curves).

The CD spectrum of Py-ISA **5c** in PB showed a minimum at 191 nm which indicated a random coil secondary structure^[58] and corresponds to the hydrogen bond interactions of the peptide backbone (Figure 3.12, left, turquoise line).^[59,60] Two maxima were observed at 206 nm and 233 nm which can be attributed to $n-\pi^*$ transitions. In addition, a cotton effect with four positive maxima at 278 nm, 290 nm, 334 nm and 355 nm appears which can be assigned to the $\pi-\pi^*$ transitions of the aromatic pyrene groups, demonstrating the importance

of them in the self-assembly process.^[27] The cotton effect is the characteristic change in circular dichroism near an absorption band of a molecule (compare Figure 3.12, right).^[61] In contrast to the spectra of the linear peptide **5c**, the CD spectrum of the furin-responsive depeptide **3c** in PB did not show obvious CD signals above 200 nm (Figure 3.12, left, blue line). Around 200 nm a minimum was observed indicating a random coil secondary structure. Interestingly, Py-ISA **5c** in Milli-Q water did not show any signals within the hole wavelength area which could indicate that self-assembly heavily depends on the solute-solvent interactions and the ionic strength of the solvent. Additional ions might increase the polarity which results in a stronger hydrophobic effect causing more non-covalent interactions between the aromatic units.^[62]

Another CD experiment was performed to examine the stability of the Py-ISA **5c** fibers at higher temperatures. For this reason, the temperature of the sample was increased in ten-degree steps, starting at 20 °C and ending at 80 °C (Figure 3.13) and decreased in a similar fashion back to the starting temperature. The effects of the temperature of the self-assembly behavior were additionally visualized by TEM images.

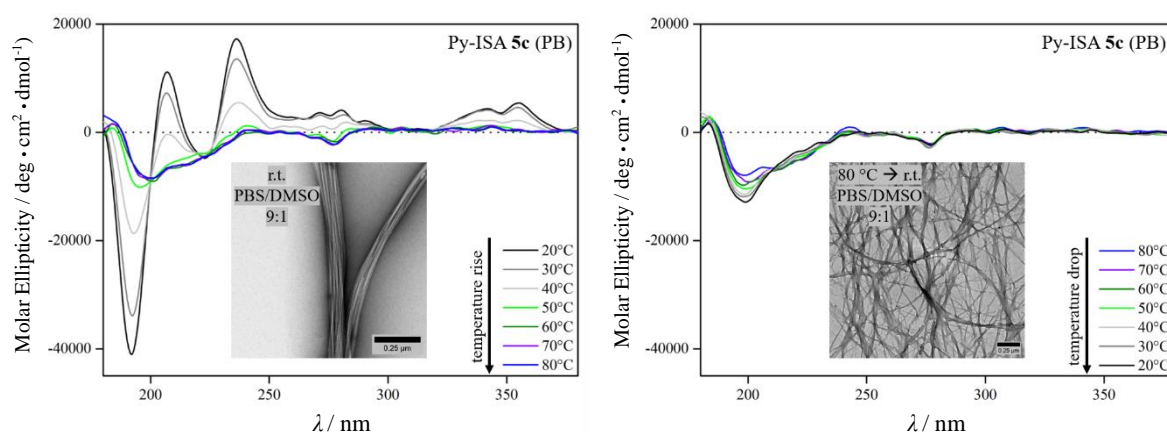


Figure 3.13: Temperature dependent CD spectra of Py-ISA **5c** ($c = 100 \mu\text{M}$) in PB and respective TEM images at room temperature (left) and 80 °C \rightarrow room temperature (right).

An increase of ten degrees caused signal intensity losses resulting in a complete vanishing of the maxima above 200 nm at 50 °C. Instead, the CD spectra measured at 50 °C or higher showed a distinct random coil structure indicating that above 50 °C the secondary structure of Py-ISA **5c** is disrupted. After cooling the sample back down to 20 °C the CD spectrum did not display similar signals as the one of the unheated sample which could hint at a loss of superstructures due to the heating and cooling cycle. To visualize potential morphological changes caused by heat, a TEM study after incubating Py-ISA **5c** for 24 h at 80 °C was performed (Figure 3.13, right). The TEM image shows a clear change in morphology, since

Results and Discussion

the sample with the linear peptide that underwent heating and cooling did not display any bundled nanofibers anymore but instead showed a network of individual thin fibers.

3.3.4 NMR Spectroscopy

The temperature-dependent self-assembly behavior of Py-ISA **5c** was further investigated on a molecular level by ^1H -NMR spectroscopy (Figure 3.14). For a better comparison with the previously performed CD experiments, the same solvent conditions were used but with deuterated solvents instead (PB/DMSO- d_6 9:1). The concentration of the peptide **5c** for the NMR experiment was at 804 μM (0.43 mg/ml) and thus higher than in the other analytical methods. However, this was necessary to acquire adequate NMR signals. In this experiment, the temperature was increased in five-degree steps from 25 $^\circ\text{C}$ to 80 $^\circ\text{C}$. After cooling down, the sample was measured again at 25 $^\circ\text{C}$ (Figure 3.14).

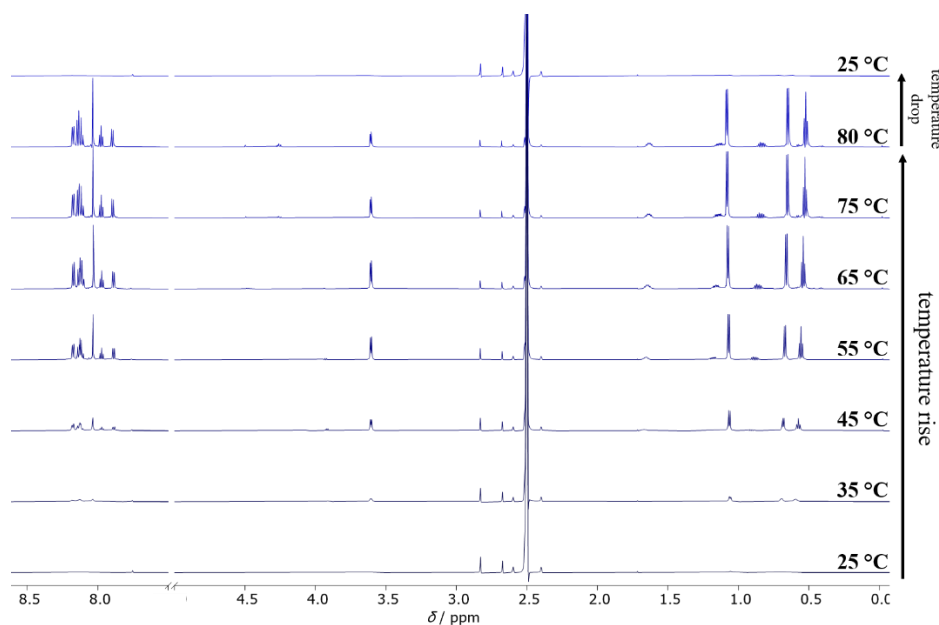


Figure 3.14: Temperature-dependent ^1H -NMR spectra of Py-ISA **5c** (0.43 mg/ml) in PB/DMSO- d_6 9:1.

At 25 $^\circ\text{C}$ no signals, in both aromatic and aliphatic region, belonging to Py-ISA **5c** were visible which indicates the self-assembly of the linear peptide. Increasing the temperature led to the appearance of signals at 35 $^\circ\text{C}$ and grew more intense up until 75 $^\circ\text{C}$. These observations suggest that the self-assembled structures disassemble at elevated temperatures and that Py-ISA **5c** is then present as a monomer. After the sample was cooled back to 25 $^\circ\text{C}$, the signals in the ^1H -NMR spectrum disappeared again suggesting that supramolecular nanostructures are formed once more. These results are in line with the data acquired from temperature-dependent CD measurements and TEM studies that indicate a change in secondary structure and morphology upon heating (Figure 3.13).

3.4 Cell Uptake Studies and Intracellular Structure Formation

To analyze the intracellular behavior and the cytotoxicity of the furin-responsive depsipeptides, various experiments were performed in collaboration with *Sarah Chagri* who carried out the culturing, treatment and analysis of the cells.

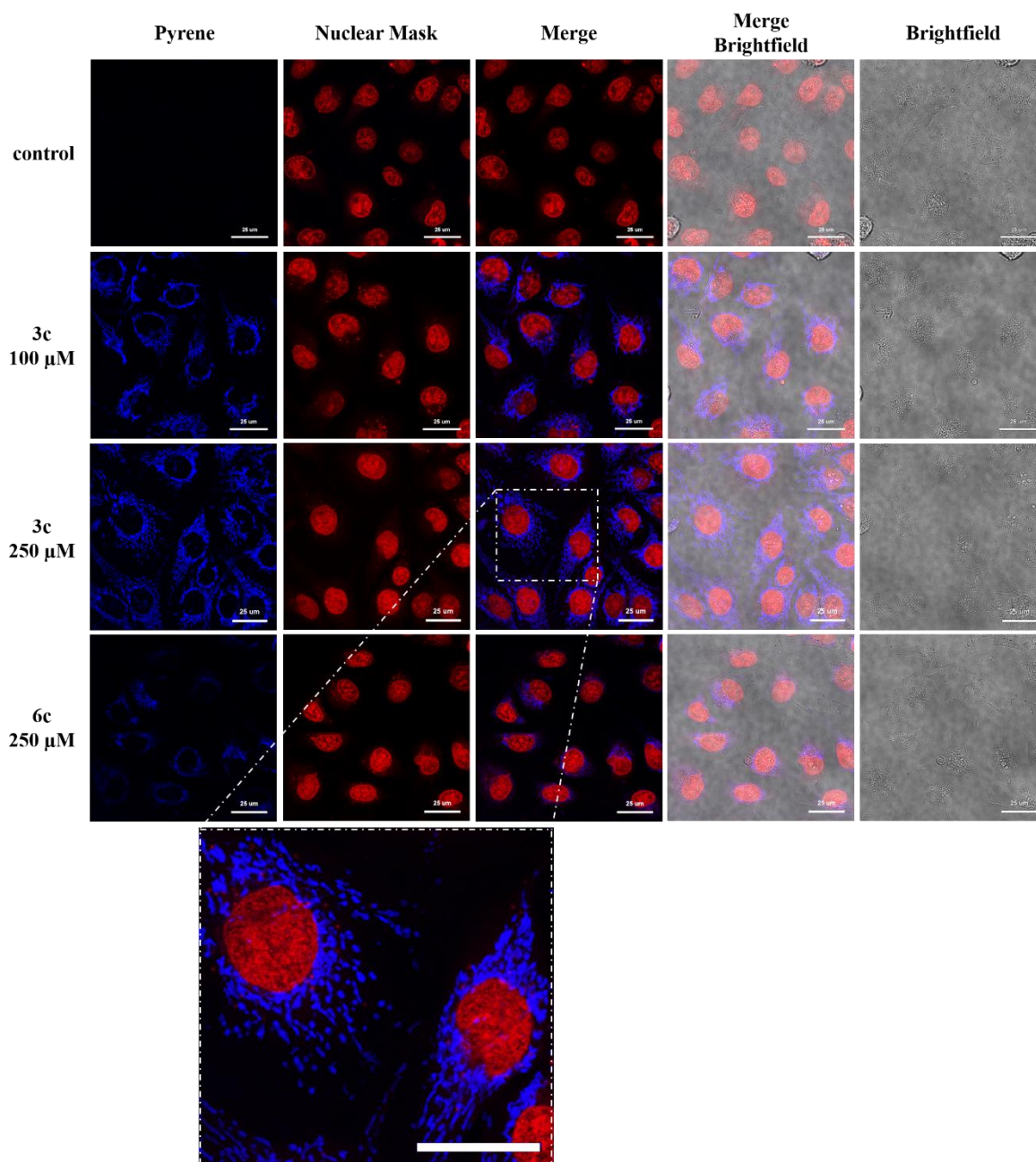


Figure 3.15: Confocal laser scanning micrographs of MDA-MB-231 cells treated for 24 h with furin-sensitive depsipeptide **3c** (2nd row, $c = 100 \mu\text{M}$, 3rd row, $c = 250 \mu\text{M}$) and non-cleavable control depsipeptide **6c** (4th row, $c = 250 \mu\text{M}$) to show cellular uptake and intracellular structure formation. Scale bars: 25 μm .

The cellular uptake of the furin-sensitive depsipeptides **3** and the subsequent intracellular structure formation of the linearized peptides **5** as a result of furin-induced cleavage was investigated. As a control substance the non-cleavable scrambled depsipeptides **6** were

Results and Discussion

employed which were expected to only show cellular uptake but no further enzymatic conversion as demonstrated via HPLC analysis in the presence of furin (chapter 3.2). For the cell experiments the breast cancer cell line MDA-MB-231 was used which has been shown to exhibit an increased furin expression.^[47] First, the pyrene-modified depsipeptides **3c**/**6c** were tested (Figure 3.15) at concentrations of 100 μ M (**3c**) and 250 μ M (**3c**/**6c**) which are necessary to surpass the critical fibrillation concentration.

The confocal microscopy images show cellular uptake of both pyrene-modified depsipeptides **3c** (RVRR motif) and **6c** (scrambled RRRV motif) but the intracellular fluorescence signal was significantly higher for the samples treated with the furin-sensitive peptide sequence **3c**. This suggests that the enzymatic conversion and subsequent intracellular structure formation and aggregation of the linearized peptide **5c** in these samples caused an accumulation of the fluorescent peptide inside the cells. In contrast to that, the non-cleavable depsipeptide **6c** would have a much lower tendency to aggregate due to electrostatic repulsion of the arginine side chains and would therefore still be able to leave the cell in a non-assembled state. This hypothesis is further supported by the lack of defined structures formed by **6c** inside cells. This lower accumulation tendency of **6c** could be the reason for its lower intracellular fluorescence signal compared to the cells treated with **3c**. This finding underlines the importance of in situ supramolecular structure formation for the retainment of synthetic material inside cells. For additional proof that the linearized Py-ISA **5c** was formed inside the cells treated with the furin-sensitive depsipeptide **3c**, the cell lysate was analyzed by analytical HPLC (Figure 3.16).

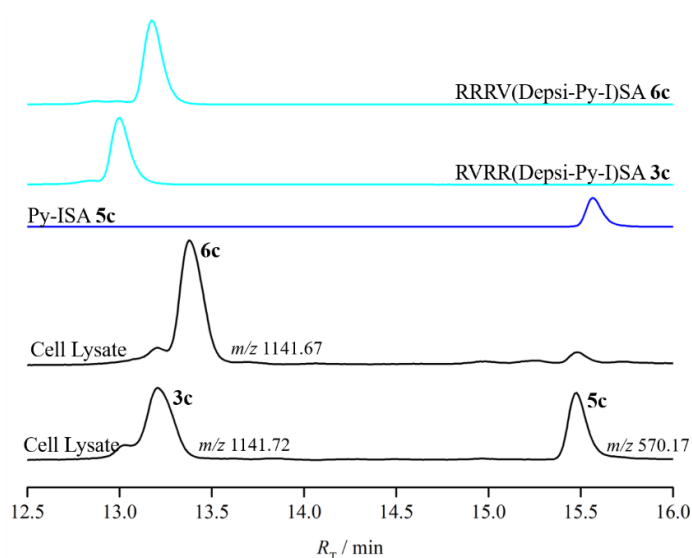


Figure 3.16: HPLC traces of reference compounds **3c**, **5c** and **6c** (turquoise and blue), and of the cell lysates of the cells treated with either cleavable depsipeptide **3c** or non-cleavable control depsipeptide **6c** (black) (detection at 340 nm).

The HPLC trace of the lysate of cells treated with the active depsipeptide **3c** shows both the peak of the starting material and of the linearized Py-ISA **5c** as confirmed via MALDI-TOF measurements (Figure 8.22, Figure 8.23, Figure 8.24, see attachment). These results indicate at least a partial conversion of the furin-sensitive depsipeptide **3c** by intracellular furin inside MDA-MB-231 cells in contrast to the control depsipeptide **6c** with the scrambled sequence that could not be removed by the enzyme.

Besides the nucleus, the Golgi apparatus was also stained in additional cell studies (Figure 3.17, yellow) to check if the pyrene fluorescence signal was concentrated near the organelle where furin is mainly located. For this reason, a commercial Golgi stain was used before doing the confocal imaging (BODIPYTM FL C₅-ceramide stain, complexed to bovine serum albumin).

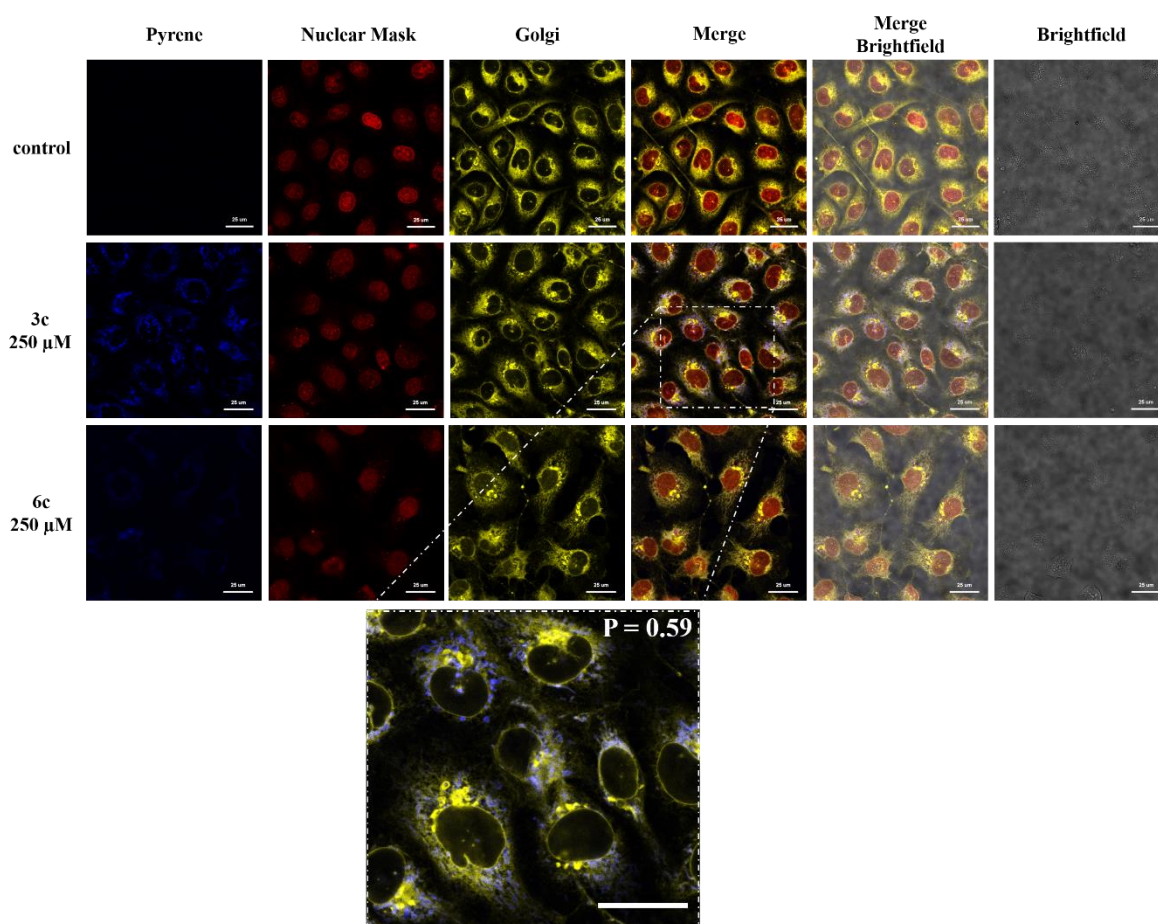


Figure 3.17: Confocal laser scanning micrographs of MDA-MB-231 cells treated for 24 h with depsipeptide **3c** (2nd row, $c = 250 \mu\text{M}$) and depsipeptide **6c** (3rd row, $c = 250 \mu\text{M}$) to show cellular uptake and intracellular structure formation. *HCS NuclearMask Deep Red* (red) and BODIPYTM FL C₅-ceramide, complexed to BSA Golgi stain (yellow). Scale bars: 25 μm .

The *Pearson's* correlation coefficient was calculated to 0.59 for depsipeptide **3c**. Compared with the literature the result does indicate just a weak Golgi affinity.^[63] For the scrambled

Results and Discussion

depsipeptide **6c** the value is less lower with 0.54 probably due to the possibility to diffuse away from the furin location and by possibly crossing the cell membrane again. In addition, the structures look more amorphous and less fiber-like as in the previous cell experiment which perhaps can result from the Golgi stain. In further experiments the concentration of the Golgi apparatus stain should be decreased for a less competitive fluorescence signal compared to pyrene luminescence. In addition, parallel it could prepare samples with just a stained nucleus in the same experiment to check if the Golgi stain disturbs the fiber formation.

MDA-MB-231 cells were also treated with the Fmoc- and C343-modified depsipeptides **3a/3b** (5:1) to investigate their cell uptake and intracellular structure formation (Figure 3.18). For this experiment, the incubation time was 14 h which was sufficient because of the higher fluorescence intensity of C343 in comparison to pyrene which facilitated the detection.

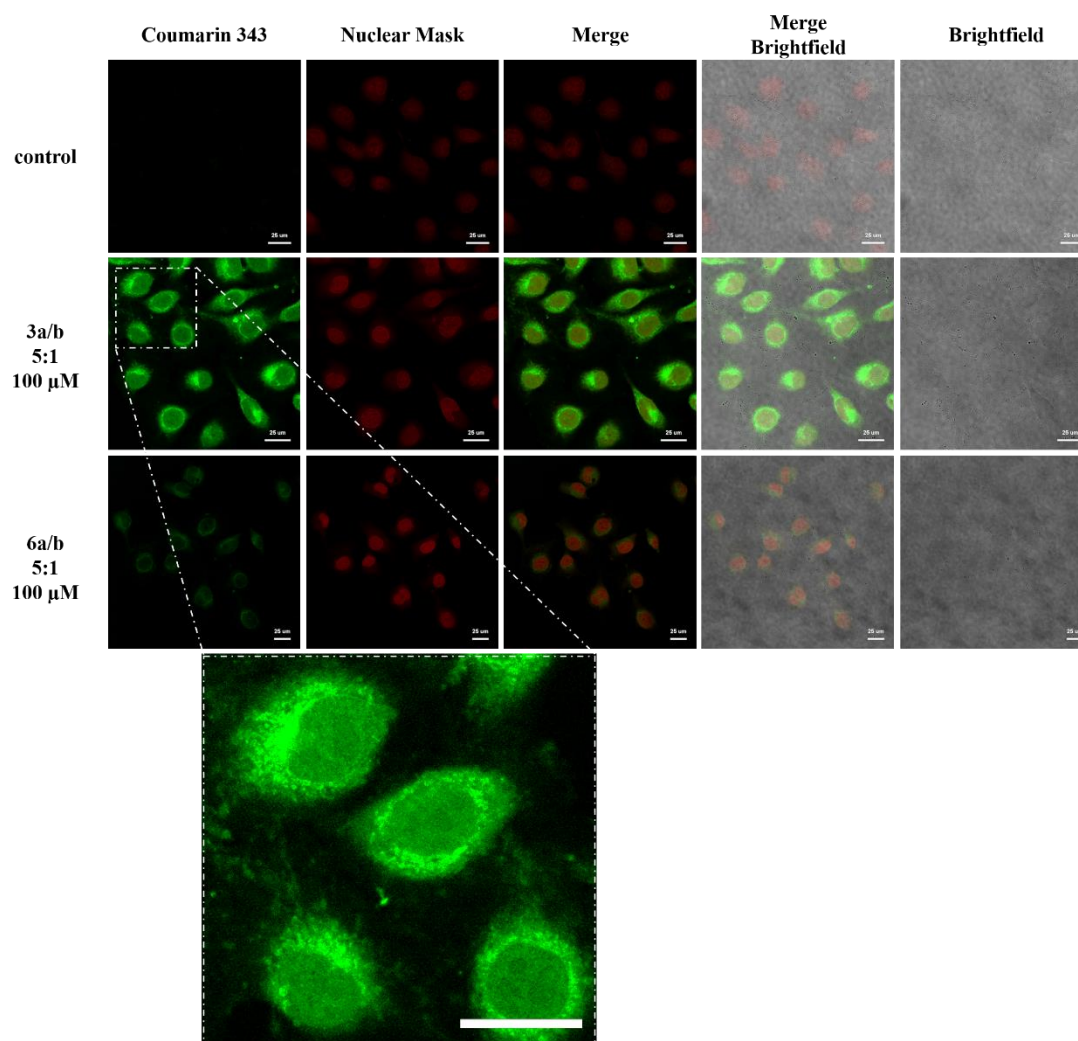


Figure 3.18: Confocal laser scanning micrographs of MDA-MB-231 cells treated for 14 h with depsipeptides **3a/3b** 5:1 (2nd row, $c = 100 \mu\text{M}$) and depsipeptide **6a/6b** 5:1 (3rd row, $c = 100 \mu\text{M}$) to show cellular uptake and intracellular structure formation. *HCS NuclearMask Deep Red* (red). Scale bars: 25 μm.

Analogous to the pyrene-modified depsipeptides **3c/6c** both the active and the scrambled peptides **3a/b** and **6a/b** show cellular uptake but with a significantly higher fluorescence signal in the cells treated with the enzyme-responsive molecules **3a/b** (Figure 3.18, middle row) which again suggests enzymatic conversion and subsequent intracellular co-assembly and accumulation of the linearized peptides **5a/b**.

3.5 Cell Viability

The cytotoxicity of the pyrene-modified depsipeptides **3c/6c** was investigated using a cell viability assay (Figure 3.19). MDA-MB-231 cells were treated for 24 h with different concentrations of the furin-responsive **3c** and the scrambled control depsipeptide **6c** and subsequently analyzed.

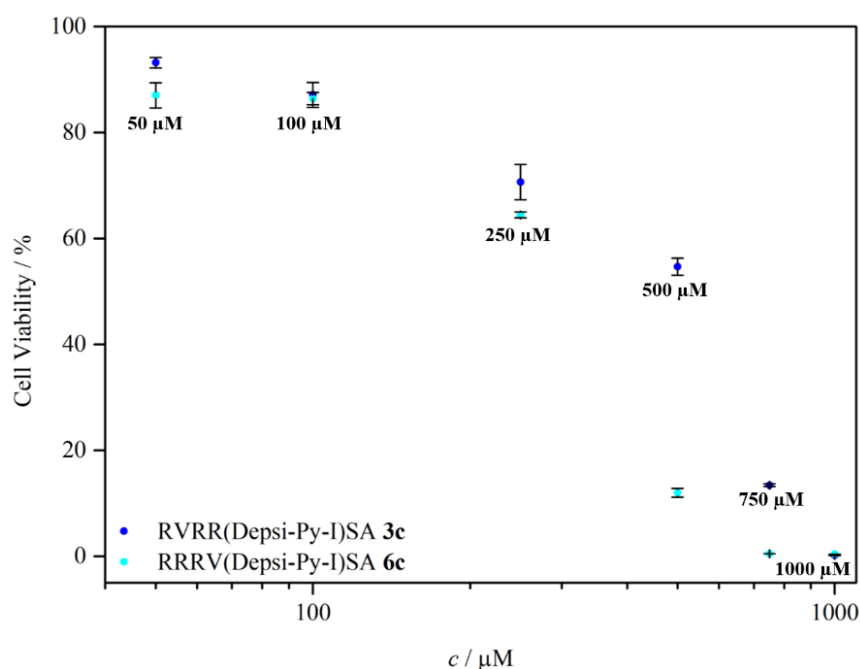


Figure 3.19: Cell viability of MDA-MB-231 cells treated for 24 h with different concentrations of depsipeptides **3c/6c**.

The cell viability after 24 h of incubation was similar for the active **3c** and scrambled depsipeptide **6c** for concentrations up to 250 μM. However, at 500 μM a strong difference in cell viability were observed between the two materials with the depsipeptide **6c** being significantly more toxic. This is an interesting observation since it suggests that the intracellular conversion of the furin-responsive depsipeptide **3c** decreases its toxicity compared to the non-cleavable control peptide **6c**. For **3c** the IC_{50} (half maximal inhibitory concentration) is 578 μM and for **6c** 322 μM. However, more measurements should be made in the future to reduce the error of the calculated IC_{50} values. Regarding the role of the intracellular

Results and Discussion

self-assembly, it is important to note that the furin-sensitive depsipeptide **3c** caused the formation of fluorescent intracellular nanostructures at a concentration of 100 μM that could be observed via confocal microscopy. However, at this sample concentration the MDA-MB-231 cells still displayed 87 % viability. While other peptide materials for intracellular self-assembly have been shown to be significantly more toxic^[27,60] making them interesting for a therapeutic application. The low cytotoxicity of the furin-responsive depsipeptide **3c** offers a new possibility to build synthetic structures inside cells without directly causing a cell death.

4 Conclusion and Outlook

In this thesis, an enzyme-responsive material was developed to achieve the controlled formation of intracellular nanostructures triggered by the protease furin. For this purpose, three different furin-responsive depsipeptides **3** were synthesized which were either Fmoc- (**3a**), C343- (**3b**) or pyrene-substituted (**3c**). As non-cleavable control compounds, the scrambled counterparts **6** were synthesized, also by using solid-phase peptide synthesis and by attaching Fmoc-, C343- or pyrene-modified isoleucine at the free hydroxy group of serine via a *Steglich* esterification. For the additional investigation of the self-assembling behavior of the linearized version of the peptides, the respective linear peptides **5** were also obtained.

Using commercial furin in buffered solution, the cleavage of the active depsipeptides **3** downstream of the R_VR_R motif and the subsequent *O,N*-acyl shift of the free depsipeptides could be shown successfully via HPLC analysis. Furthermore, the stability of the depsipeptides **6** with a non-cleavable R_RR_RV motif in the presence of the enzyme could be demonstrated as well.

Using the linear pyrene-modified peptide **5c** the self-assembling behavior was investigated with different analytical methods. This included TEM studies to visualize the morphology of the formed supramolecular structures. At concentrations from 100 μ M and higher, long twisted peptide fibers resulting in strands up to a thickness of approximately 150 nm were observed. At a concentration of 75 μ M, only amorphous aggregates could be observed. Further investigation of the peptide nanofibers, formed by the linear peptide **5c** was performed by CD spectroscopy. The signals in the recorded spectra are in line with the TEM images, indicating the formation of supramolecular structures. In addition, it could also be shown that the branched pyrene-modified depsipeptide **3c** do not form any ordered structures, which proves that there is no self-assembling behavior of the enzyme-responsive precursor that is comparable to the linear fibrillating Py-ISA **5c**. The stability of the self-assembling structures as well as the behavior of the π - π -stacking of the aromatic fluorophores was investigated via temperature-dependent CD and ¹H-NMR studies. The results showed changes in the self-assembly and π - π -stacking behavior at temperatures around 40 °C. Morphological changes of the fibrillating linear peptide **5c** caused by heat could be made visible with TEM studies where no bundled nanofibers were displayed after an incubation time at 80 °C anymore but instead showed a network of individual thin fibers. In addition, optical properties of the pyrene-modified linear peptide **5c** were investigated by UV/VIS spectroscopy. Changes in concentrations above and below the critical fibrillation concentration show differences in the signal intensity providing further hints towards self-assembly of **5c**.

Conclusion and Outlook

Finally, MDA-MB-231 cells which show an increased furin expression^[47] were each treated with depsipeptide **3c** or **6c** and analyzed using confocal laser scanning fluorescence microscopy. After an incubation time of 24 h, fiber-like structures were observed in the cells treated with the furin-responsive pyrene-modified depsipeptide **3c**. The cell lysate was subjected to HPLC analysis, which confirmed the presence of the linearized peptide **5c**. In comparison, the non-cleavable depsipeptide **6c** had a weaker fluorescence intensity signal inside cells and did not show obvious structure formation. In order to examine whether there is a localization of the fibers within the cell at the Golgi apparatus, where furin is mainly found, co-staining experiments were performed. However, experimental conditions including the concentration of the stain need to be optimized, as it has not yet been possible to make a precise statement about the localization of the fluorescent nanostructures. Lastly, the cytotoxicity of the depsipeptides **3c/6c** was investigated, showing a lower cytotoxicity of the compounds compared to other already known materials that are able to form sophisticated structures within cells.^[27,60] Interestingly, the furin-responsive depsipeptide **3c** displays a weaker toxicity than its non-cleavable control molecule **6c** (IC_{50} (**3c**) = 578 μ M, IC_{50} (**6c**) = 322 μ M).

In summary, it could be shown that the synthesized active depsipeptides **3** are suitable for intracellular self-assembly and are only activated inside the cell due to the furin-responsive cleavage site (RVRR), allowing the control of assembly formation. The comparatively low cytotoxicity also opens up the possibility of building supramolecular structures in the cell without triggering directly cell death.

A further aim of this project could be the controlled disassembly of these architectures, for example, via an intracellular click reaction with a highly polar compound on the surface of the assemblies (Figure 4.1). To realize this idea, preliminary experiments were performed as a proof of concept. First, an azido group was introduced to the free C-terminus of the linear pyrene-modified peptide **5c** to generate a self-assembling peptide monomer with a clickable group. As a hydrophilic click partner, a tetraarginine sequence was prepared and linked to dibenzocyclooctene (DBCO) at the N-terminus. After a successful click reaction, the polar tetraarginine sequence should disrupt the assemblies of the linear pyrene-modified peptide due to electrostatic repulsion of the positively charged arginine's. The strain-promoted alkyne-azide cycloaddition (SPAAC) has already been successfully performed in cells. These reactions are fully biocompatible, and they proceed at physiological conditions without the addition of any potentially toxic catalyst,^[64] such as copper which is often used for the activation of click reactions.

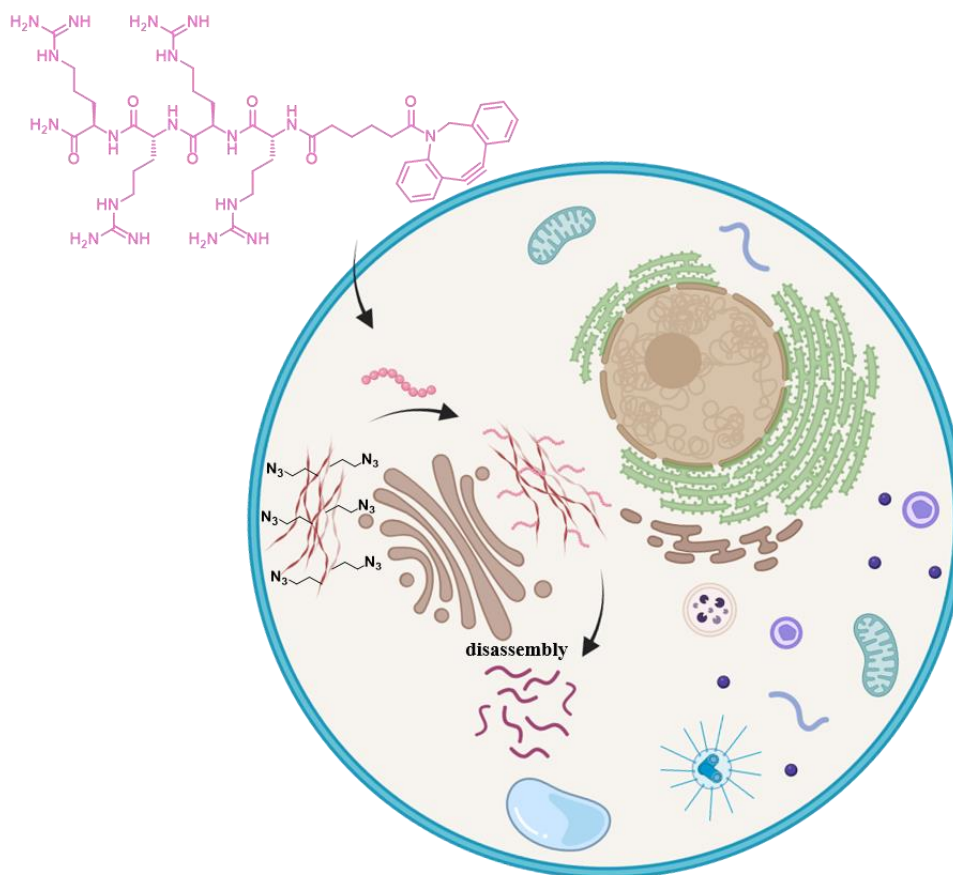


Figure 4.1: Schematic representation of click-induced disassembly of synthetic structures inside cells. The tetraarginine sequence connected with DBCO is uptaken by the cell after synthetic nanostructures were formed via enzyme-responsive transformation of an assembly precursor. The click reaction between DBCO and the C-terminal azide at the self-assembled structures changes the hydrophobicity of the peptide monomers resulting in the disassembly of the intracellular structures.

During this thesis, the click reaction was already tested outside the cell, whereby the desired product could be detected in the MALDI mass spectrum. In the future, further experiments should be carried out, for instance, TEM studies to check whether disassembly of previously formed fibers via click reaction is possible.

In general, controlling both the assembly and the disassembly of the synthetic nanomaterial inside living cells would be a milestone in this research field and would bring the community closer to the imitation of natural supramolecular systems within cellular environment.

5 Experimental Section

5.1 Instruments and Methods

The methods used for the purification, analysis and characterization of the reaction mixtures and products as well as detailed preparation procedures and other kinds of experiments are described below.

Reagents and Solvents

All reagents and solvents were purchased from commercial sources and used without further purification. For peptide synthesis special DMF with reduced amine content was used.

Thin Layer Chromatography

The analysis of compounds by means of thin layer chromatography was carried out using Alugram Sil G/UV₂₅₄ plates, by *Macherey-Nagel*. The analytes were detected by extinction of UV absorption at a wavelength of 254 nm or 365 nm.

Flash Chromatography

For the purification by column chromatography, silica gel with an average particle size of 0.04 – 0.063 mm, by *Macherey-Nagel* was used for the stationary phase. The mobile phase was freshly prepared from analytical grade solvents.

Nuclear Magnetic Resonance Spectroscopy (NMR)

NMR-spectra were recorded on an Avance III 400 (400 MHz) or an Avance III 850 (850 MHz) spectrometer by *Bruker* in deuterated solvents. The chemical shifts δ (in ppm) refer to the proton signal of the deuterated solvent relative to the tetramethyl silane standard (= 0.00 ppm). For further analysis of the fibrillating peptides a temperature dependent NMR analysis with an Avance III 700 (700 MHz) spectrometer was performed. The peptide Py-ISA **5c** (0.43 mg/mL) was dissolved in DMSO-*d*₆ and diluted with aqueous (D₂O) 50 mM phosphate buffer (1:9). The temperature was increased in 5 °C steps from 25 °C to 80 °C. After cooling down, another spectrum at 25 °C was recorded. The *MestReNova 10.0.2* software by *MESTRELAB RESEARCH* was used to analyze the spectra.

Solid Phase Microwave Peptide Synthesizer (SPPS)

All peptides were synthesized by using a Liberty Blue Automated Microwave Peptide Synthesizer by *CEM Corporation*. The resin was swollen for at least 1 h in special DMF with

reduced amine content before the synthesis. All amino acids were dissolved in DMF at a concentration of 0.2 M. As activator DIC (0.5 M in DMF) was used and Oxyma[®] as activator base (1 M in DMF). Further information of the individual methods are described below for each peptide separately.

High Performance Liquid Chromatography (HPLC)

All peptides were purified via preparative HPLC by *Shimadzu* equipped with a Kinetex 5 μm EVO C18 100 Å LC column (size: 150 \times 30.0 mm) with a flowrate of 25 mL/min. Further purification steps and analytical measurements were performed via semi-preparative or rather analytical HPLC equipped with an Agilent Eclipse XDB-C18 5 μm column (size: 9.4 \times 250 mm) with a flowrate of 4 mL/min.

For both HPLC instruments the mobile phase consisting of ACN and Milli-Q water, each acidified with 0.1 % TFA were prepared freshly. The absorbance was recorded at 214 nm, 254 nm, 340 nm (for pyrene-modified peptides) and 437 nm (for C343-modified peptides) according to the photophysical properties of the compound. Further information on the method used is described below for each peptide separately.

Liquid Chromatography - Mass Spectrometry (LC-MS)

For compound analysis a LC-MS 2020 by *Shimadzu* equipped with a Kinetex 2.6 μm EVO C18 100 Å column (size: 50 \times 2.1 mm) was used. For the mobile phase ACN and Milli-Q water were utilized, each acidified with 0.1 % formic acid. All measurements were started with 5 % ACN while it was linearly increased to 95 % in 12 minutes. The samples were dissolved in ACN, MeOH and/or Milli-Q water.

Matrix-Assisted Laser Desorption/Ionization – Time of Flight Mass Spectrometry (MALDI-TOF)

For further characterization of the peptides, MALDI-TOF spectra were recorded on a rapiflex MALDI-TOF/TOF by *Bruker*. The samples were solved in ACN, MeOH and/or Milli-Q water and mixed with a saturated solution of the matrix α -cyano-4-hydroxycinnamic acid (CHCA) in water/ACN (1:1) and 0.1 % TFA before measuring. The software *mMass* was used to analyze the spectra.

UV/VIS Spectroscopy

To perform fluorescence intensity and absorbance scans, a SPARK 20M microplate reader by the company *Tecan group Ltd.* was used. The samples were measured in a *Greiner* 384

Experimental Section

flat transparent well plate and the data were evaluated via Excel and Origin. The samples were prepared in different ratios of DMSO/PBS or in pure DMSO depending on the experiment.

Circular Dichroism Spectroscopy (CD)

For further investigation of fibrillating molecules CD spectra were recorded on a JASCO J-1500 spectrometer in a 1 mm High Precision Cell by *HellmaAnalytics*. Data were processed in Spectra Analysis by JASCO and Origin. The samples were prepared in Milli-Q water or 10 mM phosphate buffer with a peptide concentration of 100 μM . To fully dissolve the peptide sample solutions, they were sonicated. After an incubation time of 24 h, CD spectra were recorded at wavelengths from 180 nm to 380 nm with a bandwidth of 1 nm, data pitch of 0.2 nm and scanning speed at 5 nm/min. Spectra were measured three times and then averaged. For temperature dependent measurements, the temperature was increased and decreased in 10 $^{\circ}\text{C}$ steps.

Transmission Electron Microscopy (TEM)

TEM images were recorded on a JEOL 1400 transmission electron microscope with a voltage of 120 kV. The images were visualized with the software *ImageJ*. Unless noted otherwise, all samples were prepared in DMSO/PBS (9:1) solution and incubated between 20 h and 24 h at room temperature while shaking. The samples were applied to plasma-cleaned Formvar/carbon-film coated copper grids (300 mesh) by *Plano GmbH*. To prepare the TEM grids, a 3 μL drop of the sample solution was placed on the grid and incubated for 5 minutes. The excess solution was removed and then the grids were stained with uranyl acetate for 2.5 minutes. After washing three times with Milli-Q water, the grids were dried before being used for microscopy.

Furin Degradation Analysis

To check if the depsipeptides can be enzymatically cleaved, commercial furin (PeProtech) was utilized. The peptides (sample concentration: 100 μM) were dissolved in a buffer solution prepared of HEPES, TCEP and CaCl_2 in Milli-Q water with 2 μg of furin. The pH was adjusted to 7.4 using 1M HCl and diluted NH_3 . A second identical sample without the enzyme was prepared and both were shaken at 37 $^{\circ}\text{C}$. After 0.5 h, 1 h, 2 h, 4 h and 8 h, 150 μL of the sample were removed and the same volume of methanol was added (1:1 150 μL /150 μL). After centrifugation for 5 minutes at 12,000 rpm, 200 μL of the supernatant

was injected into an analytical HPLC and the cleavage of the peptide by furin and its subsequent linearization were monitored.

Cell Uptake Studies

For cell uptake studies MDA-MB-231 cells cultured in DMEM medium were utilized. The cells were seeded in an 8-well confocal plate with 15,000 cells per well. The peptides were dissolved in DMSO to obtain a 10 mM stock solution which was diluted with PBS (1:9). After an additional dilution with DMEM (1:9), the cells were treated with the sample solutions ($c = 100 \mu\text{M}$) and were incubated at 37°C for 14 h or 24 h dependent on the experiment. Then the cells were fixed with 4 % paraformaldehyde for 15 minutes at room temperature (this step was skipped for live cell imaging). For nucleus staining (30 min at 37°C) *HCS NuclearMask Deep Red Stain* and for Golgi stain BODIPYTM FL C₅-ceramide complexed to BSA was utilized (30 min at 4°C). Before imaging with confocal laser microscopy, the nucleus staining solution was removed and fresh DMEM was added. After Golgi staining the cells were incubated again with fresh medium (30 min at 37°C).

Confocal Laser Scanning Microscopy

Cells were imaged on a *Leica Stellaris*[®] 8 microscope (40x glycerol immersion objective) with a fast lifetime contrast (FALCON) module. Excitation of the samples was performed by using a 40 MHz pulsed white laser. A HyD[®]X (GaAsP hybrid photocathode) detector was used to detect emitted photons.

Intracellular Linearization of Depsipeptides

After the cells were incubated in a confocal plate (8-well, 15000 cells/well) four wells were treated with R_{VRR}(Depsi-Py-I)SA **3c** and the other half with R_{RRV}(Depsi-Py-I)SA **6c** (each $250 \mu\text{M}$) for 24 h. Then the cells were washed with PBS three times and lysed using $100 \mu\text{L}$ RIPA buffer on ice for 5 min. The cells were treated using a cell scraper and the cell lysates were transferred into two different PCR tubes. $400 \mu\text{L}$ of each cell lysate were mixed with $1600 \mu\text{L}$ methanol to precipitate proteins from the lysate. After centrifugation at 13,000 rpm at 4°C for 15 min to remove the proteins and cellular debris, $400 \mu\text{L}$ of each supernatant was analyzed by analytical HPLC.

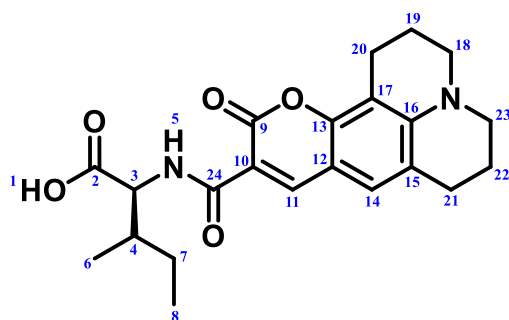
Experimental Section

Cell Viability Assay

MDA-MB-231 cells were seeded in a white 96 half area well plate (1500 cells/well) and were left to adhere overnight. The cells were treated with different concentrations ($c = 50 \mu\text{M}$, $100 \mu\text{M}$, $250 \mu\text{M}$, $500 \mu\text{M}$, $1000 \mu\text{M}$) of $50 \mu\text{L}$ sample solution of depsipeptides **3c/6c** such as **5c** ($c = 250 \mu\text{M}$) and incubated for 24 h. After the incubation was finished, the same volume of *CellTiterGlo* Assay solution (prepared according to the protocol of the supplier) was added to the sample. After incubation for 10 min at room temperature, the luminescence was read out using the well plate reader *Promega GloMax[®]-Multi Detection System*, using the settings the instrument was supplied with. The assay was performed in quadruplicates.

5.2 Synthesis

C343-Ile (**1b**)



Method A:

C343-Ile **1b** was synthesized using solid-phase supported synthesis. First, Fmoc-Ile *Wang* resin (65.59 mg, 0.50 mmol, 1.0 eq.) was swollen in DMF for 1 h. Then the Fmoc-protecting group was removed by adding a solution of 20 % piperidine in DMF ($2 \times 8 \text{ mL}$). The reaction solution was shaken 2×10 minutes. After removing the piperidine solution, the resin was washed with DMF and DCM. C343 (171.18 mg, 0.60 mmol, 1.2 eq.) and PyBOP (520.40 mg, 1.00 mmol, 2.0 eq.) were dissolved in dry DMF (5 mL) and DIPEA (0.35 mL, 2.00 mmol, 4.0 eq.) was added dropwise. The mixture was added to the resin suspended in dry DMF (3 mL) and the reaction solution was shaken over night at room temperature. After the reaction was completed, the solvent was removed and the resin was washed with DMF and DCM. Finally, the product was cleaved from the resin by adding a mixture of TFA (4.75 mL, 95 %), TIPS (0.125 mL, 2.5 %) and H_2O (0.125 mL, 2.5 %). The mixture was shaken for 2.5 h and the solvent was removed under reduced pressure. The crude product was purified by flash chromatography on silica (EA/CH = 3:1 \rightarrow 5:1, DCM/MeOH = 5:1).

Method B:

C343 (427.95 mg, 1.50 mmol, 1.0 eq.) was dissolved in dry DCM (5 mL) and DIPEA (1.6 mL, 9.00 mmol, 6.0 eq.) was added. PyBOP (1561.20 mg, 3.00 mmol, 2.0 eq.) and ^tBu-L-Ile × HCl (335.61 mg, 1.50 mmol, 1.0 eq.) were also dissolved in dry DCM (5 mL) and added to the previous prepared solution. The reaction mixture was stirred at room temperature for 3 h before the solvent was removed under reduced pressure. The crude product was purified via column chromatography (CH/EA, 2:1). In a last step, the *tert*-butyl-protecting group was removed by adding a mixture of DCM/TFA (10 mL, 1:1). After stirring at room temperature for 3 h the solvent was removed under reduced pressure.

Yield: A: 199.23 mg (0.50 mmol, *quant.*), dark yellow amorphous solid.

B: 541.60 mg (1.36 mmol, 91 %).

MF: C₂₂H₂₆N₂O₅ **MW:** 398.46 g/mol [398.18].

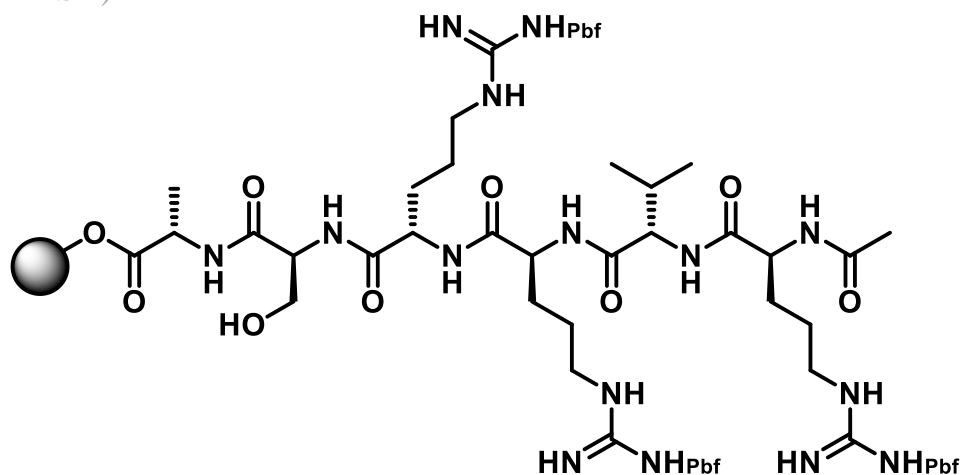
R_F = 0.18 (CH/EA, 2:1, HCOOH).

¹H-NMR, COSY (500 MHz, DMF) δ/ppm = 9.25 (d, *J* = 8.43 Hz, 1H, H-11), 8.59 (s, 1H, H-14), 7.27 (s, 1H, H-5), 4.64 (dd, *J* = 4.65 Hz, 8.47 Hz 1H, H-3), 3.40 (p, *J* = 3.66 Hz, 3.70 Hz, 4H, H-18, H-23), 2.93 (m, 2H, H-20), 2.77 (m, 2H, H-21), 1.96 (m, 4H, H-19, H-22), 1.58 (ddd, *J* = 5.01 Hz, 7.42 Hz, 12.76 Hz, 1H, H-4), 1.28 (p, *J* = 7.62 Hz, 7.36 Hz, 2H, H-7), 0.96 (m, 6H, H-6, H-8).

¹³C-NMR (500 MHz, DMF) δ/ppm = 152.95 (C-2), 148.76 (C-9, C-24), 148.02 (C-11), 127.62 (C-14), 120.23 (C-13), 108.33 (C-16), 108.15 (C-15), 106.37 (C-17), 57.15 (C-3), 50.16 (C-12), 49.64 (C-10), 38.04 (C-4), 27.40 (C-18, C-23), 25.42 (C-21), 21.16 (C-7), 20.19 (C-20), 20.08 (C-19, C-22), 15.63 (C-6), 11.54 (C-8).

Acetyl-L-arginyl-L-valyl-L-arginyl-L-arginyl-L-seryl-L-alanine (2.1)

(Ac-RVRRSA)



Experimental Section

The peptides were synthesized using the afore-mentioned solid-phase peptide synthesizer. Two different methods for the preparation of Ac-RVRRSA were carried out.

Method A:

Before using the peptide synthesizer, the Fmoc-Ala *Wang* resin (0.705 g) was swollen in DMF for 1h. To prepare 0.5 mmol of the peptide, Fmoc-Ser (unprotected side chain) (0.82 g), Fmoc-Arg(Pbf) (6.23 g), Fmoc-Val (0.82 g) and Ac-Arg(Pbf) (2.24 g) were dissolved in DMF (12 mL, 48 mL, 12 mL, 24 mL) as well as the activator base Oxyma[®] (3.13 g in 22 mL DMF) and the activator DIC (3.68 mL in 49 mL DMF). The swollen resin was transferred into the reaction vessel of the peptide synthesizer and the amino acids as well as activator and activator base were placed at the appropriate positions. The selected method was started whereby the Fmoc group of alanine was removed first, using 20 % piperidine solution in DMF followed by a washing step with DMF. Next Fmoc-Ser was coupled to the *N*-Terminus of Ala using Oxyma[®] and DIC. The removal of the Fmoc protecting group and the coupling of the next amino acid were carried out alternately till the peptide sequence was completely finished. For the couplings of arginine, double coupling and additional washing steps were performed. Because of the acetyl protecting group at the *N*-terminal arginine the final Fmoc-deprotection step was omitted. The finished peptide at the solid phase was removed from the reaction vessel and washed with DMF and DCM.

Method B:

Before using the peptide synthesizer, the Fmoc-Ala *Wang* resin (0.705 g) was swollen in DMF for 1h. To prepare 0.5 mmol of the peptide, Fmoc-Ser (unprotected side chain) (0.82 g), Fmoc-Arg(Pbf) (9.35 g) and Fmoc-Val (0.82 g) were dissolved in DMF (12 mL, 72 mL, 12 mL) as well as the activator base Oxyma[®] (3.13 g in 22 mL DMF) and the activator DIC (3.68 mL in 49 mL DMF). The swollen resin was transferred into the reaction vessel of the peptide synthesizer and the amino acids such as activator and activator base in DMF were placed at the appropriate positions. The selected method was started whereby the Fmoc group of Ala was removed first, using 20 % piperidine solution in DMF followed by a washing step with DMF. Next Fmoc-Ser was coupled to the *N*-Terminus of Ala using Oxyma[®] and DIC. The removal of the Fmoc protecting group and the coupling of the next amino acid were carried out alternately till the peptide sequence was completely finished. For the couplings of arginine, a double coupling and additional washing steps were performed. The finished peptide (with a free *N*-terminus) at the solid phase was removed from the reaction vessel and washed with DMF and DCM. Then acetic acid (0.04 mL, 0.75 mmol,

Experimental Section

4k rpm the supernatant was removed. The crude was dissolved in water and CAN and purified via HPLC (10 % to 100 % ACN in 20 min).

Yield: 34.2 mg (0.03 mmol, 12 %), yellow amorphous solid.

MF: C₅₃H₈₃N₁₆O₁₃ **MW:** 1166.35 g/mol [1165.64].

MALDI-TOF: m/z: [M+H]⁺ 1166.38 (calc. 1166.65), [M+Na]⁺ 1188.36 (calc. 1188.63).

R_T (semipreparative HPLC) = 12.8 min.

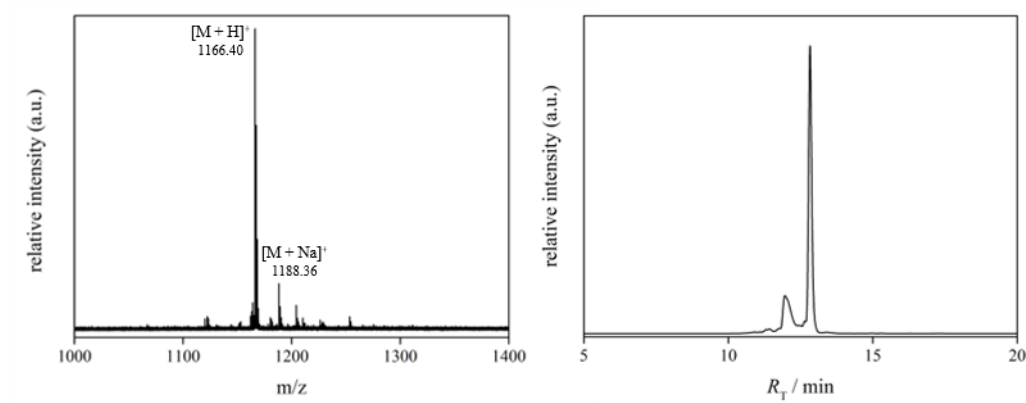
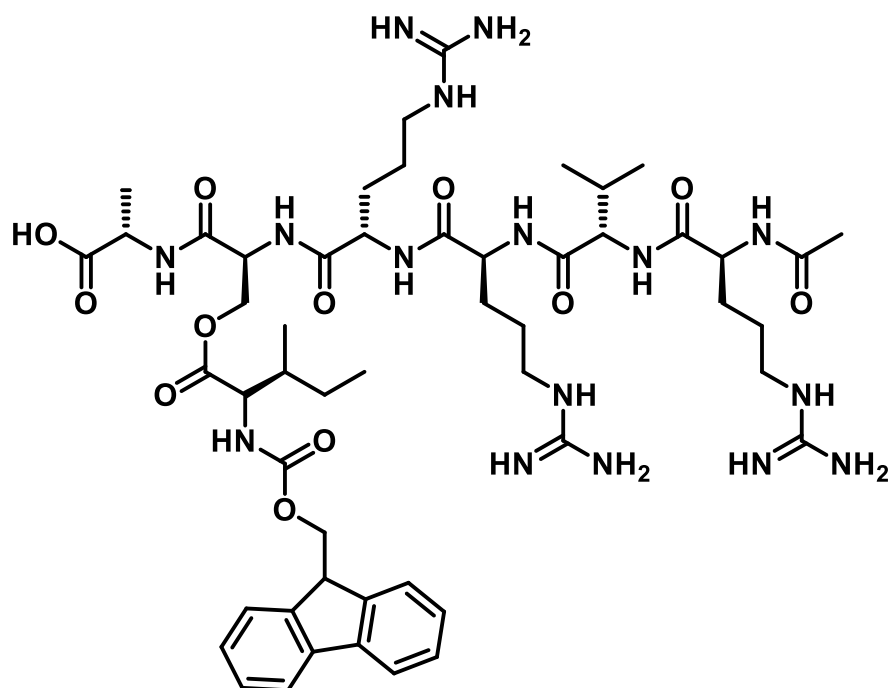


Figure 5.1: MALDI-TOF spectrum (left) and HPLC trace (right) of RVRR(Depsi-C343-I)SA.

RVRR(Depsi-Fmoc-I)SA (3a)



Fmoc-Ile **1a** (353.42 mg, 1.00 mmol, 4 eq.) and DMAP (30.54 mg, 0.25) were dissolved in dry DMF (5 mL) and DIC (0.16 mL, 1.00 mmol, 4 eq.) was added to the solution. To the resin (0.25 mmol) loaded with Ac-RVRRSA **2.1** dry DMF (3 mL) was added and the previously prepared mixture was added dropwise. The suspension was shaken over night at room

temperature. Afterwards, the resin was washed repeatedly with DMF and DCM. To cleave the peptide sequence from the resin, a mixture of TFA (4.75 mL, 95 %), TIPS (0.125 mL, 2.5 %) and H₂O (0.125 mL, 2.5 %) was added and the suspension was shaken for 2.5 h at room temperature. The solution was separated from the resin and the crude product was precipitated in ice cold Et₂O. After centrifugation for 20 minutes at 4k rpm the supernatant was removed. The crude was dissolved in water and ACN and purified via HPLC (10 % to 100 % CAN in 20 min).

Yield: 2.00 mg (1.78 μmol, 1 %), colorless amorphous solid.

MF: C₅₂H₈₀N₁₆O₁₂ **MW:** 1121.31 g/mol [1120.61].

MALDI-TOF: m/z: [M+H]⁺ 1121.68 (calc. 1121.62), [M+Na]⁺ 1143.66 (calc. 1143.60).

R_T (semipreparative HPLC) = 13.0 min.

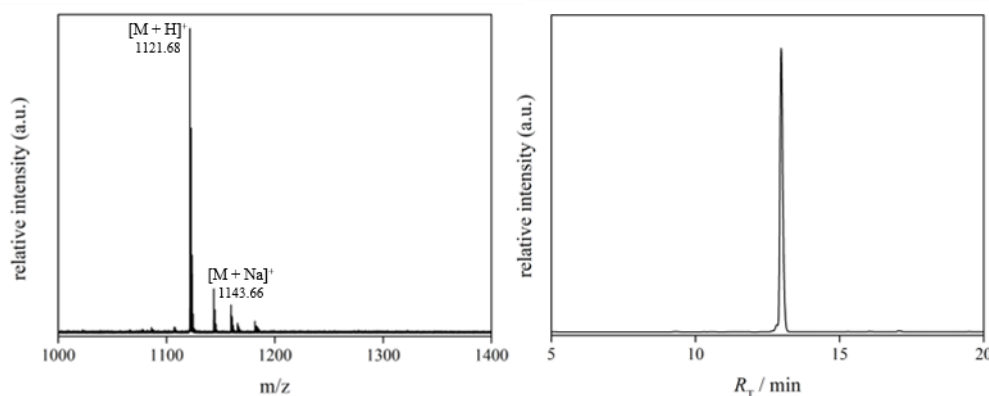
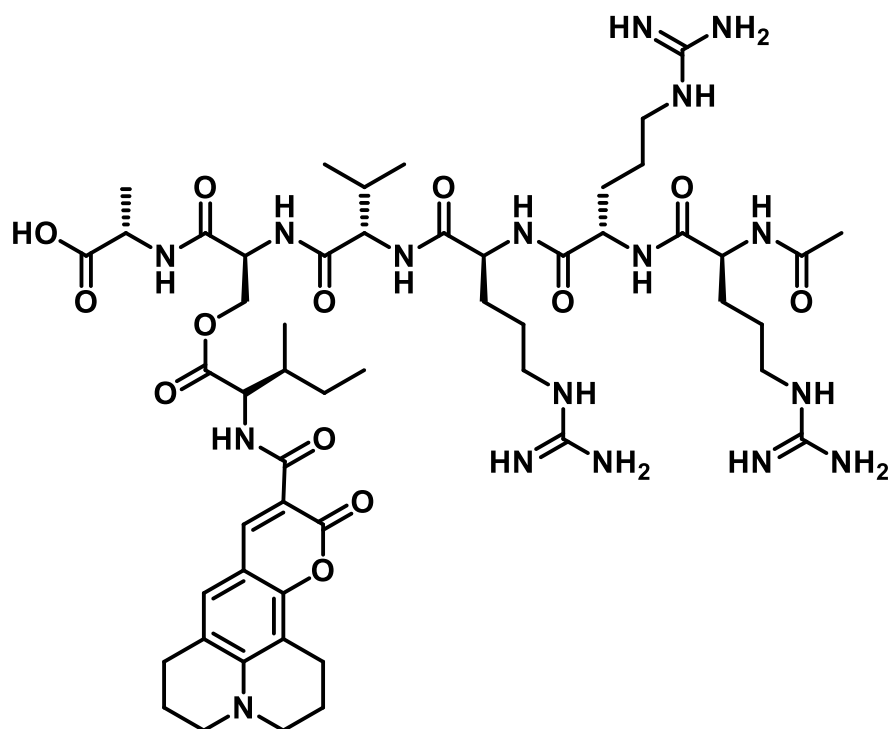


Figure 5.2: MALDI-TOF spectrum (left) and HPLC trace (right) of RVRRR(Depsi-Fmoc-I)SA.

RRRV(Depsi-C343-I)SA (6b)



RRRV(Depsi-C343-I)SA **6b** was synthesized analogously to RVRR(Depsi-C343-I)SA **3b**. Only the amino acid sequence in the method of the peptide synthesizer was changed to get the scrambled peptide. Because of a triple arginine coupling in a row the method was adjusted accordingly by accomplishing more washing steps.

Yield: 40.0 mg (0.03 mmol, 12 %), yellow amorphous solid.

MF: C₅₃H₈₃N₁₆O₁₃ **MW:** 1166.35 g/mol [1165.64].

MALDI-TOF: m/z: [M+H]⁺ 1166.38 (calc. 1166.65).

R_T (analytical HPLC) = 13.0 min.

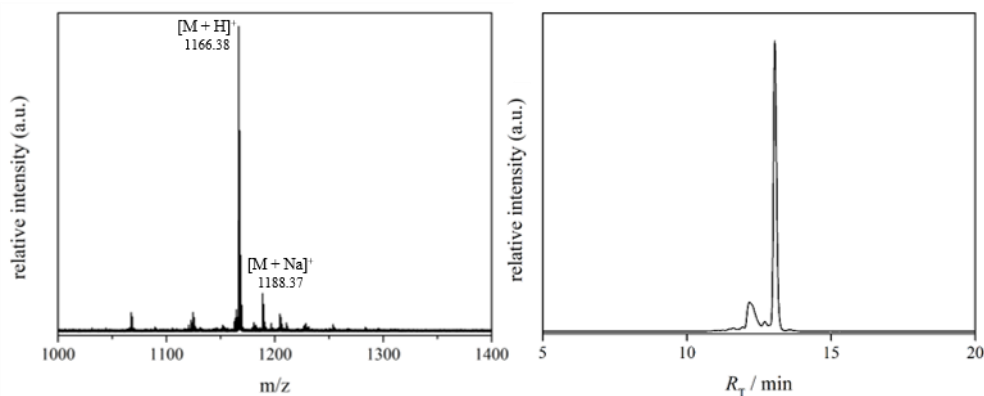
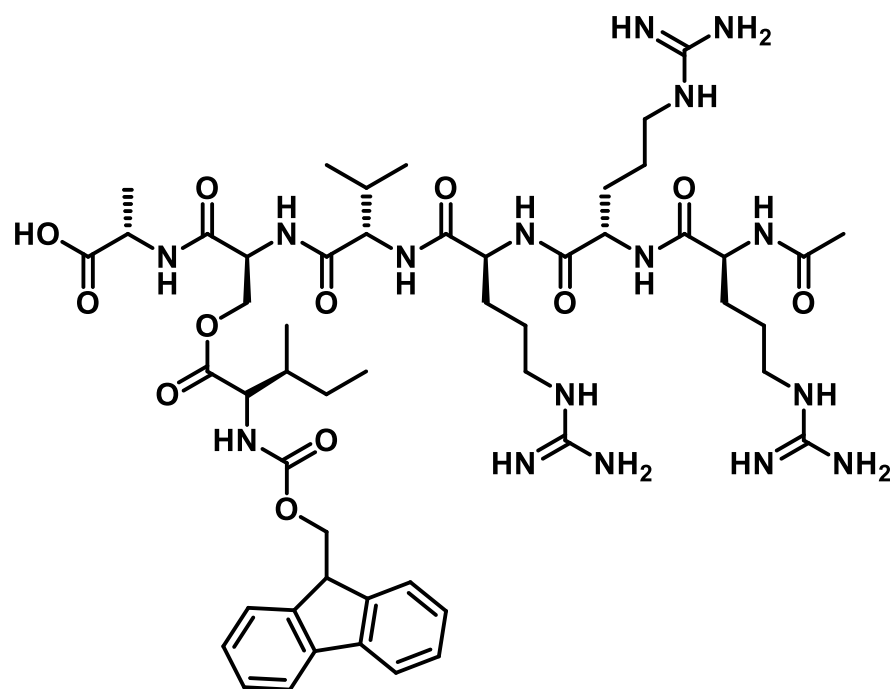


Figure 5.3: MALDI-TOF spectrum (left) and HPLC trace (right) of RRRV(Depsi-C343-I)SA.

RRRV(Depsi-Fmoc-I)SA (6a)



RRRV(Depsi-Fmoc-I)SA **6a** was synthesized analogously to RVRV(Depsi-Fmoc-I)SA **3a**. Only the amino acid sequence in the method of the peptide synthesizer was changed to get the scrambled peptide. Because of a triple arginine coupling in a row the method was adjusted accordingly by accomplishing more washing steps.

Yield: 64.2 mg (57.2 μmol , 12 %), colorless amorphous solid.

MF: $\text{C}_{52}\text{H}_{80}\text{N}_{16}\text{O}_{12}$ **MW:** 1121.31 g/mol [1120.61].

MALDI-TOF: m/z : $[\text{M}+\text{H}]^+$ 1121.77 (calc. 1121.62), $[\text{M}+\text{Na}]^+$ 1144.76 (calc. 1143.60).

R_T (analytical HPLC) = 13.2 min.

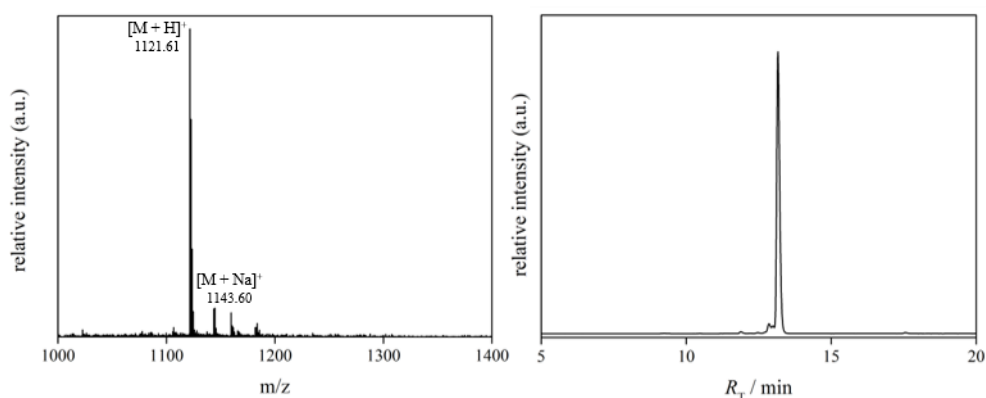
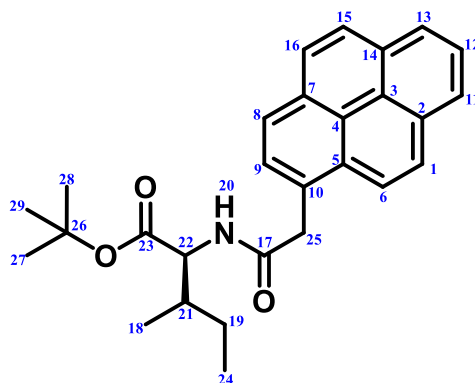


Figure 5.4: MALDI-TOF spectrum (left) and HPLC trace (right) of RRRV(Depsi-Fmoc-I)SA.

Experimental Section

(2-(pyren-1-yl)acetyl)-L-isoleucinate (1c)

(Py-Ile)



2-(Pyren-1-yl)acetic acid (130.15 mg, 0.50 mmol, 1.0 eq.) was dissolved in dry DMF (5 mL) before DIPEA (0.50 mL, 3.00 mmol, 6.0 eq.) was added. Then PyBOP (520.4 mg, 1.00 mmol, 2.0 eq.) and ^tBu-L-Ile × HCl (111.87 mg, 0.50 mmol, 1.0 eq.) were also dissolved in dry DMF (5 mL) and added to the previous prepared solution. The reaction mixture was stirred at room temperature for 3 h before the solvent was removed under reduced pressure. The crude product was purified via column chromatography (CH/Ea, 2:1). In a last step the *tert*-butyl-protecting group was removed by adding a mixture of DCM/TFA (10 mL, 1:1). After stirring at room temperature for 3 h the solvent was removed under reduced pressure. The yield determination and characterization were performed before *tert*-butyl was removed.

Yield: 191.5 mg (0.44 mol, 89 %), colorless crystalline solid.

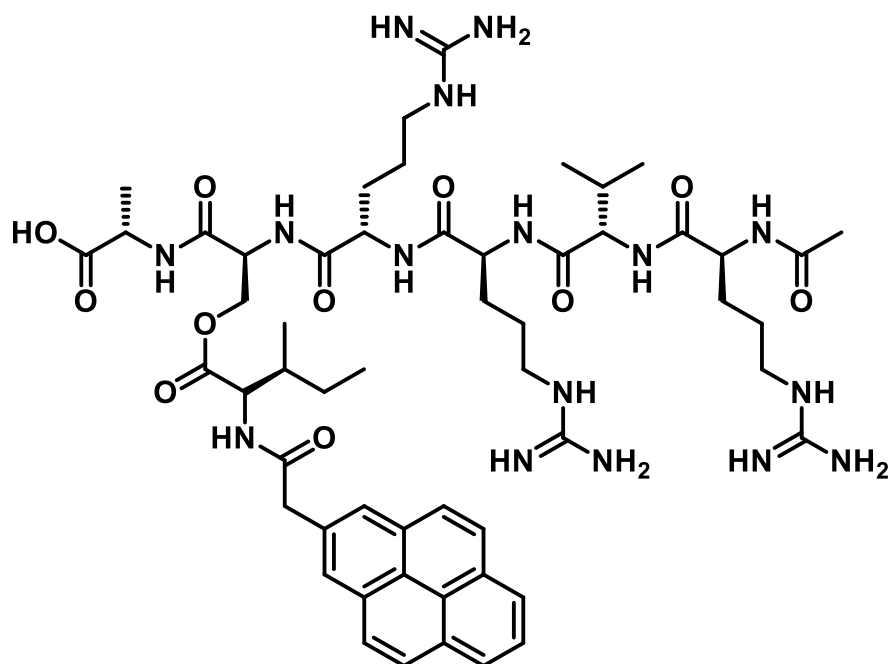
MF: C₂₈H₃₁NO₃ **MW:** 429.56 g/mol [429.23].

R_F = 0.65 (CH/Ea, 2:1).

¹H-NMR (400 MHz, DMF) δ/ppm = 8.55 (d, *J* = 9.27 Hz, 1H, H-13), 8.42 – 8.22 (m, 9H, H-1, H-6, H-8, H-9, H-11, H-12, H-15, H-16, H-20), 4.46 (q, *J* = 8.00 Hz, 2H, H-25), 4.32 (dd, *J* = 8.39 Hz, 5.96 Hz, 1H, H-22), 1.89 (m, 1H, H-21), 1.59 – 1.24 (m, 2H, H-19), 1.41 (s, 9H, H-27, H-28, H-29), 0.92 (m, 6H, H-18, H-24).

MALDI-TOF: m/z: [M-^tBu+H]⁺ 374.10 (calc. 374.18), [M+H]⁺ 429.15 (calc. 430.24), [M+Na]⁺ 468.11 (calc. 468.19).

RVRR(Depsi-Py-I)SA (3c)



Py-Ile **1c** (102.70 mg, 0.275 mmol, 1.1 eq.) and DMAP (30.54 mg, 0.25 mmol, 1.0 eq.) were dissolved in dry DCM (5 mL) and DIC (0.16 mL, 1.00 mmol, 4 eq.) was added to the solution. To the resin (0.25 mmol) loaded with Ac-RVRRSA dry DCM (3 mL) was added and the previously prepared mixture was added dropwise. The suspension was shaken over night at room temperature. To cleave the peptide sequence from the resin, a mixture of TFA (4.75 mL, 95 %), TIPS (0.125 mL, 2.5 %) and H₂O (0.125 mL, 2.5 %) was added and the suspension was shaken for 2.5 h at room temperature. The solution was separated from the resin and the crude product was precipitated in ice-cold Et₂O. After centrifugation for 20 minutes at 4k rpm the supernatant was removed and the crude was dissolved in water and ACN and purified via HPLC (10 % to 100 % ACN in 20 min).

Yield: 9.4 mg (8.23 μ mol, 3 %), beige amorphous solid.

MF: C₅₅H₈₀N₁₆O₁₁ **MW:** 1141.35 g/mol [1140.62].

MALDI-TOF: m/z: [M+H]⁺ 1141.37 (calc. 1141.63), [M+Na]⁺ 1163.35 (calc. 1163.61).

R_T (analytical HPLC) = 13.0 min.

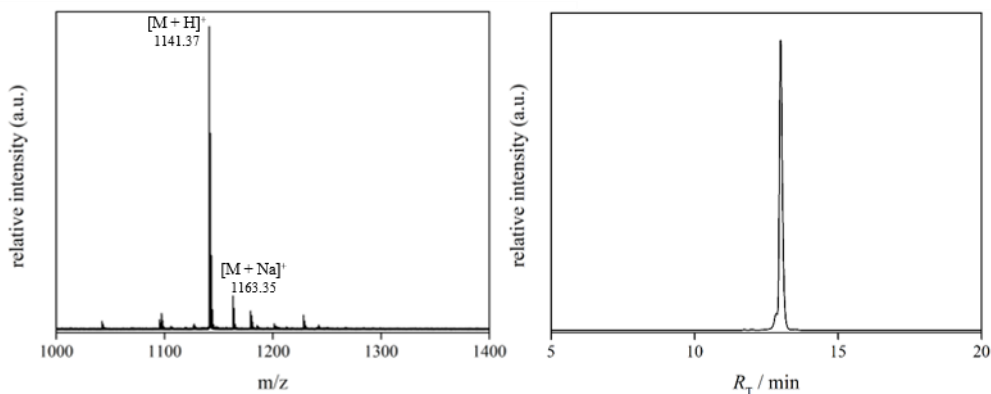
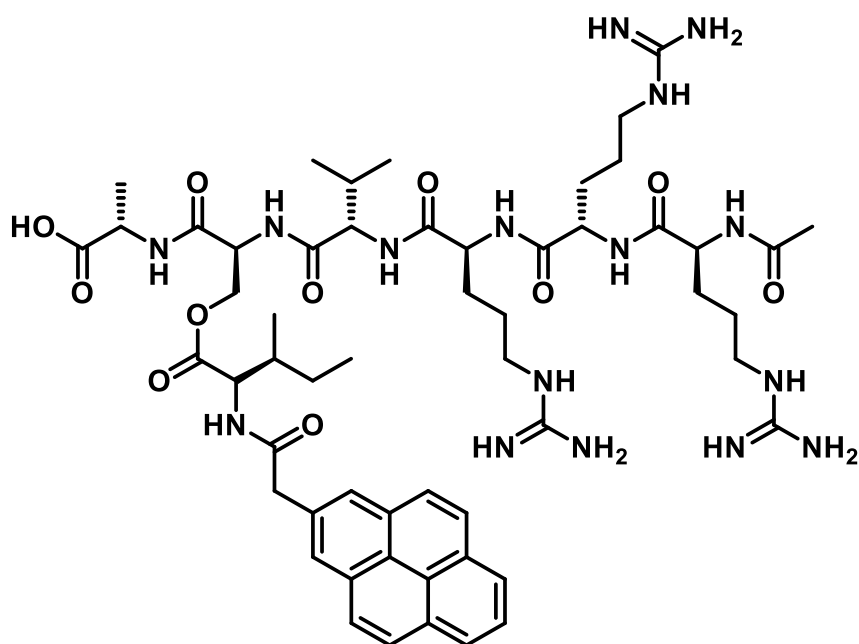


Figure 5.5: MALDI-TOF spectrum (left) and HPLC trace (right) of RVRR(Depsi-Py-I)SA.

RRRV(Depsi-Py-I)SA (6c)



RRRV(Depsi-Py-I)SA **6c** was synthesized analogously to RVRR(Depsi-Py-I)SA **3c**. Only the amino acid sequence in the method of the peptide synthesizer was changed to get the scrambled peptide. Because of a triple arginine coupling in a row the method was adjusted accordingly by accomplishing more washing steps.

Yield: 34.6 mg (0.03 mmol, 12 %), beige amorphous solid.

MF: C₅₅H₈₀N₁₆O₁₁ **MW:** 1141.35 g/mol [1140.62].

MALDI-TOF: m/z: [M+H]⁺ 1141.56 (calc. 1141.63), [M+Na]⁺ 1163.54 (calc. 1163.61).

R_T (analytical HPLC) = 13.2 min.

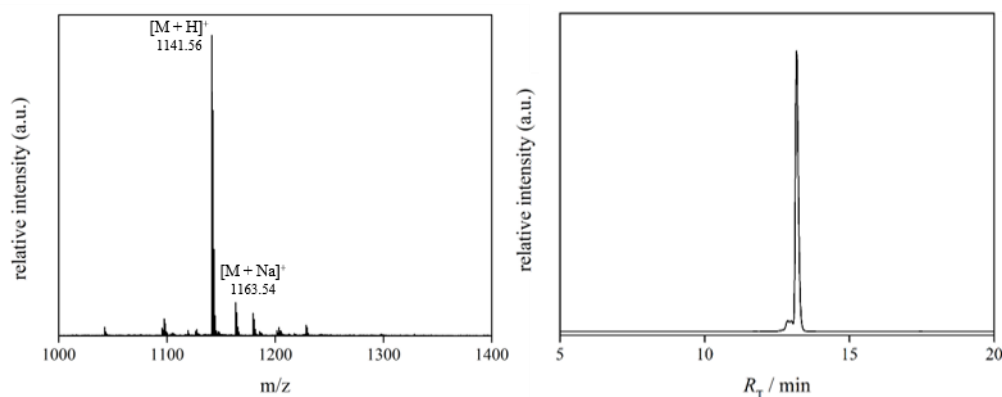
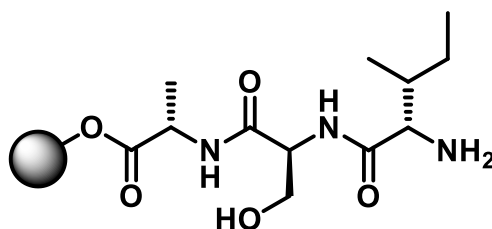


Figure 5.6: MALDI-TOF spectrum (left) and HPLC trace (right) of RRRV(Depsi-Py-I)SA.

L-Isoleucyl-L-seryl-L-alanine (4) (ISA)



The peptide was synthesized using the afore-mentioned solid-phase peptide synthesizer. Before using the peptide synthesizer, the Fmoc-Ala Wang resin (0.704 g) was swollen in DMF for 1h. To prepare 0.5 mmol of the peptide, Fmoc-Ser (unprotected side chain) (0.82 g) and Fmoc-Ile (0.85 g) were dissolved in DMF (12 mL each) as well as the activator base Oxyma[®] (0.99 g in 7 mL DMF) and the activator DIC (0.94 mL in 12 mL DMF). The swollen resin was transferred into the reaction vessel of the peptide synthesizer and the amino acids as well as activator and activator base were placed at the appropriate positions. The selected method was started whereby the Fmoc group of alanine was removed first, using 20 % piperidine solution in DMF followed by a washing step with DMF. Next Fmoc-Ser was coupled to the *N*-Terminus of Ala using Oxyma[®] and DIC by a following removal of the Fmoc-protecting group and the coupling of the last Fmoc-Ile analogous to the first coupling. After a final deprotection step of Fmoc the finished peptide at the solid phase was removed from the reaction vessel and washed with DMF and DCM.

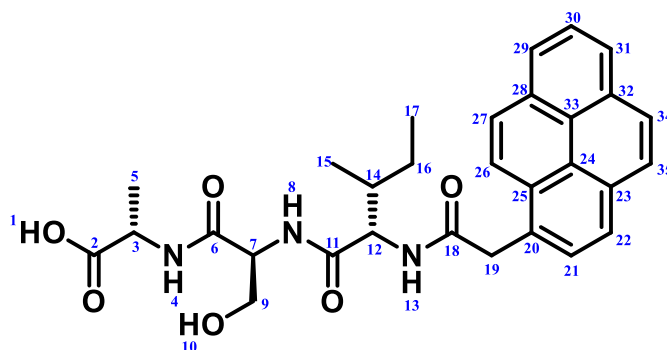
MF: C₁₂H₂₃N₃O₅

MW: 289.33 g/mol

[289.13].

(2-(Pyrene-1-yl)acetyl)-L-isoleucyl-L-seryl-L-alanine (5c)

(Py-ISA)



2-(Pyrene-1-yl)acetic acid (156.17 mg, 0.600 mmol, 1.2 eq.) and PyBOP (520.4 mg, 1.00 mmol, 2.0 eq.) were dissolved in dry DMF (5 mL) and DIPEA (0.35 mL, 2.00 mmol, 4 eq.) was added to the solution. To the resin (0.50 mmol) loaded with ISA dry DMF (3 mL) was added and the previously prepared mixture was added dropwise. The suspension was shaken for 2.5 h at room temperature and the resin was subsequently washed with DMF and DCM. To cleave the peptide sequence from the resin, a mixture of TFA (4.75 mL, 95 %), TIPS (0.125 mL, 2.5 %) and H₂O (0.125 mL, 2.5 %) was added and it was shaken 2.5 h at room temperature. The solution was separated from the resin and the crude product was precipitated in ice cold Et₂O. After centrifugation for 20 minutes at 4k rpm the supernatant was removed. The crude was dissolved in water and ACN and purified via HPLC (10 % to 100 % ACN in 20 min).

Yield: 26.0 mg (48.9 μmol, 10 %), colorless amorphous solid.

MF: C₃₀H₃₃N₃O₆ **MW:** 531.61 g/mol [531.24].

¹H-NMR, COSY (850 MHz, DMSO) δ/ppm = 8.41 (d, *J* = 9.15 Hz, 1H, H-26), 8.39 (d, *J* = 8.93 Hz, 1H, H-13), 8.28 (t, *J* = 7.28 Hz, 2H, H-29, H-31), 8.24 (d, *J* = 7.71 Hz, 1H, H-22), 8.20 (d, *J* = 9.17 Hz, 1H, H-27), 8.15 (s, 2H, H-34, H-35), 8.07 (d, *J* = 7.51 Hz, 1H, H-30), 8.05 (t, *J* = 8.50 Hz, 1H, H-8), 8.02 (d, *J* = 7.73 Hz, 1H, H-21), 7.95 (m, 1H, H-4), 4.37 (d, *J* = 15.00 Hz, 1H, H-19.1), 4.33 (q, *J* = 6.42 Hz, 1H, H-7), 4.27 (dd, *J* = 7.20 Hz, 8.95 Hz, 1H, H-12), 4.23 (d, *J* = 15.00 Hz, 1H, H-19.2), 4.18 (m, 1H, H-3), 3.57 (m, 2H, H-9), 1.78 (m, 1H, H-14), 1.46 (m, 1H, H-16.1), 1.21 (d, *J* = 7.29 Hz, 3H, H-5), 1.12 (m, 1H, H-16.2), 0.84 (d, *J* = 6.83 Hz, 3H, H-15), 0.78 (t, *J* = 7.43 Hz, 3H, H-17).

MALDI-TOF: m/z: [M+H]⁺ 554.11 (calc. 554.23).

R_T (analytical HPLC) = 15.6 min.

6 References

- [1] A. C. Mendes, E. T. Baran, R. L. Reis, H. S. Azevedo, *Wiley Interdiscip. Rev. Nanomed. Nanobiotechnol.* **2013**, *5*, 582–612.
- [2] B. Alberts, A. Johnson, J. Lewis, D. Morgan, M. Raff, K. Roberts, P. Walt, *Molekularbiologie der Zelle*, John Wiley & Sons, Incorporated, Weinheim, Germany, **2017**.
- [3] Y. Tu, F. Peng, A. Adawy, Y. Men, L. K. E. A. Abdelmohsen, D. A. Wilson, *Chem. Rev.* **2016**, *116*, 2023–2078.
- [4] G.-B. Qi, Y.-J. Gao, L. Wang, H. Wang, *Adv. Mater.* **2018**, *30*, 1703444 (1-34).
- [5] D. M. Bradshaw, R. J. Arceci, *J. Clin. Oncol.* **1998**, *16*, 3674–3690.
- [6] D.-B. Cheng, D. Wang, Y.-J. Gao, L. Wang, Z.-Y. Qiao, H. Wang, *J. Am. Chem. Soc.* **2019**, *141*, 4406–4411.
- [7] C. Fouquey, J.-M. Lehn, A.-M. Levelut, *Adv. Mater.* **1990**, *2*, 254–257.
- [8] J.-M. Lehn, *Angew. Chem.* **1988**, *100*, 91–116.
- [9] K. Gloe, K. Gloe, H. Heßke und L. F. Lindoy, *Wiss. Z. TU Dresden* **2007**, *56*, 32–38.
- [10] G. M. Whitesides, B. Grzybowski, *Science* **2002**, *295*, 2418–2421.
- [11] J. D. Watson, F. H. Crick, *Nature* **1953**, *171*, 737–738.
- [12] J. Wang, K. Liu, R. Xing, X. Yan, *Chem. Soc. Rev.* **2016**, *45*, 5589–5604.
- [13] P. Zhu, X. Yan, Y. Su, Y. Yang, J. Li, *Chem. Eur. J.* **2010**, *16*, 3176–3183.
- [14] J. Kim, T. H. Han, Y.-I. Kim, J. S. Park, J. Choi, D. G. Churchill, S. O. Kim, H. Ihee, *Adv. Mater.* **2010**, *22*, 583–587.
- [15] C. G. Pappas, P. W. J. M. Frederix, T. Mutasa, S. Fleming, Y. M. Abul-Haija, S. M. Kelly, A. Gachagan, D. Kalafatovic, J. Trevino, R. V. Ulijn et al., *Chem. Commun.* **2015**, *51*, 8465–8468.
- [16] G. Krauss, *Biochemistry of Signal Transduction and Regulation*, Wiley-VCH, Weinheim, Germany, **2014**.
- [17] S. Chagri, D. Y. W. Ng, T. Weil, *Nat. Rev. Chem.* **2022**, *6*, 320–338.

References

- [18] B. A. Webb, M. Chimenti, M. P. Jacobson, D. L. Barber, *Nat. Rev. Cancer* **2011**, *11*, 671–677.
- [19] a) M. Marsh, M. Marsh (Eds.) *Frontiers in molecular biology*, Vol. 36, Oxford University Press, Oxford, **2001**; b) J. R. Casey, S. Grinstein, J. Orlowski, *Nat. Rev. Mol. Cell Biol.* **2010**, *11*, 50–61.
- [20] M. Waqas, W. Jeong, Y.-J. Lee, D.-H. Kim, C. Ryou, Y. Lim, *Biomacromolecules* **2017**, *18*, 943–950.
- [21] S. C. Lu, *FASEB J.* **1999**, *13*, 1169–1183.
- [22] J. F. Quinn, M. R. Whittaker, T. P. Davis, *Polym. Chem.* **2017**, *8*, 97–126.
- [23] W.-W. Guo, Z.-T. Zhang, Q. Wei, Y. Zhou, M.-T. Lin, J.-J. Chen, T.-T. Wang, N.-N. Guo, X.-C. Zhong, Y.-Y. Lu et al., *Biomacromolecules* **2020**, *21*, 444–453.
- [24] E. A. Veal, A. M. Day, B. A. Morgan, *Mol. Cell* **2007**, *26*, 1–14.
- [25] R. Spooner, O. Yilmaz, *Int. J. Mol. Sci.* **2011**, *12*, 334–352.
- [26] B. C. Dickinson, C. J. Chang, *Nat. Chem. Biol.* **2011**, *7*, 504–511.
- [27] M. Pieszka, S. Han, C. Volkmann, R. Graf, I. Lieberwirth, K. Landfester, D. Y. W. Ng, T. Weil, *J. Am. Chem. Soc.* **2020**, *142*, 15780–15789.
- [28] B. Liu, S. Thayumanavan, *Cell. Rep. Phys. Sci.* **2020**, *1*, 100271.
- [29] Y. Yuan, G. Liang, *Org. Biomol. Chem.* **2014**, *12*, 865–871.
- [30] G. Liang, H. Ren, J. Rao, *Nat. Chem.* **2010**, *2*, 54–60.
- [31] J. M. Berg, J. L. Tymoczko, G. J. Gatto jr., L. Stryer, *Stryer Biochemie*, Springer Berlin Heidelberg, Berlin, Heidelberg, **2018**.
- [32] P. C. Heinrich, M. Müller, L. Graeve (Eds.) *Löffler/Petrides Biochemie und Pathobiochemie*, Springer Berlin Heidelberg, Berlin, Heidelberg, **2014**.
- [33] L. Pauling, R. B. Corey, H. R. BRANSON, *Proc. Natl. Acad. Sci. USA* **1951**, *37*, 205–211.
- [34] D. Eisenberg, *Proc. Natl. Acad. Sci. USA* **2003**, *100*, 11207–11210.
- [35] L. Pauling, R. B. Corey, *Proc. Natl. Acad. Sci. USA* **1951**, *37*, 235–240.

- [36] L. Pauling, R. B. Corey, *Proc. Natl. Acad. Sci. USA* **1951**, *37*, 251–256.
- [37] R. B. Merrifield, *J. Am. Chem. Soc.* **1963**, *85*, 2149–2154.
- [38] R. B. Merrifield, *Angew. Chem. Int. Ed. Engl.* **1985**, *24*, 799–810.
- [39] IUPAC-IUB Joint Commission on Biochemical Nomenclature (JCBN), *Eur. J. Biochem.* **1984**, *138*, 9–37.
- [40] C. E. Ballard, H. Yu, B. Wang, *Curr. Med. Chem.*, *9*, 471–498.
- [41] I. Coin, R. Dölling, E. Krause, M. Bienert, M. Beyermann, C. D. Sferdean, L. A. Carpino, *J. Org. Chem.* **2006**, *71*, 6171–6177.
- [42] S. S. Molloy, P. A. Bresnahan, S. H. Leppla, K. R. Klimpel, G. Thomas, *J. Biolog. Chem.* **1992**, *267*, 16396–16402.
- [43] R. J. Siezen, J. W. Creemers, W. J. van de Ven, *Eur. J. Biochem.* **1994**, *222*, 255–266.
- [44] S. O. Dahms, M. Arciniega, T. Steinmetzer, R. Huber, M. E. Than, *Proc. Natl. Acad. Sci. USA* **2016**, *113*, 11196–11201.
- [45] N. C. Rockwell, R. S. Fuller, *J. Biolog. Chem.* **2002**, *277*, 17531–17537.
- [46] G. Griffiths, K. Simons, *Science* **1986**, *234*, 438–443.
- [47] Y. Yuan, L. Wang, W. Du, Z. Ding, J. Zhang, T. Han, L. An, H. Zhang, G. Liang, *Angew. Chem. Int. Ed.* **2015**, *54*, 9700–9704.
- [48] M. Montalti, S. L. Murov, *Handbook of photochemistry*, CRC/Taylor & Francis, Boca Raton, **2006**.
- [49] J. R. Lakowicz, *Principles of fluorescence spectroscopy*, Springer, New York, NY, **2006**.
- [50] H. Sahoo (Ed.) *Optical Spectroscopic and Microscopic Techniques. Analysis of Biological Molecules*, Springer Singapore; Imprint: Springer, Singapore, **2022**.
- [51] J. C. Stockert, A. Blázquez-Castro, *Fluorescence Microscopy In Life Sciences*, Bentham Science Publishers, Sharjah, **2017**.
- [52] G. A. Reynolds, K. H. Drexhage, *Opt. Commun.* **1975**, *13*, 222–225.
- [53] I. B. Berlman, *Handbook of fluorescence spectra of aromatic molecules. 2.ed*, Academic Press, New York, N., **1971**.

References

- [54] P.-P. Yang, Q. Luo, G.-B. Qi, Y.-J. Gao, B.-N. Li, J.-P. Zhang, L. Wang, H. Wang, *Adv. Mater. (Deerfield Beach, Fla.)* **2017**, *29*.
- [55] a) Z. Chen, M. Chen, Y. Cheng, T. Kowada, J. Xie, X. Zheng, J. Rao, *Angew. Chem. Int. Ed.* **2020**, *59*, 3272–3279; b) Z. Feng, H. Wang, S. Wang, Q. Zhang, X. Zhang, A. A. Rodal, B. Xu, *J. Am. Chem. Soc.* **2018**, *140*, 9566–9573; c) Y. Gao, J. Shi, D. Yuan, B. Xu, *Nat. Commun.* **2012**, *3*, 1033.
- [56] A. Juris, L. Prodi, *New J. Chem.* **2001**, *25*, 1132–1135.
- [57] S. A. Schmid, R. Abbel, A. P. H. J. Schenning, E. W. Meijer, L. M. Herz, *Phil. Trans. R. Soc. A* **2012**, *370*, 3787–3801.
- [58] S. W. Provencher, J. Glöckner, *Biochemistry* **1981**, *20*, 33–37.
- [59] S. Fleming, R. V. Ulijn, *Chem. Soc. Rev.* **2014**, *43*, 8150–8177.
- [60] Z. Zhou, K. Maxeiner, P. Moscariello, S. Xiang, Y. Wu, Y. Ren, C. J. Whitfield, L. Xu, A. Kaltbeitzel, S. Han et al., *J. Am. Chem. Soc.* **2022**, *144*, 12219–12228.
- [61] A. Cotton, *C. R. Acad. Sci.* **1895**, *120*, 989–991.
- [62] S. Bartocci, I. Morbioli, M. Maggini, M. Mba, *J. Pept. Sci.* **2015**, *21*, 871–878.
- [63] X. Hu, Z. Hai, C. Wu, W. Zhan, G. Liang, *Anal. Chem.* **2021**, *93*, 1636–1642.
- [64] I. Nikić, J. H. Kang, G. E. Girona, I. V. Aramburu, E. A. Lemke, *Nat. Protoc.* **2015**, *10*, 780–791.

7 List of Figures and Schemes

Figures

- Figure 1.1: Schematic representation of the eukaryotic cell and its compartments harboring different conditions in terms of self-assembly triggers such as ROS, glutathione, pH or enzymes.^[17] 3
- Figure 1.2: Possible chemical transformations of precursors induced by different intracellular stimuli which lead to the generation of self-assembling monomers.^[17] 5
- Figure 1.3: Material classes for intracellular self-assembly and their supramolecular structures.^[17] 6
- Figure 1.4: Mesomeric structures of the peptide bond to show its partial double bond character..... 7
- Figure 1.5: Schematic representations of the α -Helix (left) and two types of β -pleated sheets (right). **a** C^α atoms (black) and side chains (green) in a helical band. **b** Illustration of the hydrogen bonds (dashed lines) between carbonyl oxygens (black, next to pink oxygen atoms) and amide protons (white). **c** Antiparallel β -pleated sheet with the β -strands running in opposite directions. **d** Parallel β -pleated sheet with the β -strands running in the same direction.^[31] 8
- Figure 1.6: Conversion of a depsipeptide to a linear peptide through the removal of a *N*-terminal protecting group (R_2) and a subsequent *O,N*-acyl shift..... 10
- Figure 1.7: **Left:** Optimal recognition sequence of the enzyme furin. (Arg = arginine, Lys = lysine, X, Z = any amino acids). **Right:** Overall structure of human unliganded furin (catalytic domains = gold, P-domains = blue). The catalytic residues (cyan stick model), the substrate binding pockets (labeled S1–S5), and bound ions (Na^+ (purple), Ca^{2+} (green)) are indicated.^[44] 11
- Figure 1.8: Possible depiction of a *Jablonski* diagram. S_0 , S_1 , S_2 : singlet ground/excited states; T_1 : triplet excited state; 0, 1, 2: vibrational states within an electronic energy level. 13
- Figure 1.9: Chemical structures as well as absorption and emission spectra of the fluorophores coumarin-343 (top)^[52] and 1-pyrene acetic acid (bottom).^[53] 14

List of Figures and Schemes

- Figure 2.1: Chemical structures of furin-responsive depsipeptides with Fmoc (violet), coumarin-343 (turquoise) and pyrene (blue) as aromatic residues. 16
- Figure 2.2: Reaction cascade to induce self-assembly inside and outside cells. Depsipeptide **3** is uptaken by the cell due to the polar arginine's (black) and subsequently cleaved by the enzyme furin resulting in peptide **3.2**. The subsequent *O,N*-acyl shift linearizes the peptide, enabling it to self-assemble and generate supramolecular networks. 17
- Figure 3.1: Chemical structures of the depsipeptides **3/6** and the linear peptide sequences **5**. 19
- Figure 3.2: ¹H-NMR spectra of C343-Ile **1b** (top, DMF-*d*₇, 500 MHz, 298 K) and Py-Ile-¹BuO (bottom, DMF-*d*₇, 400 MHz, 298 K). 21
- Figure 3.3: MALDI-TOF spectra and HPLC traces of the synthesized with Fmoc-, C343- and pyrene-modified depsipeptides **3** and **6**. 23
- Figure 3.4: ¹H-NMR spectrum of Py-ISA **5c** (DMSO-*d*₆, 850 MHz, 298 K). 24
- Figure 3.5: **Left:** HPLC traces of furin (*c* = 25.6 nM) induced removal of the RVRP cleavage site to get **3.2c** and linearization to **5c** and its reference spectrum (blue, second row). HPLC trace without furin (blue, first row) to show the stability of **3c** in HEPES buffer solution. **Right:** HPLC traces to show the stability of **6c** in the presence (*c* = 21.4 nM) and absence (blue) of furin in HEPES buffer solution. 26
- Figure 3.6: **Left:** HPLC traces of furin (*c* = 14.7 nM) induced removal of the RVRP cleavage site to get **3.2a** and linearization to **5a** and its reference spectrum (violet, second row). HPLC trace without furin to show the stability of **3a** in HEPES buffer solution (violet, first row). **Right:** HPLC traces to show the stability of **6a** in the presence (*c* = 19.8 nM) and absence (violet) of furin in HEPES buffer solution. 27
- Figure 3.7: **Left:** HPLC traces of furin (*c* = 15.0 nM) induced removal of the RVRP cleavage site to get **3.2b** and linearization to **5b** and its reference spectrum (turquoise, second row). HPLC spectrum without furin to show the stability of **3b** in HEPES buffer solution (turquoise, first row). **Right:** HPLC traces to show the stability of **6b** in the presence (*c* = 23.8 nM) and absence (turquoise) of furin in HEPES buffer solution. 27

Figure 3.8: TEM images of Py-ISA 5c at different concentrations in 9:1 PBS/DMSO (pH 7.4). Scale bars = 250 nm.	28
Figure 3.9: TEM images of RVRR(Depsi-Py-I)SA 3c at a concentration of $c = 250 \mu\text{M}$ in 9:1 PBS/DMSO (pH 7.4). Scale bars = 250 nm.	29
Figure 3.10: Absorption (a) and emission spectra of Py-ISA 5c (b) and Py-COOH (c) with different concentrations in PBS/DMSO 9:1.	30
Figure 3.11: Top: Absorption (left) and emission (right) spectra of Py-ISA 5c ($c = 100 \mu\text{M}$) with different ratios of PBS/DMSO. Bottom: TEM images of Py-ISA 5c ($c = 100 \mu\text{M}$) with two different ratios of PBS/DMSO.	31
Figure 3.12: CD spectra (left) and absorption spectra (right) of Py-ISA 5c ($c = 100 \mu\text{M}$) in phosphate buffer (PB, 10 mM) (turquoise curves) and Milli-Q (black curves) and RVRR(Depsi-Py-I)SA 3c ($c = 100 \mu\text{M}$) in phosphate buffer (PB, 10 mM) (blue curves).	32
Figure 3.13: Temperature dependent CD spectra of Py-ISA 5c ($c = 100 \mu\text{M}$) in PB and respective TEM images at room temperature (left) and $80 \text{ }^\circ\text{C} \rightarrow$ room temperature (right).	33
Figure 3.14: Temperature-dependent $^1\text{H-NMR}$ spectra of Py-ISA 5c (0.43 mg/ml) in PB/DMSO- d_6 9:1.	34
Figure 3.15: Confocal laser scanning micrographs of MDA-MB-231 cells treated for 24 h with furin-sensitive depsipeptide 3c (2 nd row, $c = 100 \mu\text{M}$, 3 rd row, $c = 250 \mu\text{M}$) and non-cleavable control depsipeptide 6c (4 th row, $c = 250 \mu\text{M}$) to show cellular uptake and intracellular structure formation. Scale bars: 25 μm	35
Figure 3.16: HPLC traces of reference compounds 3c , 5c and 6c (turquoise and blue), and of the cell lysates of the cells treated with either cleavable depsipeptide 3c or non-cleavable control depsipeptide 6c (black) (detection at 340 nm).	36
Figure 3.17: Confocal laser scanning micrographs of MDA-MB-231 cells treated for 24 h with depsipeptide 3c (2 nd row, $c = 250 \mu\text{M}$) and depsipeptide 6c (3 rd row, $c = 250 \mu\text{M}$) to show cellular uptake and intracellular structure formation. <i>HCS NuclearMask Deep Red</i> (red) and BODIPY TM FL C ₅ -ceramide, complexed to BSA Golgi stain (yellow). Scale bars: 25 μm	37

List of Figures and Schemes

Figure 3.18: Confocal laser scanning micrographs of MDA-MB-231 cells treated for 14 h with depsipeptides 3a/3b 5:1 (2 nd row, $c = 100 \mu\text{M}$) and depsipeptide 6a/6b 5:1 (3 rd row, $c = 100 \mu\text{M}$) to show cellular uptake and intracellular structure formation. <i>HCS NuclearMask Deep Red</i> (red). Scale bars: 25 μm	38
Figure 3.19: Cell viability of MDA-MB-231 cells treated for 24 h with different concentrations of depsipeptides 3c/6c	39
Figure 4.1: Schematic representation of click-induced disassembly of synthetic structures inside cells. The tetraarginine sequence connected with DBCO is uptaken by the cell after synthetic nanostructures were formed via enzyme-responsive transformation of an assembly precursor. The click reaction between DBCO and the C-terminal azide at the self-assembled structures changes the hydrophobicity of the peptide monomers resulting in the disassembly of the intracellular structures.....	43
Figure 5.1: MALDI-TOF spectrum (left) and HPLC trace (right) of RVRR(Depsi-C343-I)SA.....	52
Figure 5.2: MALDI-TOF spectrum (left) and HPLC trace (right) of RVRR(Depsi-Fmoc-I)SA.....	53
Figure 5.3: MALDI-TOF spectrum (left) and HPLC trace (right) of RRRV(Depsi-C343-I)SA.....	54
Figure 5.4: MALDI-TOF spectrum (left) and HPLC trace (right) of RRRV(Depsi-Fmoc-I)SA.....	55
Figure 5.5: MALDI-TOF spectrum (left) and HPLC trace (right) of RVRR(Depsi-Py-I)SA.....	58
Figure 5.6: MALDI-TOF spectrum (left) and HPLC trace (right) of RRRV(Depsi-Py-I)SA.....	59
Figure 8.1: ¹ H-NMR spectrum of C343-Ile (DMF- <i>d</i> ₇ , 500 MHz, 298 K).....	71
Figure 8.2: ¹³ C-NMR spectrum of C343-Ile (DMF- <i>d</i> ₇ , 500 MHz, 298 K).....	71
Figure 8.3: COSY spectrum of C343-Ile (DMF- <i>d</i> ₇ , 500 MHz, 298 K).....	72

Figure 8.4 MALDI spectrum of Ac-RVRR (test cleavage without purification).....	72
Figure 8.5: MALDI spectrum of RVRR(Depsi-C343-I)SA.....	73
Figure 8.6: Chromatogram of RVRR(Depsi-C343-I)SA.	73
Figure 8.7: MALDI spectrum of RVRR(Depsi-Fmoc-I)SA.	74
Figure 8.8: Chromatogram of RVRR(Depsi-Fmoc-I)SA.....	74
Figure 8.9: MALDI spectrum of RRRV(Depsi-C343-I)SA.....	75
Figure 8.10: Chromatogram of RRRV(Depsi-C343-I)SA.	75
Figure 8.11: MALDI spectrum of RRRV(Depsi-Fmoc-I)SA.	76
Figure 8.12: Chromatogram of RRRV(Depsi-Fmoc-I)SA.....	76
Figure 8.13: ¹ H-NMR spectrum of Py-Ile (DMF- <i>d</i> ₇ , 400 MHz, 298 K).....	77
Figure 8.14: MALDI spectrum of Py-Ile.....	77
Figure 8.15: MALDI spectrum of RVRR(Depsi-Py-I)SA.	78
Figure 8.16: Chromatogram of RVRR(Depsi-Py-I)SA.....	78
Figure 8.17: MALDI spectrum of RRRV(Depsi-Py-I)SA.	79
Figure 8.18: Chromatogram of RRRV(Depsi-Py-I)SA.....	79
Figure 8.19: ¹ H-NMR spectrum of Py-ISA (DMSO- <i>d</i> ₆ , 850 MHz, 298 K).....	80
Figure 8.20: MALDI spectrum of Py-ISA.	80
Figure 8.21 Chromatogram of Py-ISA.	81
Figure 8.22: MALDI spectrum of RVRR(Depsi-Py-I)SA after cell lysate analysis by analytical HPLC.	81
Figure 8.23: MALDI spectrum of RRRV(Depsi-Py-I)SA after cell lysate analysis by analytical HPLC.	82
Figure 8.24: MALDI spectrum of Py-ISA after cell lysate analysis by analytical HPLC. .	82

List of Figures and Schemes

Schemes

- Scheme 3.1: Both synthesized peptide sequences. **Left:** active sequence **2.1** (**RVRRSA**), cleavable by furin. **Right:** scrambled sequence **2.2** (**RRRVSA**), not cleavable by furin... 20
- Scheme 3.2: Synthesis scheme of C343-Ile **1b** and Py-Ile **1c** at the solid-phase and in solution..... 20
- Scheme 3.3: Synthesis scheme of the final synthesis step of the depsipeptides **3/6** and subsequent cleavage from the resin..... 22
- Scheme 3.5: Synthesis scheme of the linear pyrene-modified peptide **5c** and subsequent cleavage from the resin. 24
- Scheme 3.6: Cleavage of depsipeptides **3** by the enzyme furin at the RVRR cleavage site and a subsequent *O,N*-acyl shift to get the linearized peptides **5**. 25

8 Attachment

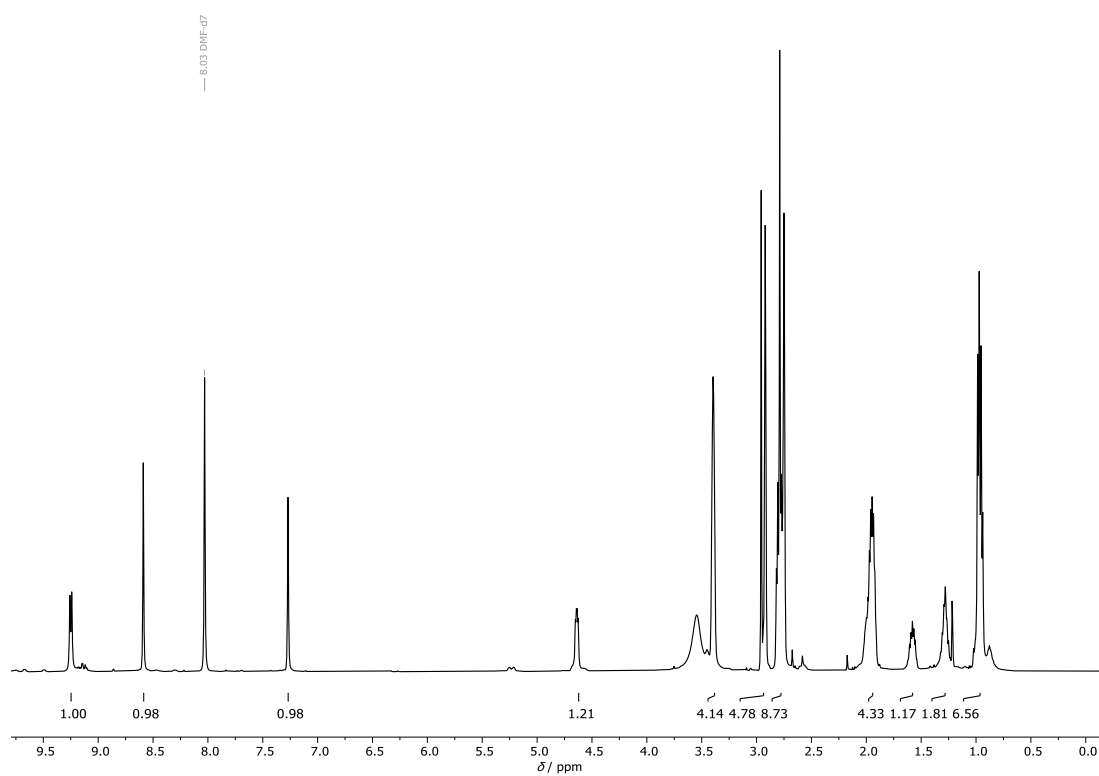


Figure 8.1: $^1\text{H-NMR}$ spectrum of C343-Ile (DMF- d_7 , 500 MHz, 298 K).

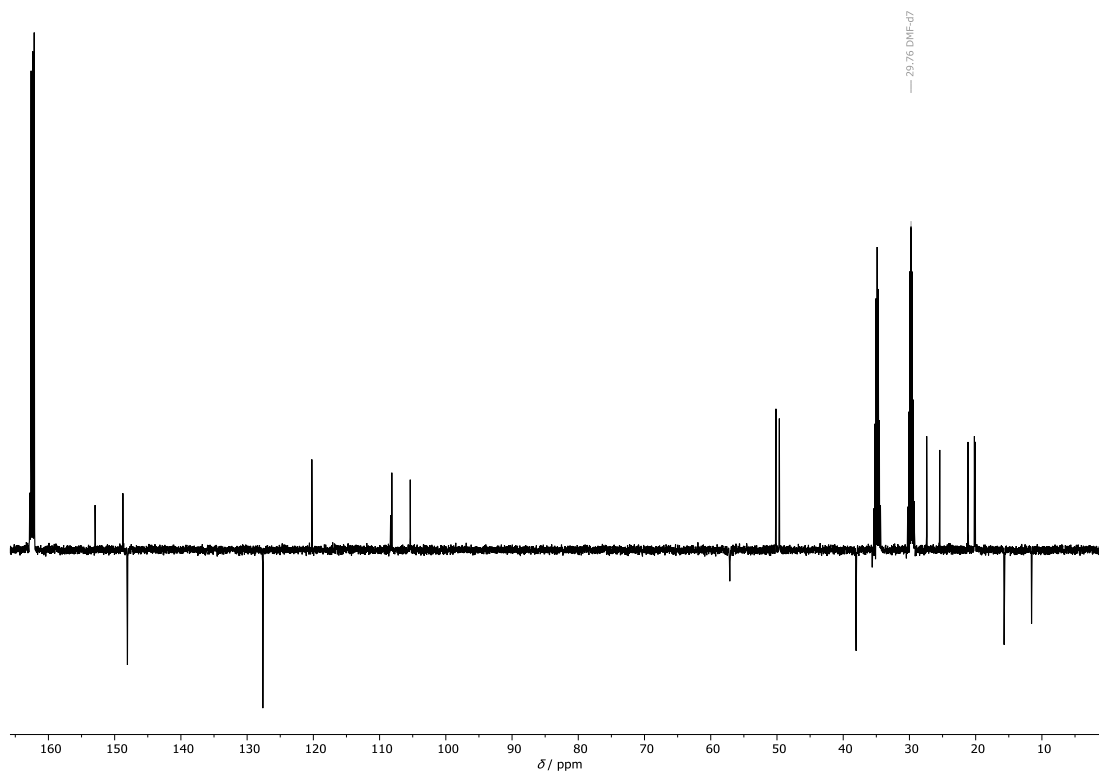


Figure 8.2: $^{13}\text{C-NMR}$ spectrum of C343-Ile (DMF- d_7 , 500 MHz, 298 K).

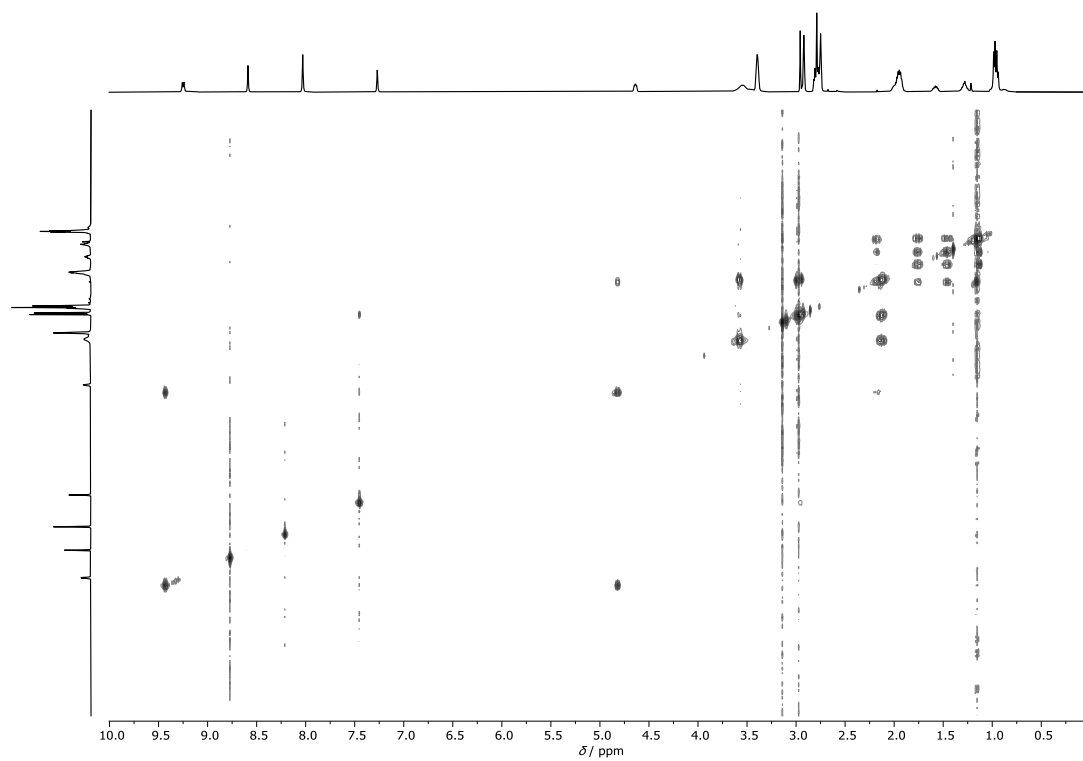


Figure 8.3: COSY spectrum of C343-Ile (DMF- d_7 , 500 MHz, 298 K).

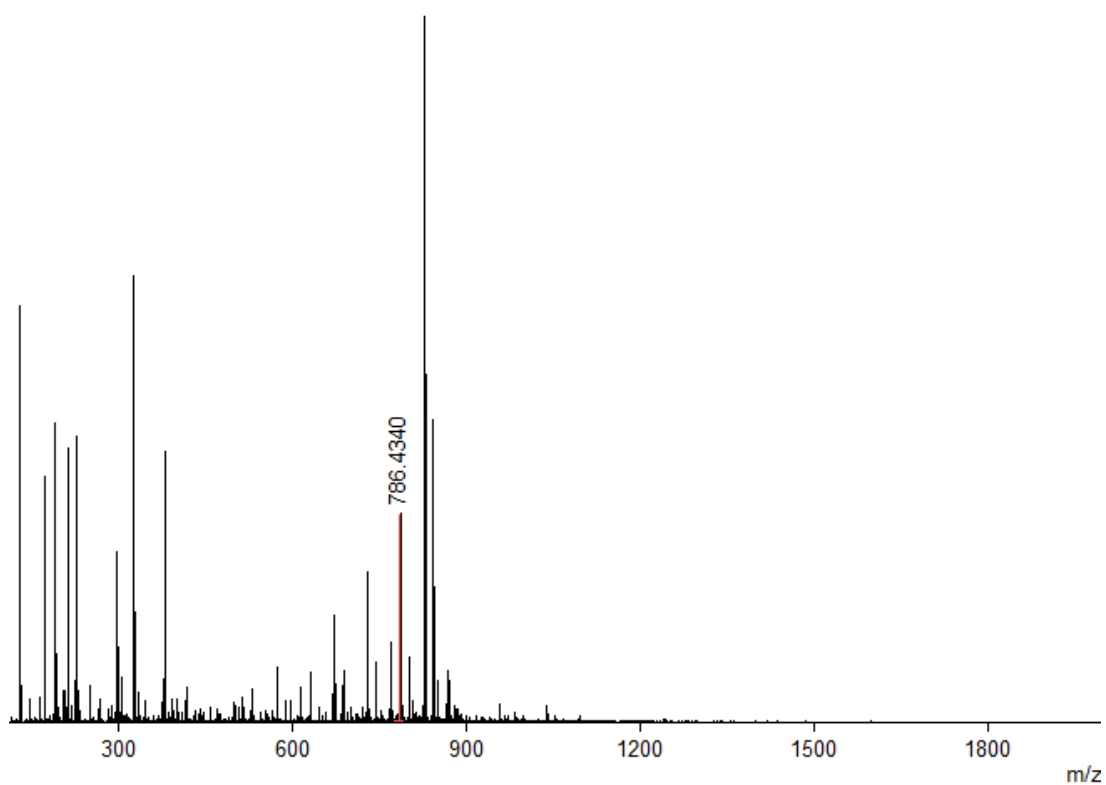


Figure 8.4 MALDI spectrum of Ac-RVRR (test cleavage without purification).

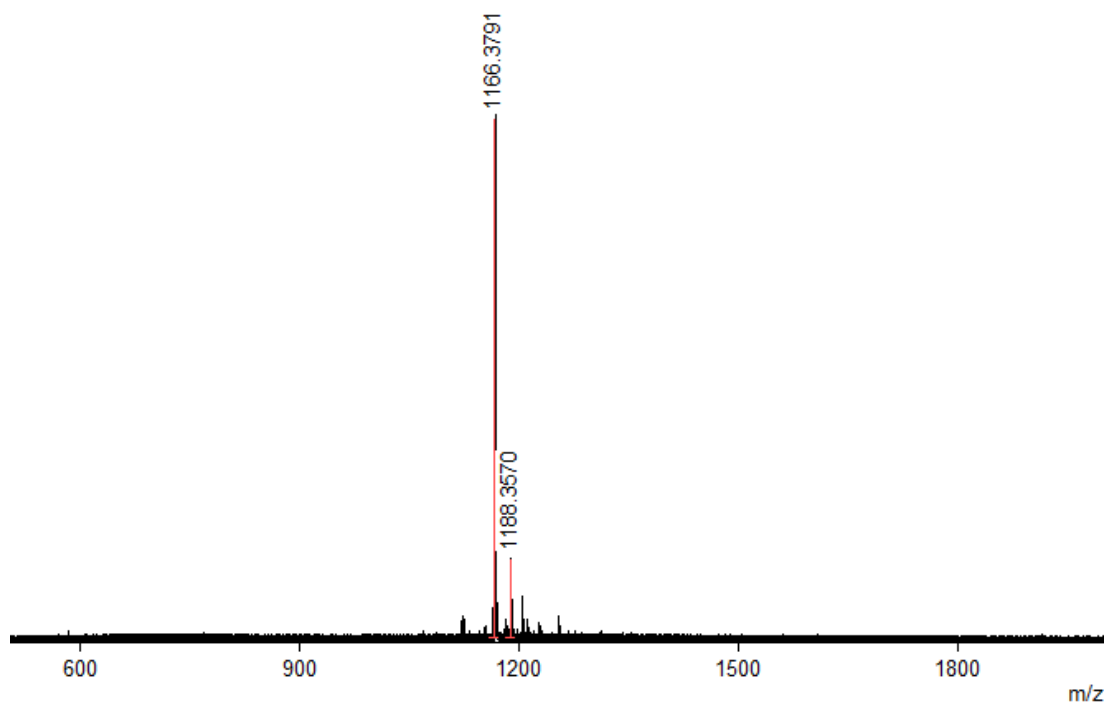


Figure 8.5: MALDI spectrum of RVR(Depsi-C343-I)SA.

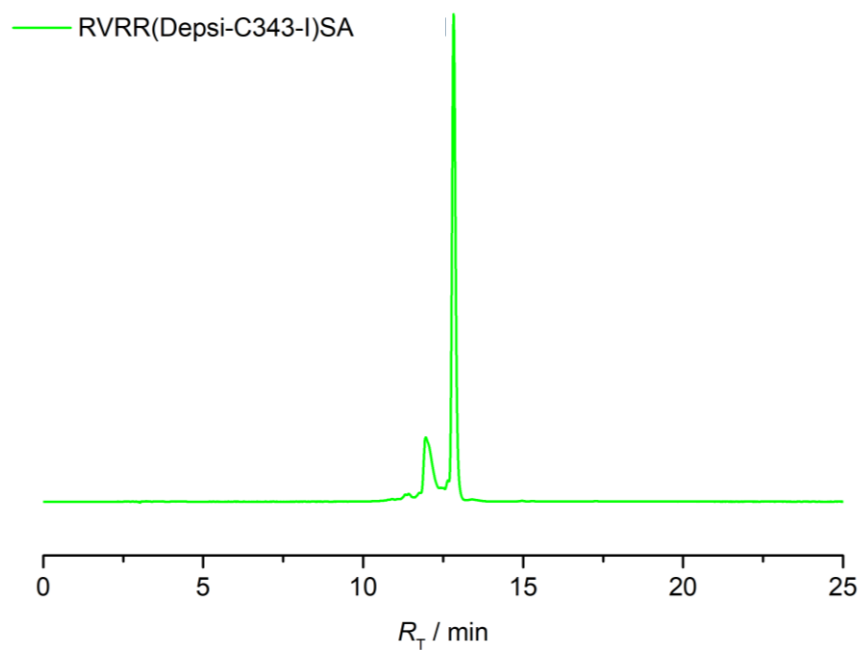


Figure 8.6: Chromatogram of RVR(Depsi-C343-I)SA.

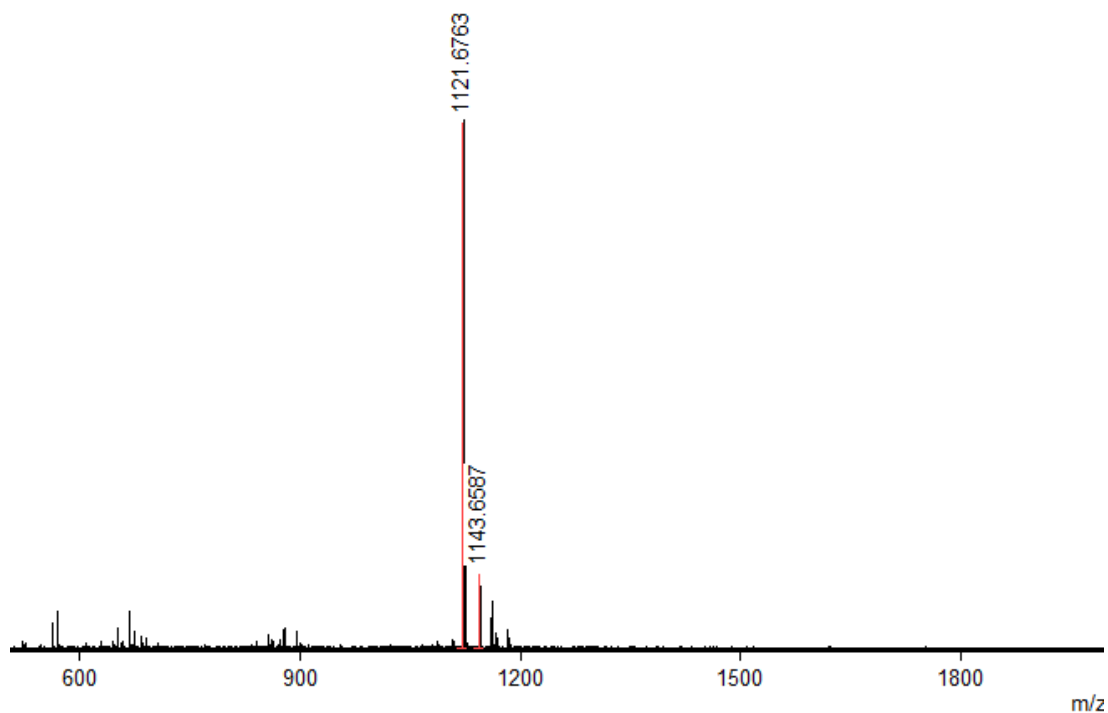


Figure 8.7: MALDI spectrum of RVRR(Depsi-Fmoc-I)SA.

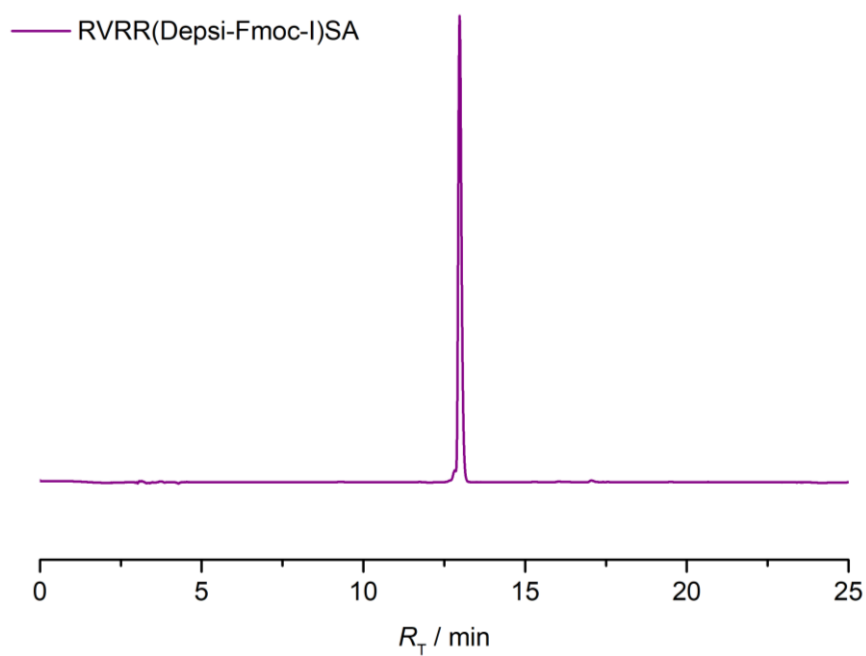


Figure 8.8: Chromatogram of RVRR(Depsi-Fmoc-I)SA.

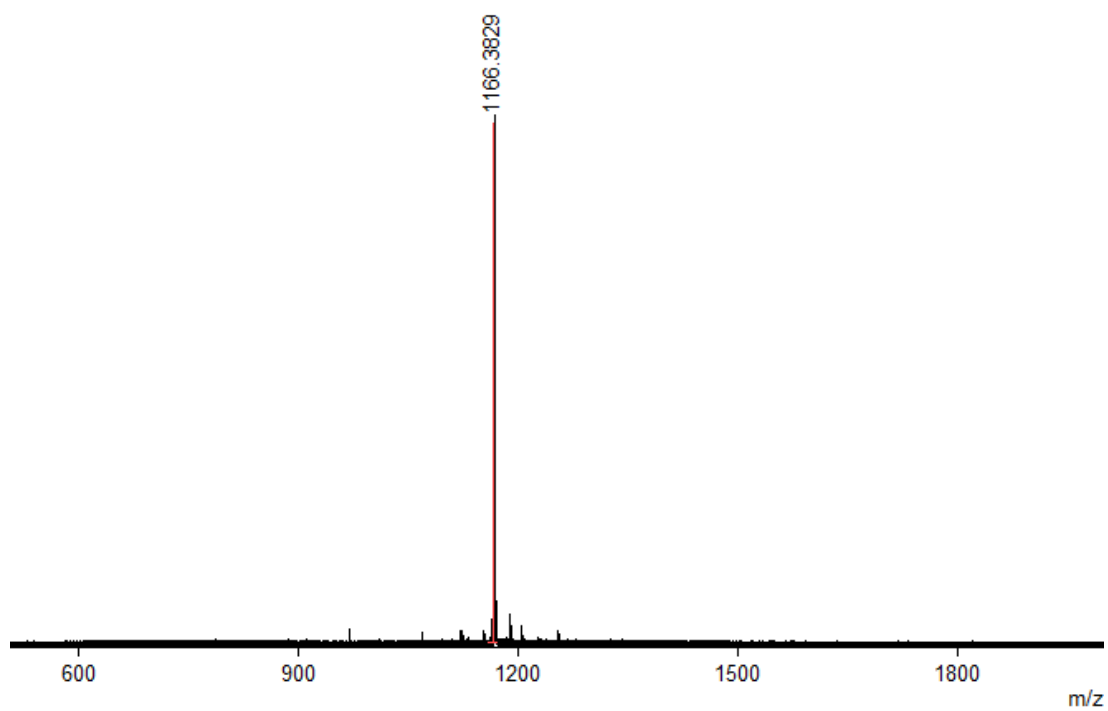


Figure 8.9: MALDI spectrum of RRRV(Depsi-C343-I)SA.

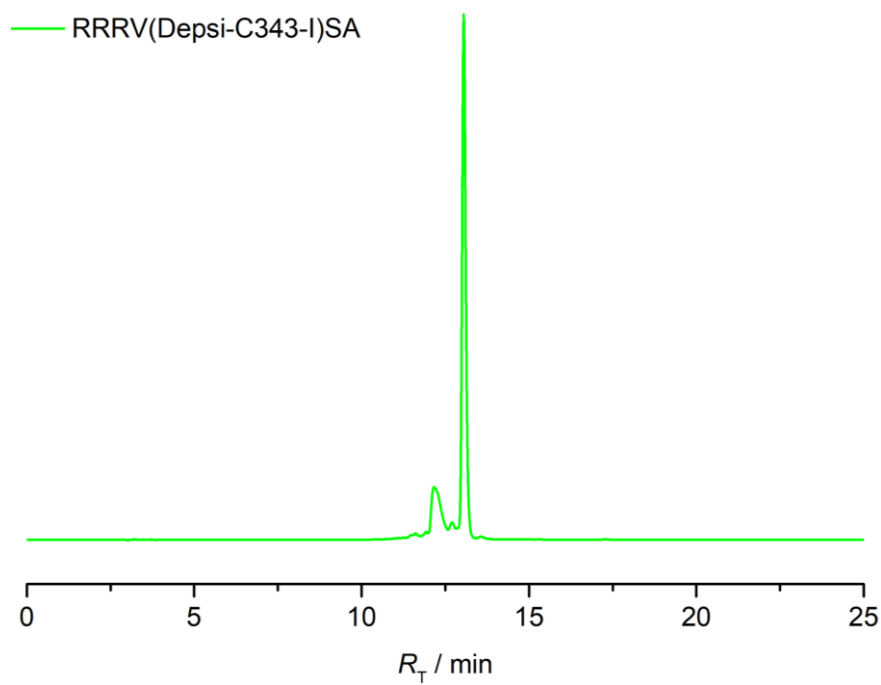


Figure 8.10: Chromatogram of RRRV(Depsi-C343-I)SA.

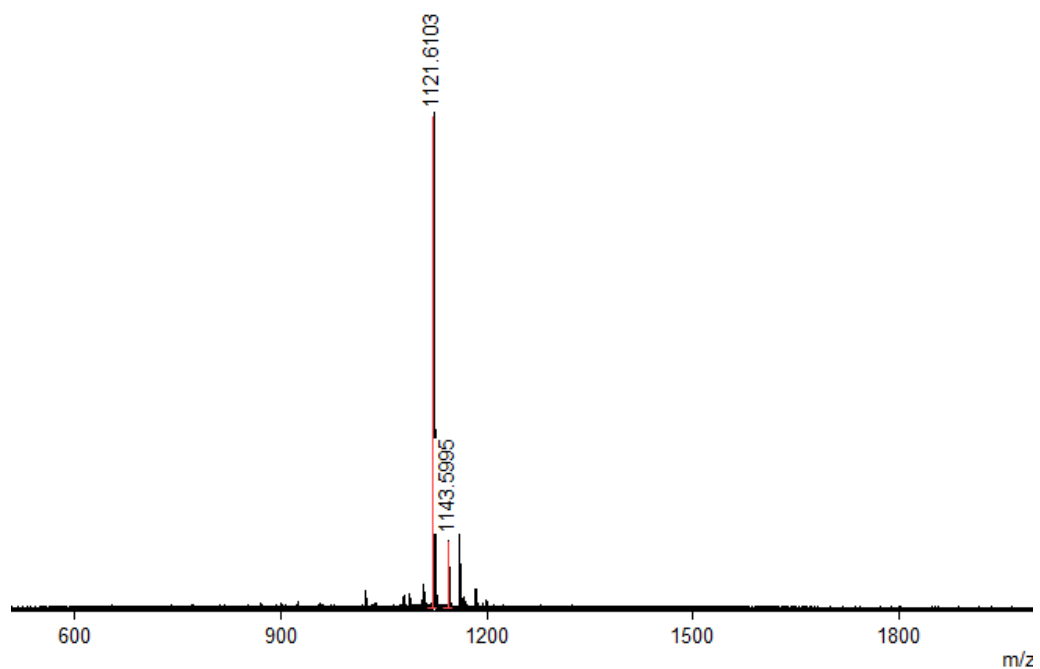


Figure 8.11: MALDI spectrum of RRRV(Depsi-Fmoc-I)SA.

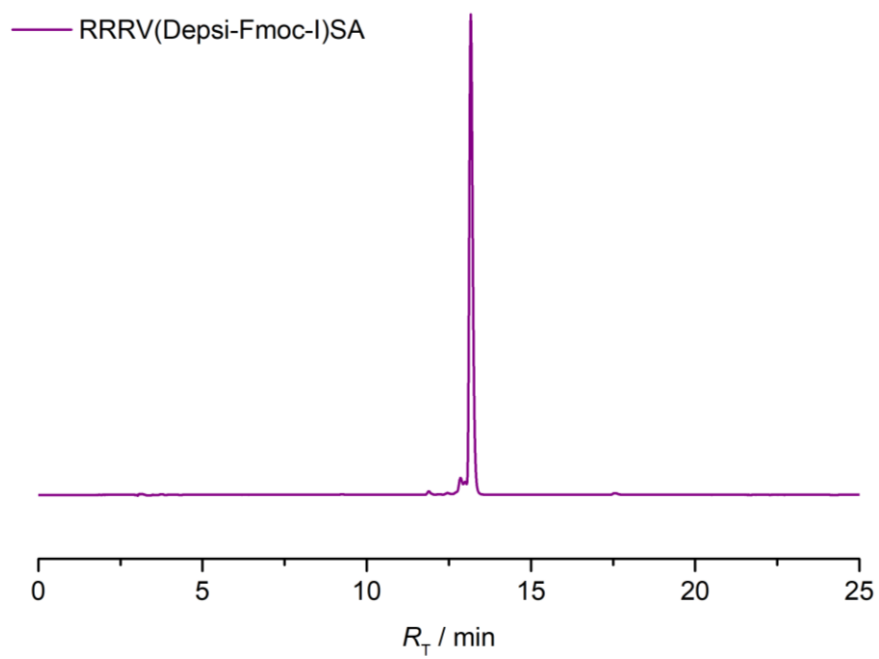


Figure 8.12: Chromatogram of RRRV(Depsi-Fmoc-I)SA.

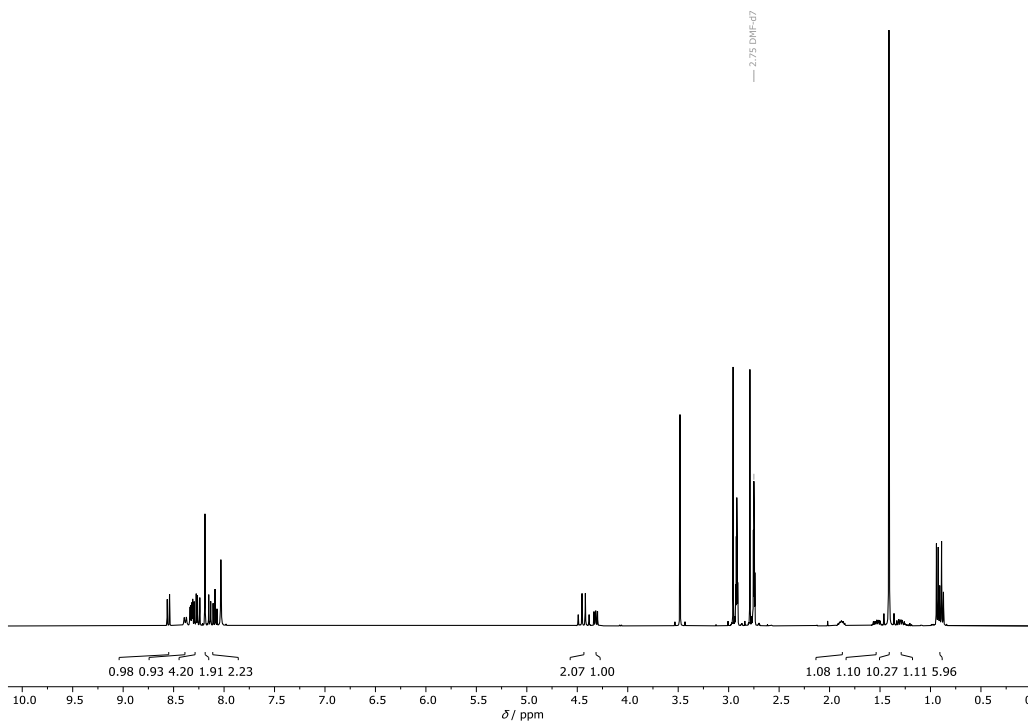


Figure 8.13: $^1\text{H-NMR}$ spectrum of Py-Ile (DMF- d_7 , 400 MHz, 298 K).

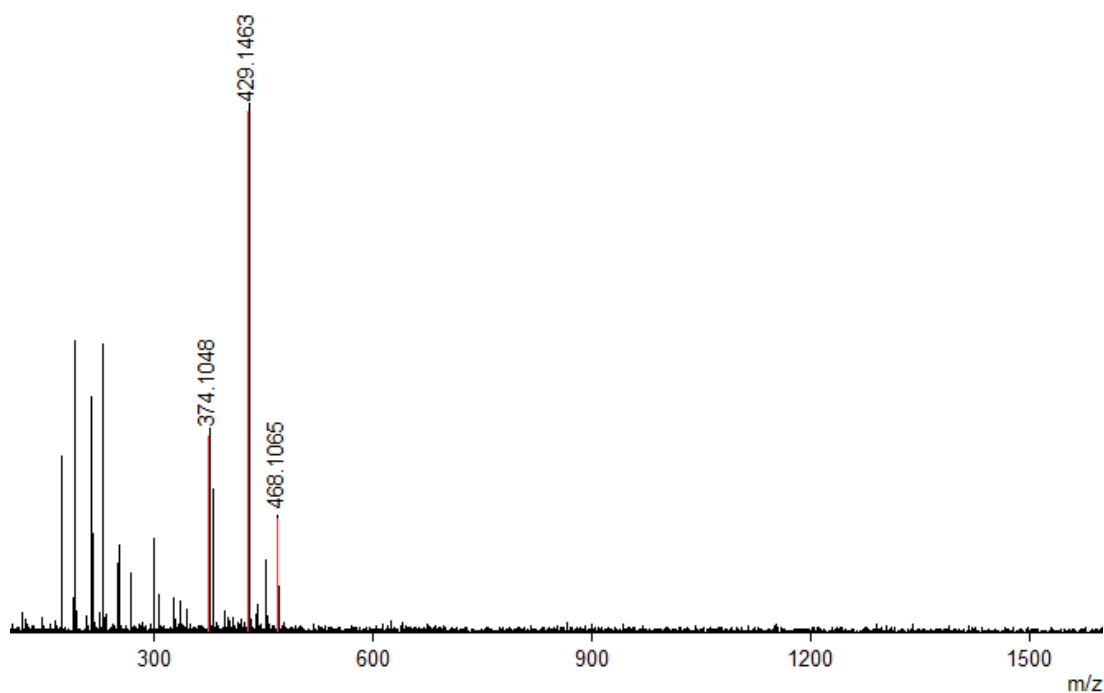


Figure 8.14: MALDI spectrum of Py-Ile.

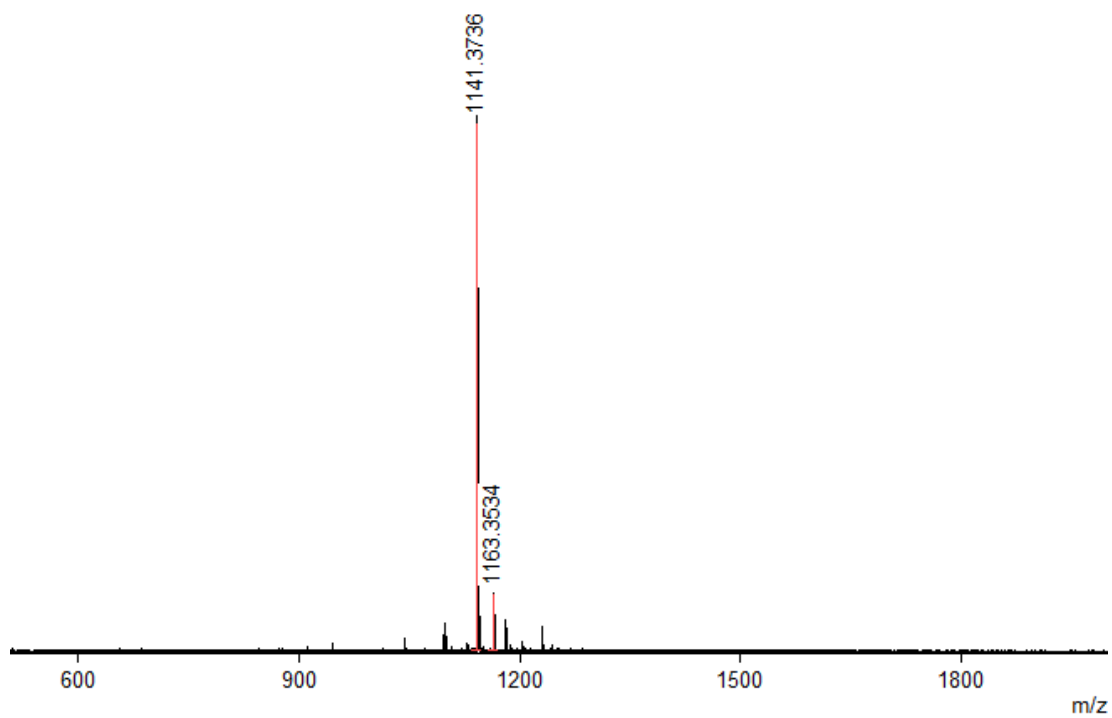


Figure 8.15: MALDI spectrum of RVRR(Depsi-Py-I)SA.

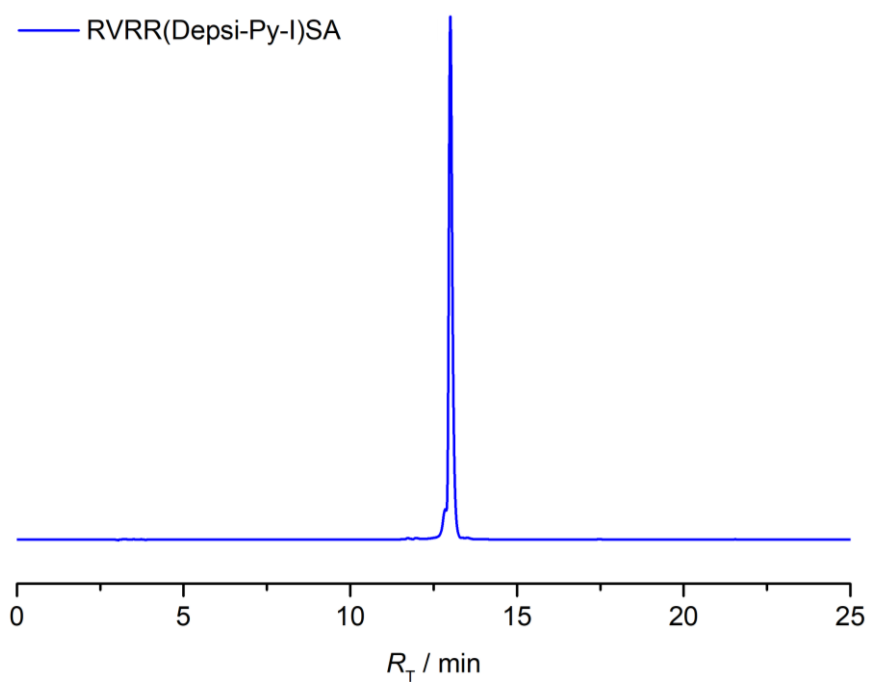


Figure 8.16: Chromatogram of RVRR(Depsi-Py-I)SA.

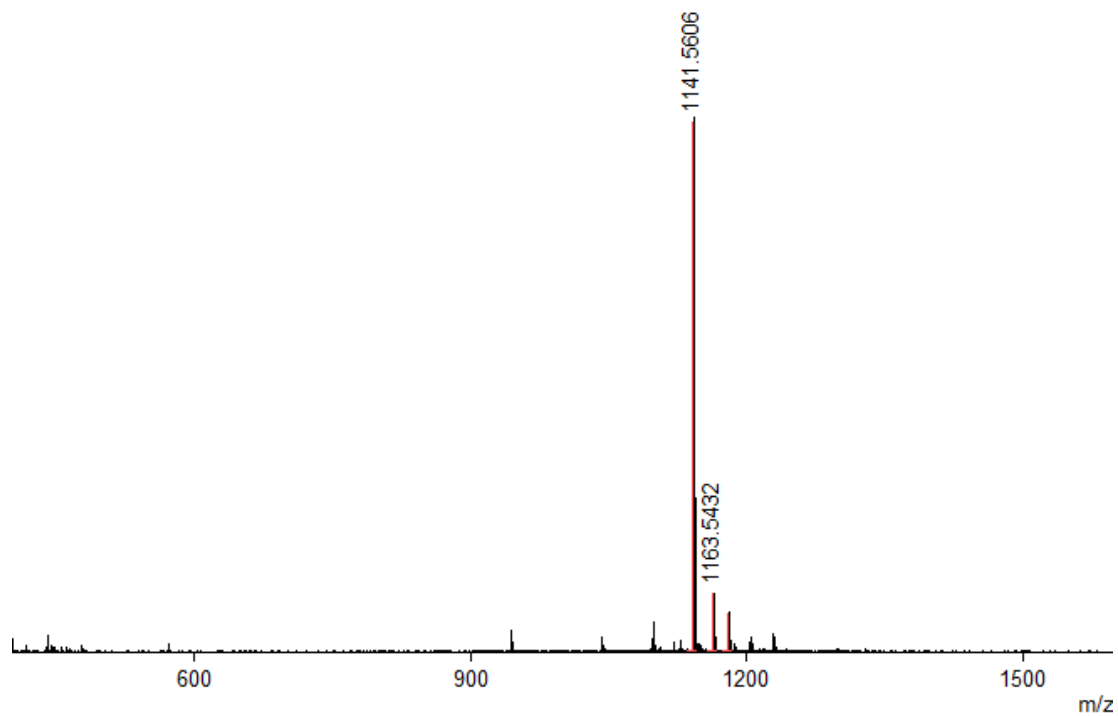


Figure 8.17: MALDI spectrum of RRRV(Depsi-Py-I)SA.

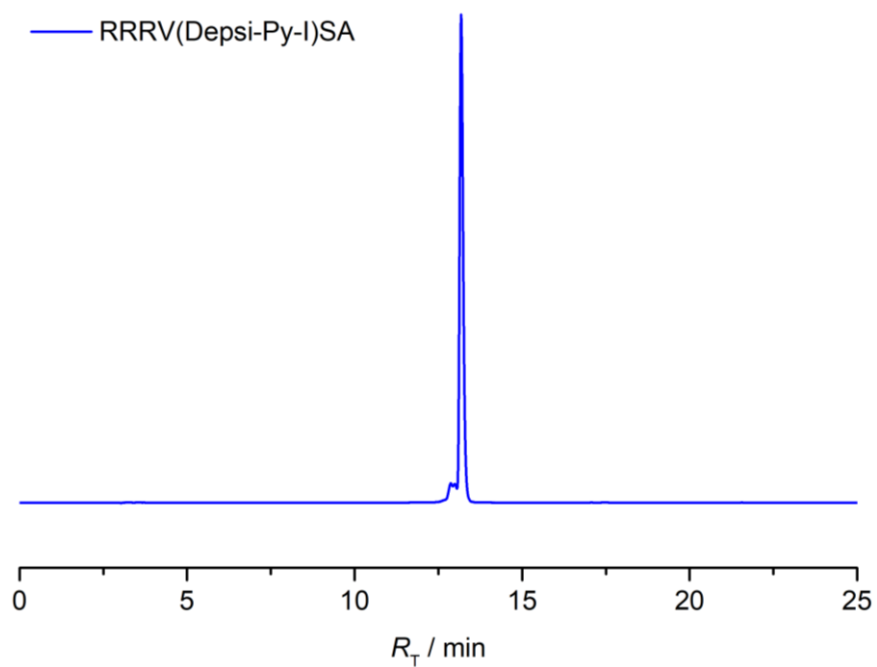


Figure 8.18: Chromatogram of RRRV(Depsi-Py-I)SA.

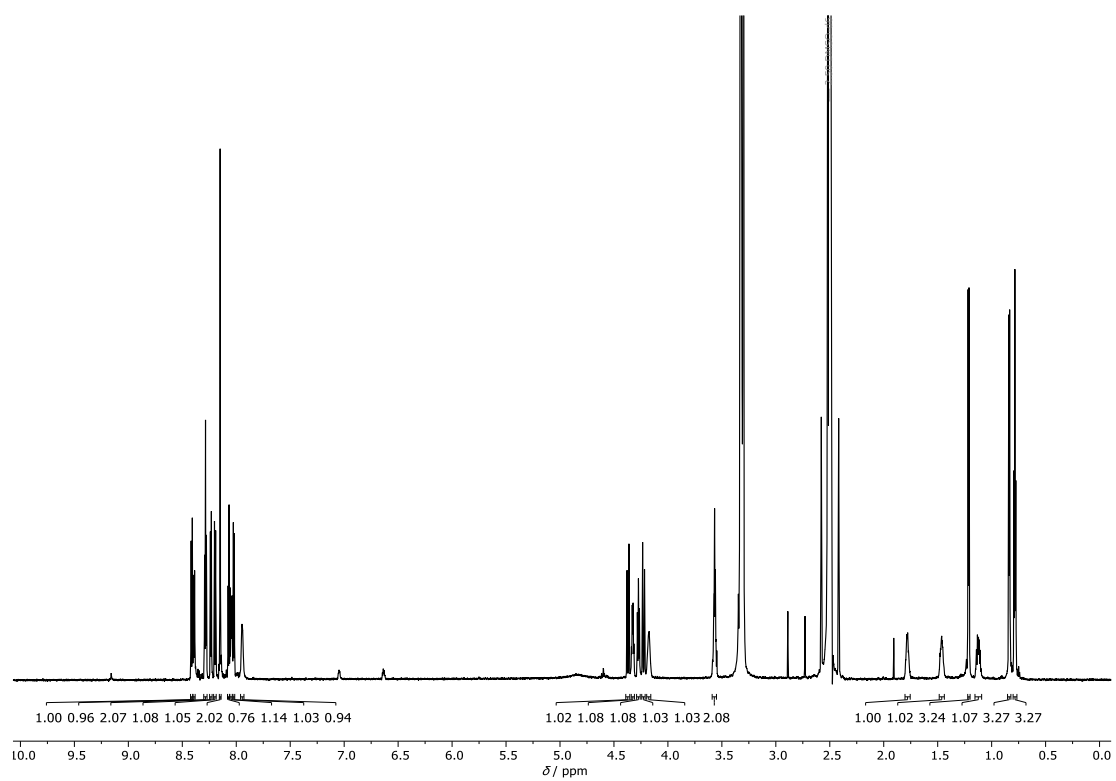


Figure 8.19: $^1\text{H-NMR}$ spectrum of Py-ISA ($\text{DMSO-}d_6$, 850 MHz, 298 K).

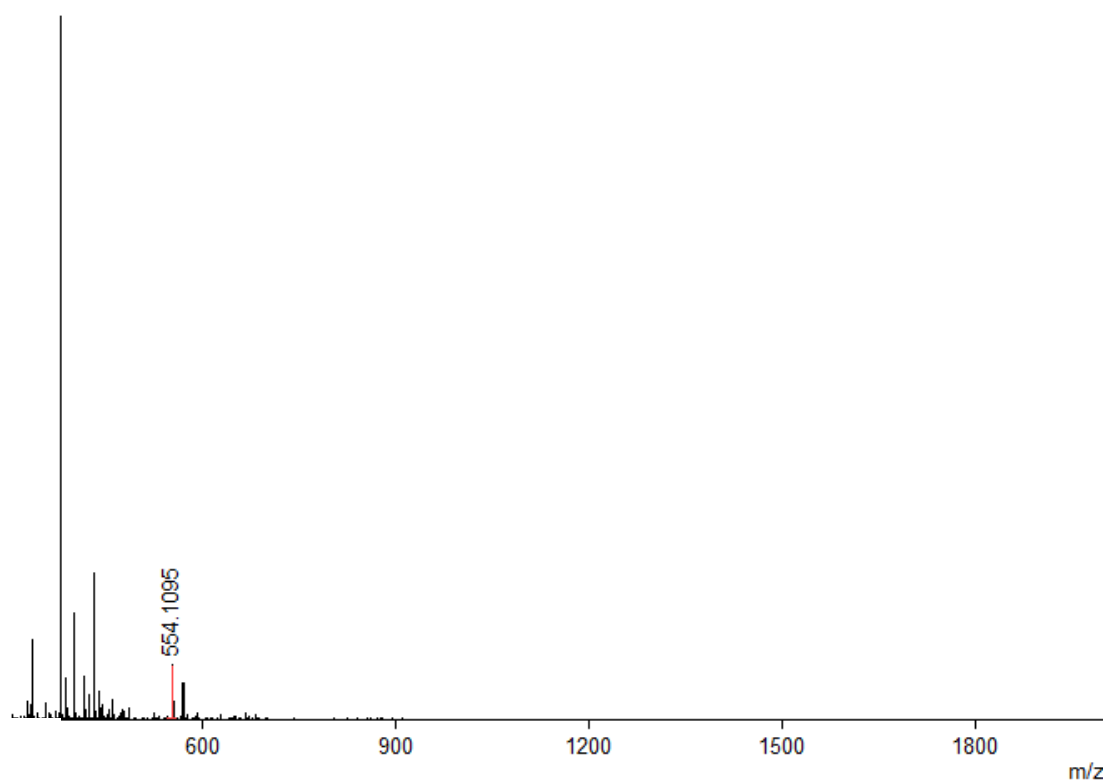


Figure 8.20: MALDI spectrum of Py-ISA.

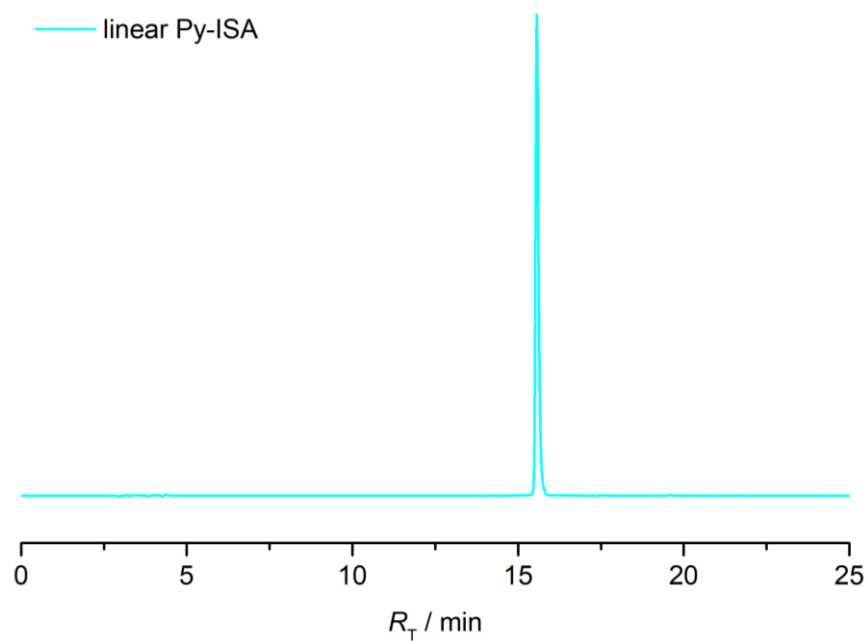


Figure 8.21 Chromatogram of Py-ISA.

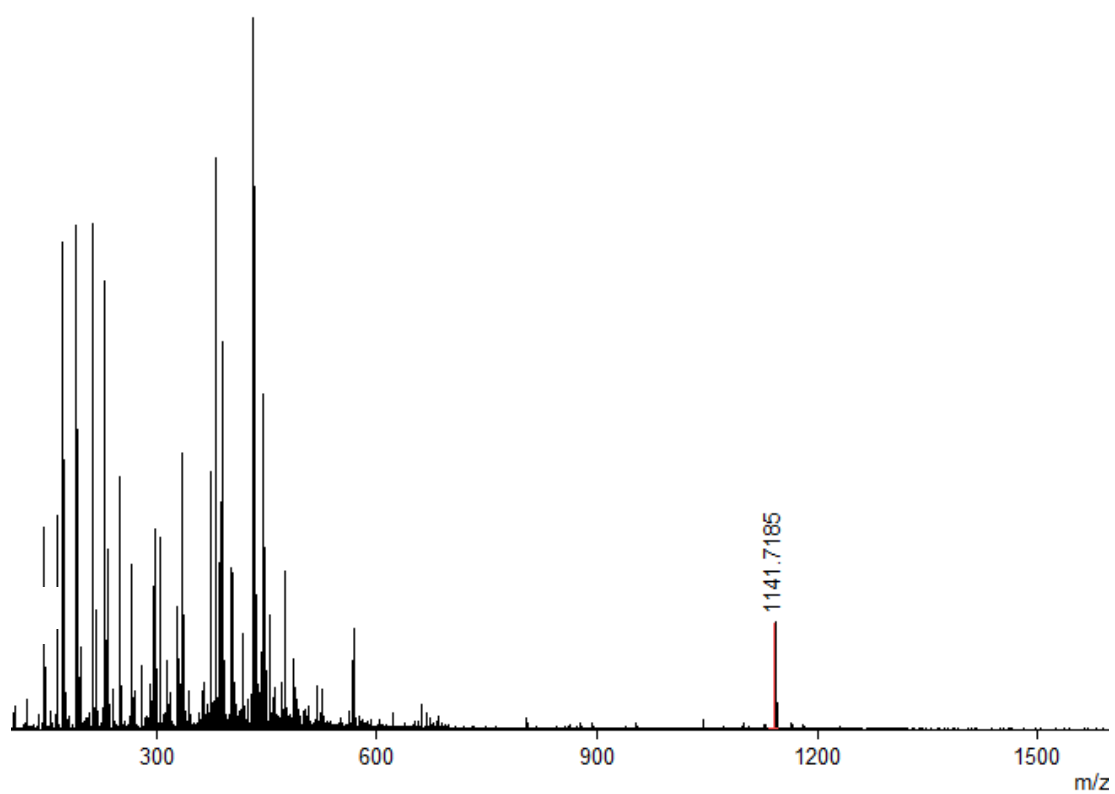


Figure 8.22: MALDI spectrum of RVRR(Depsi-Py-I)SA after cell lysate analysis by analytical HPLC.

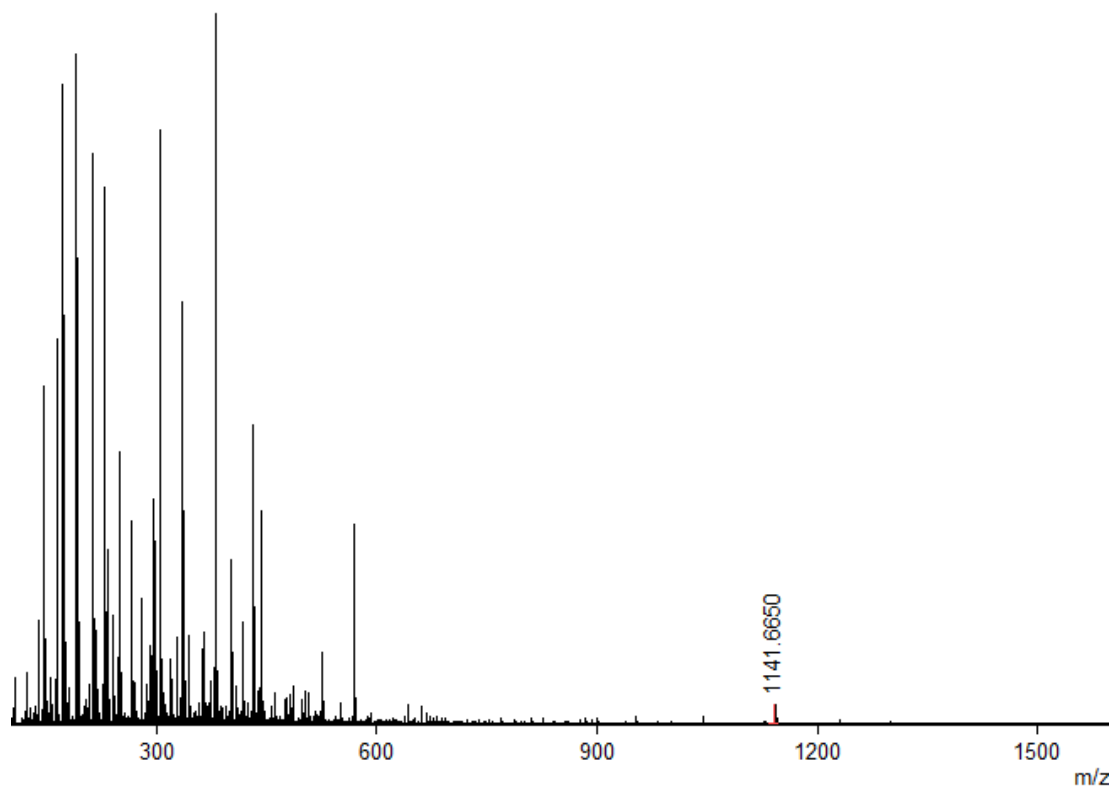


Figure 8.23: MALDI spectrum of RRRV(Depsi-Py-I)SA after cell lysate analysis by analytical HPLC.

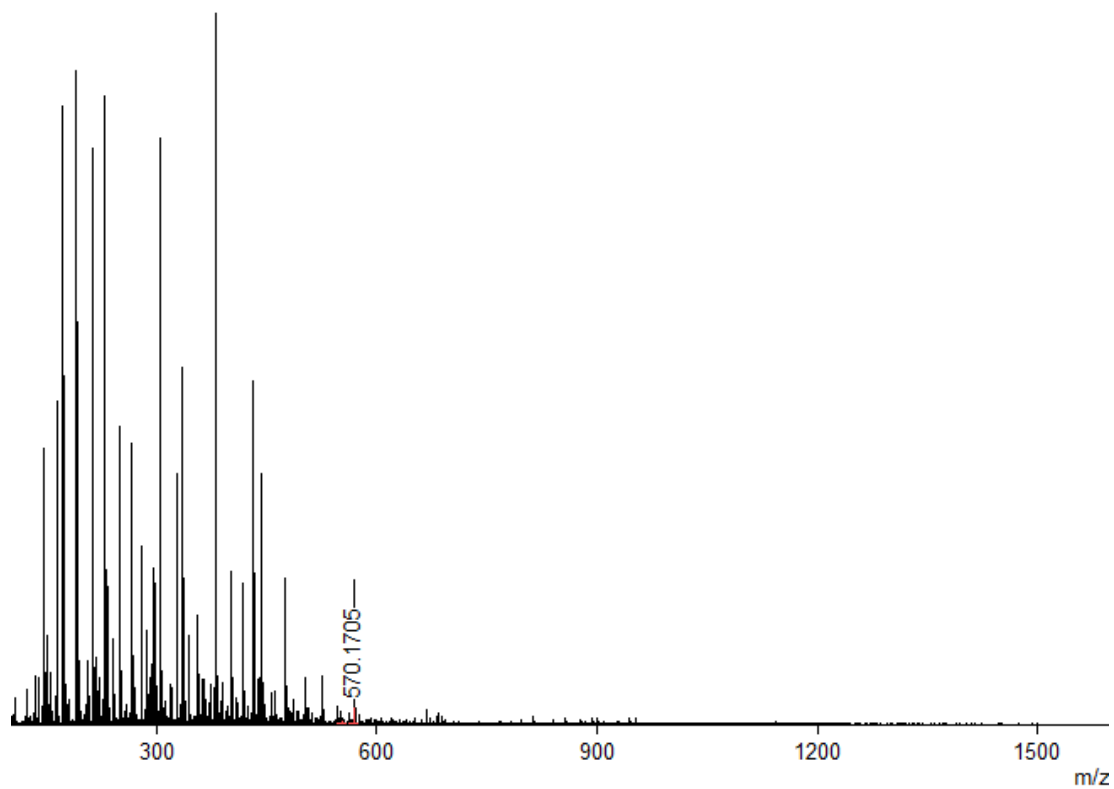


Figure 8.24: MALDI spectrum of Py-ISA after cell lysate analysis by analytical HPLC.

Danksagung

Als erstes möchte ich mich bei Frau Prof. Dr. Tanja Weil bedanken, die mir die Möglichkeit gegeben hat meine Masterarbeit in ihrem Arbeitskreis anzufertigen. Außerdem möchte ich mich für die Zeit bedanken die sie sich genommen hat, um ausführlich über meine Forschungsergebnisse zu diskutieren.

Für das Erstellen eines Zweitgutachtens meiner Masterarbeit möchte ich mich bei Herrn Prof. Dr. Andreas Walther bedanken.

Ein großer Dank geht auch an meinen Gruppenleiter Dr. David Ng, der stets eine offene Tür für jegliche Fragen hatte und mir jederzeit sehr freundlich begegnet ist. Außerdem bedanke ich mich bei ihm für die großartigen Konfokal Laser Scanning Mikroskop Aufnahmen im Rahmen der in dieser Arbeit durchgeführten Zellexperimente.

Auch vielen Dank an alle Mitarbeiter:innen des gesamten Instituts die an den Messungen meiner Proben beteiligt waren.

Mein größter Dank gilt meiner Betreuerin Sarah, die mich hier am Institut sehr liebevoll aufgenommen hat und mir alles sehr geduldig erklärt und gezeigt hat. Ich hatte jederzeit die Möglichkeit ihr Fragen zu stellen und bekam immer eine ausführliche und zufriedenstellende Antwort. Ich bedanke mich auch für die sehr hilfreichen Korrekturvorschläge meiner Arbeit, durch die ich selbst am Ende noch einiges neues dazu lernen konnte.

Ein großer Dank geht auch an den Rest der Gruppe die mich alle sehr herzlich aufgenommen haben und ebenfalls immer offen für Fragen waren. Das Kartenspielen mit Konrad, Patrick, Raphael, Julian, Laura und Nelly nach der Mittagspause werde ich definitiv vermissen. Ein besonderer Dank geht an Patrick für die Messung meiner TEM-Proben.

Mein letzter Dank geht an meine Freunde und Familie, die mich stets unterstützt haben und dafür gesorgt haben, dass ich in meiner Freizeit auch mal an etwas anderes denken konnte.